Internal Leakage Diagnosis in Valve Controlled Actuation Systems and Electrohydrostatic Actuation Systems

by

Chinenye Alozie

A Thesis submitted to the Faculty of Graduate studies of

The University of Manitoba

in partial fulfillment of the requirements of the degree of

MASTER OF SCIENCE

Department of Mechanical and Manufacturing Engineering

University of Manitoba

Winnipeg

Abstract

Diagnosis of faults associated with hydraulic actuators is essential to avoid accidents or loss of system functionality. This thesis focuses on internal leakage fault diagnosis in valve controlled hydraulic actuation systems (VCA) as well as electrohydrostatic actuation systems (EHA). For the VCA, the hydraulic actuator is driven in a closed loop mode to track a pseudorandom input signal whereas for the EHA, an actuator is driven in an open loop mode to track a sinusoidal input. Motivated by developing a method that does not rely on the model of the system or type of fault, signal processing techniques based on the ratio of metric lengths of pressure signals, autocorrelation of pressure signal, cross correlation between chamber pressure signals, and cross correlation between control signal and piston displacement is employed for internal leakage diagnosis.

For the VCA, autocorrelation of pressure signals performed well at lower lags (less than 4) and at a window size of 200 data points; both cross correlation between pressure signals and cross correlation between control signal and piston displacement performed well at higher lags (higher than 8) and at a window size of 100 data points; ratio of metric lengths of pressure signals was found to be more effective at higher lag ratios (more than 16:3). All methods were sensitive to the lowest simulated leakage of 0.047 L/min, though with different level of success; ratio of metric lengths produced 84% sensitivity, autocorrelation 19% sensitivity, cross correlation between pressure signals 25% sensitivity and cross correlation between piston displacement and control signal 20% sensitivity.

For the EHA, all methods were capable of identifying small leakage of 0.98 L/min. The ratio of metric lengths produced 6.7% sensitivity, autocorrelation 2.59% sensitivity, cross correlation between pressure signals 9.4% sensitivity and cross correlation between piston displacement and control signal 31.9% sensitivity. The low leakage detection achieved without requiring a model of the actuator or leakage type make these methods very attractive for industrial implementation

DEDICATION

Dedicated to the Lord God Almighty for given me the opportunity to come this far, Rivers State government of Nigeria for given me the initial lift in life, my future wife and my parents for their persistent prayers and support.

Acknowledgements

Firstly I will like to thank God Almighty for giving me the enablement and grace to complete this project. I am grateful to my supervisor, Prof. Nariman Sepehri, for his untiring and unwavering support, advice and direction which was paramount to the success of this work. There is no doubt, without his influence and support the success of this project would have been jeopardized. From my supervisor, I have learned a great deal about problem solving and presentation of results.

I would also like to thank Prof. Witold Kinsner for his support and very helpful suggestions from the preliminary phase to the completion of this project. My gratitude goes to the members at the fluid power and telerobotics research laboratory. They provided me with the appropriate atmosphere to complete this work. I am also very grateful to Mr. J.P. Burak for the review of my thesis and helpful comments. Finally, I am ultimately grateful to my parents who persistently prayed for my success.

Table of Contents

List of Tables

List of Figures

Nomenclature

VALVE CONTROLLED ACTUATION SYSTEM

P_1, P_2	Line pressures
$\{x_v, v_v\}$	Valve spool displacement and velocity
m	Mass of the rod
d	Effective viscous damping of the actuator
A	Annulus area of the piston
β	Effective bulk modulus of the fluid
V	Volume of fluid on each side actuator side
k_v	Valve spool position gain
w_v	Servo valve natural frequency
ξ	Servo valve damping ratio
q_1, q_2	Flows through the valve
W	Valve orifice area gradient
P_s, P_r	Supply and tank pressure
k_i	leakage coefficient
P_L	Load pressure

ELECTROHYDROSTATIC ACTUATION SYSTEM

P_1, P_2	Outlet and inlet pressure of the pump
M_{eq}	Combined mass of piston and rod
V	Input voltage
L_c	Inductance of the motor
F_v	Viscous damping coefficient
L	Actuator stroke
A_A, A_B	Piston area
V_{th}	Velocity threshold
β	Fluid bulk modulus

V	Volume of fluid on each side actuator side
q_b	Displacement of the pump
R_c	Resistance of motor
J_m	moment inertia (motor and pump)
C_e	Back electromotive force constant
ρ	Fluid Density
A_{line}	Area of line
d_{line}	Diameter of line
P_L	Load pressure
C_{dori}	Drag coefficient of orifice
C_m	Electromagnetism torque constant
F_{pr}	Pre load force at piston
P_A P_B	Chamber pressure
B_m	Damping coefficient
A_{dori}	Area of the orifice
Q_A, Q_B	Flow from the orifice

SIGNAL PROCESSING

cc_τ	Cross correlation at lag τ
F_m	Ratio of metric lengths (fractal number)
ac_τ	Autocorrelation at lag τ
N	Window size
K	Step size 1
L	Step size 2
RMS_l	Root mean square of leaking coefficients
RMS_{nl}	Rootmean square non-leaking coefficients
$Mean_{RMS}$	Mean root mean square

ABBREVIATIONS

VCA	Valve controlled actuation system
EHA	Electrohydrostatic actuation system
EKF	Extended Kalman filter
AC	Alternating current

CHAPTER 1

INTRODUCTION

1 INTRODUCTION

1.1 Background

Hydraulics is the transmission and control of forces in a liquid medium. A basic hydraulic system consists of a pump, hydraulic fluid, hoses to carry the fluid, control valves, tank and an actuator. Hydraulic actuators use pressurized hydraulic fluid to provide transmission of energy. Special features of hydraulic systems include high force to mass ratio and the lubricating properties of the fluid (Merrit, 1967). For these reasons, hydraulic actuators are broadly applied in manufacturing firms, robotic firms and aerospace.

A typical hydraulic system consists of a pump, motor, tank, control element and hydraulic lines. The pump pumps fluid from the tank to one side of the actuator; which results in higher pressure at one end of the hydraulic chamber. The pressure difference between the two chambers results in a movement of the cylinder in the direction of the lower pressure. Two types of hydraulic systems considered in this thesis are valve controlled hydraulic actuation *(VCA)* system and electrohydrostatic actuation *(EHA)* system.

Valve Controlled Actuation System

A valve controlled actuation system uses a servo valve as the control element to control linear cylinders or the rotary motor. The pro of using a servo valve is that it requires a low power electrical signal to position the actuator accurately. On the other hand, servo valves are costly, have low efficiency, and are complex. Figure 1-1 shows typical valve controlled actuation system.

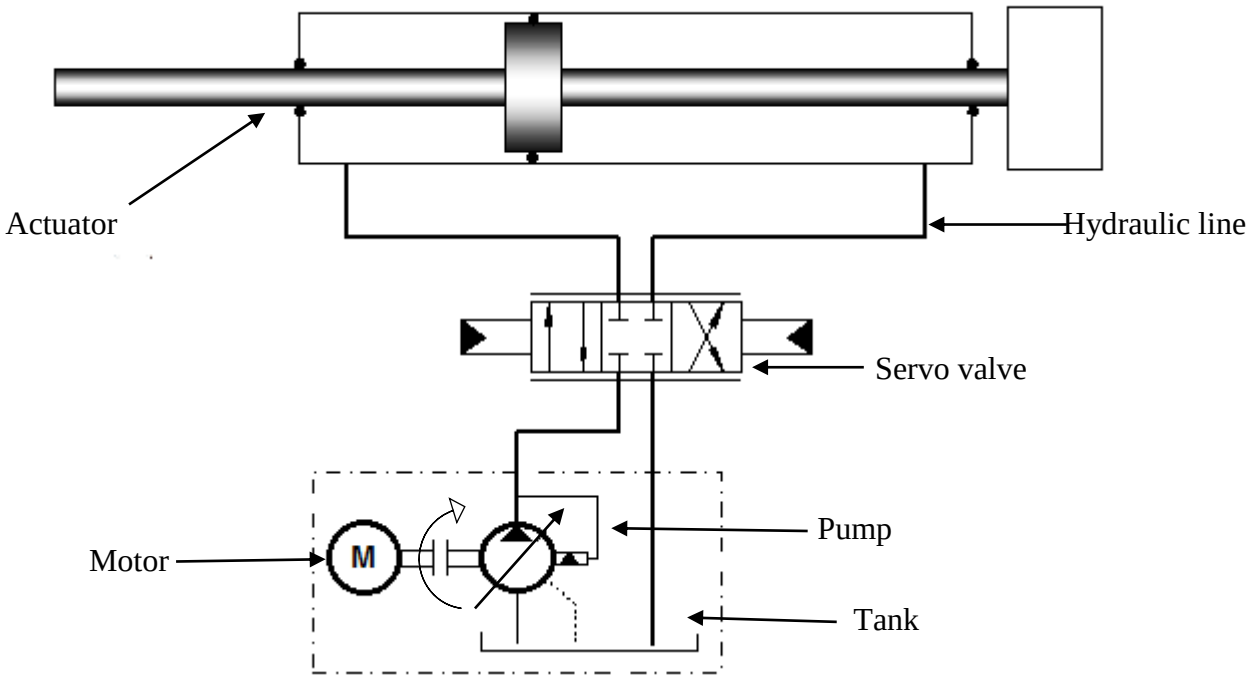

Figure 1-1: Typical valve controlled actuation system

As seen in Fig. 1-1, the motor rotates in one direction, driving the pump thus enabling the displacement of fluid. A constant volume of fluid is displaced by the pump. The displaced fluid flows through the servo valve. The servo valve is the control element in the system. It receives the control signal which determines the side of the actuator the fluid is ported. This determines the direction the actuator moves. Flow returns from the other side of the actuator to the tank.

Electrohydrostatic Actuation System

The EHA uses an AC variable speed electric motor to drive a fixed displacement pump and relies on local hydraulics for force transmission. They show promising applications in aerospace, manufacturing and robotics. The advantages of the EHA system includes high level of performance, high positioning accuracy, faster response (greater stiffness) due to compact positioning of the components and less leakage risks (Chinniah *et al.*, 2003). Figure 1-2 show typical electrohydrostatic actuation system.

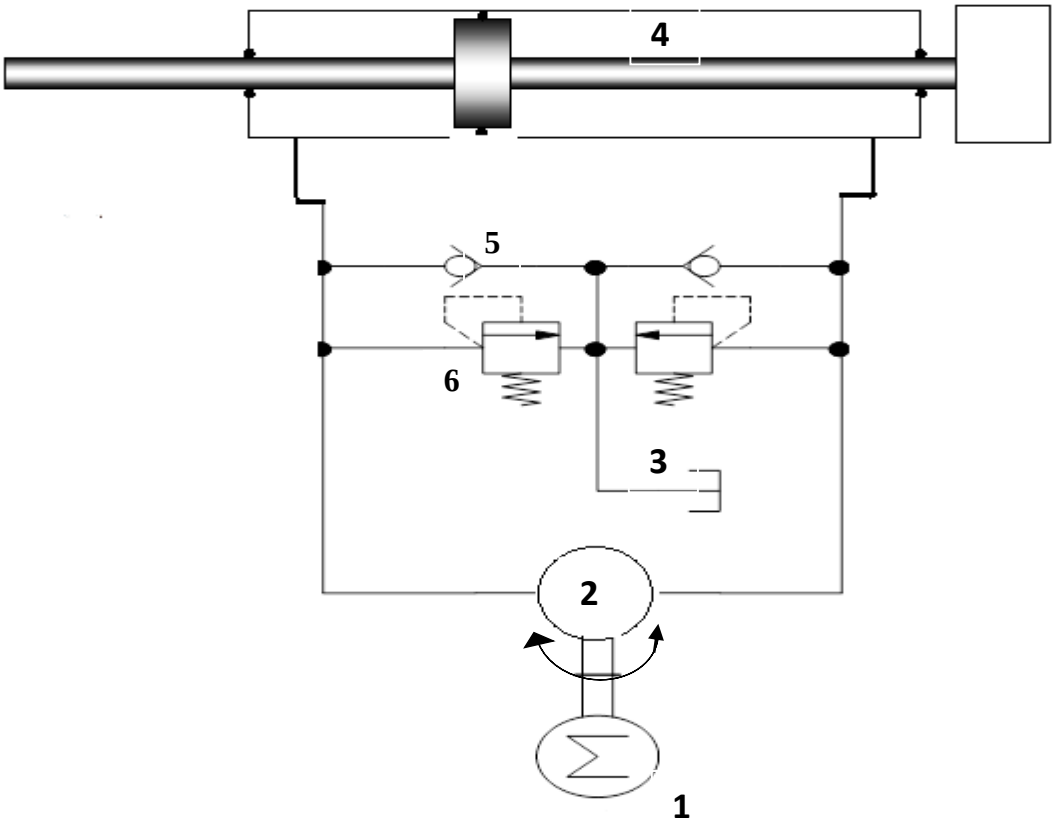

Figure 1-2: Typical electrohydrostatic actuation system

As shown in Fig. 1.2, the variable speed AC motor **1** receives the control signal and drives the fixed displacement pump **2**. The fixed displacement pump **2** pumps fluid from the accumulator **3.** The fluid flows from the pump to one side of the cylinder **4.** Check valve **5** is used for additional control purposes and pressure relief valve **6** is used for safety purposes. The fluid flows from the output port of the cylinder to the inlet of the pump and the process continues.

1.2 Hydraulic Failure

The performance of hydraulic systems is subject to various forms of failure. System failures occur due to the development of hydraulic faults. Table 1-1 illustrates the types of hydraulic failures and their causes. Examples include failures due to contamination, pressure pulsation, excessive friction, internal or external cylinder leakages (Skormin *et al.,* 1994; Zavarehi *et al.,* 1999; Zhang and Jiang, 2002; Chinniah, 2004). Detection of

faults at the early stages increases reliability, effectiveness, runtime and safety in systems. It also reduces the probability of a possible propagation of faults to other parts or components of the system, which may result to failure or possible threat to operators and the surrounding community.

Table 1-1: Common failures in hydraulic systems (Chinniah, 2004).

Feature	**Failure type**	**Failure characteristics**
Fluid pressure	Excessively high	Wear in components such as pumps/hose/tubing/pipe burst
	Excessively low	Cavitation, erosion and leaking seals
Fluid level	Low	Overheating and cessation of operations.
Flow forces in valves	High/ concentrated	Jet erosion of spool and valves.
Filtration	Clogged or blocked	Cavitation, filter burst, hose burst, back pressure.
Fluid / containment material	Incompatibility	Swelling of seals and corrosion of surfaces
Fluid borne contamination	High concentration of particles in fluid	Wear in sliding parts/ Blockage of ports
	Chemicals	Corrosion
Circuit	Excessive load	Cracks and breakage

One of the greatest concerns in fluid power systems is the leakage of hydraulic fluid. It has been documented (Leugner, 2010) that a hydraulic leak of one drop per second is equivalent to 420 gallons of oil loss in a year. It was estimated that over 100 million gallons of fluid could be saved every year in North America if hydraulic leakage from hydraulic machines and other lubricated equipment was eliminated. In Canada alone, over 12 million gallons of oil is wasted due to leakage. In economic terms the cost of this waste is overwhelming and staggering (Leugner, 2010). The economic effects of hydraulic system

leakage includes high oil consumption, premature machine component failure, inefficient machinery operation, environmental damage, accident liability, poor manufacturing quality and increased capital costs. Leakage is divided into two categories; 1) external leakage, which occurs when the hydraulic fluid leaks out of the hydraulic circuit, and 2) internal leakage, which occurs when fluid leaks into another part of the hydraulic circuit.

While external leakage can be easily inspected visually, internal leakage cannot be detected until the actuator seal is completely damaged and the actuator fails to respond (Goharrizi, 2011). As such the research for this thesis concentrates on internal leakage detection. Internal leakage has adverse effects on the entire performance and dynamics of the system.

Examples of such effect include,

1) Reduction in actuator velocity due to reduction of effective pressure arising from fluid loss (Chinniah, 2004).
2) Increase in operating temperatures (Thakur, 2011)
3) Inaccurate actuator positioning for controllers not robust to internal leakage system (Goharrizi and Sepehri, 2011)
4) Increase in the damping characteristic of the system (Goharrizi and Sepehri, 2011)
5) Decrease in Bode magnitude of the pressure signal over valve displacement, around the hydraulic natural frequency (Goharrizi and Sepehri, 2011).
6) Decrease in effective bulk modulus of the fluid, which arises due to air entrapment, consequently influencing the response of the EHA and may cause stability issues (Chinniah, 2004).

Internal leakage in the actuator is caused by wear of the seal that closes the gap between the piston and the cylinder wall. Piston seals have a crucial impact on system performance. They are a relatively soft, non-metallic ring captured in a groove, forming a sealed assembly, to block or separate fluid in reciprocating motion applications.

These seals, gradually breakdown over time and wear due to constant working, loading or impact. This leads to an undesirable flow of fluid through the seal across the hydraulic chambers, resulting to a distortion in the pressure build-up at the chambers. This may affect

the dynamics and performance of the system and if severe may lead to actuator failure. This slowly increasing flow rate continues until either the flow rate through the seal is so great that the seal is effectively non-existent, or the seal ultimately ruptures.

In common industrial practice, the seal is usually monitored or inspected at regular intervals for wears as leaks are inevitable. In order to perform these inspections, the machinery must be removed from active service, dismantled, inspected, reassembled, and then put back into active service. Seal replacement is done when necessary as it cannot be allowed to reach a non-functioning state undermining the system performance. The process of dismantling, inspecting and reassembling is very time consuming and can be extremely expensive to the operators of the machinery (May, 2012). A method for monitoring and diagnosing internal leakage faults, without necessarily dismantling and reassembling the hydraulic system is thus needful and considered in this thesis.

1.3 Literature Review

Hydraulic Fault

A fault is an undesired or abnormal occurrence which changes the behavior or dynamics of a system and often leads to system failure. Faults in hydraulic systems varies from fluid cavitations, component wear, fluid contamination, pipe leakage, swelling of seals, overheating, corrosion, breakage to external and internal leakage (Zavarehi *et al.,* 1999; Khan *et al.,* 2002; Chinniah *et al.,* 2003).

Internal leakage in the actuator affects the performance of hydraulic systems, and as such, is the focus of this thesis. This type of hydraulic fault has been rigorously studied by Goharrizi and Sepehri (2011) and the results showed that internal leakage in the actuator increases the damping characteristics of the system and reduces the bode magnitude of the pressure signal. Chinniah (2004) also showed that it leads to a reduction in actuator velocity due to reduction in effective pressure arising from fluid loss. It also leads to excessive increase in operating temperature (Thakur, 2011). All these parameters affect the dynamics and eventual performance of the system.

Actuator Internal Leakage Detection

Extensive research has been conducted in enhancing the detection of various faults in hydraulic systems (Preston *et al.,* 1996; Khan *et al*., 2002; Linaric, and Koroman, 2003; Garimella and Yao, 2005; Liu *et al.,* 2006; Murphy *et al.,* 2006; Wang and Syrmos, 2008; Ting-Tao *et al.,* 2009). However, less research work has been done in detecting faults due to actuator internal leakage despite its influence in predicting actuator seal health and system performance. Faults due to actuator internal leakage has been diagnosed using model and signal processing based schemes but with a certain level of success.

Model Based Method

An and Sepehri, (2005) employed a model based (extended Kalman filter (EKF)) scheme for internal leakage fault detection. The rationale behind this method is to linearize the system based on the most recent estimation of system states. By comparing the actual measurements and the estimated states, residual signals are obtained and then analyzed to establish the occurrence of faults. They showed that the EKF responded to faults promptly and reliably and as such is employable for internal leakage fault detection although the severity of the internal leakage detected was not quantified.

Chinniah, (2004) also employed the EKF for predicting changes in the damping coefficient of the actuator. Changes in the damping coefficient of the actuator can indicate wear in the seal or deterioration of the oil. A wear in the seal leads to internal leakage in the actuator. The disadvantages of this method are 1) a model of the system is required 2) It is hard to implement and 3) It is hard to tune.

Signal Processing Based Methods

Most signal processing based methods do not require a prior knowledge of the system model or fault type when employed for fault detection. Examples of signal processing based methods employed for internal leakage detection as documented in various literatures include wavelet transforms (Goharrizi and Sepehri, 2010; Thakur, 2011), Fast Fourier transforms (Goharrizi, 2011), Hilbert-Huang transforms (Goharrizi, 2011), Empirical Mode Decomposition (Goharrizi and Sepehri, 2011), autocorrelation and cross correlation of pressure signal (May, 2012).

Goharrizi and Sepehri, (2012) used Empirical Mode Decomposition and Hilbert Spectrum for internal leakage detection in the actuator. The pressure signal at one side of the actuator is broken into oscillatory functions called intrinsic mode functions (IMFs), and Hilbert transform is applied to each IMF to generate the instantaneous amplitude. It was reported that the root mean square of the instantaneous amplitude associated with the first IMF revealed a feature pattern that was effectively used to detect internal leakage. With this method, they were able to detect leakages as low as 0.124 L/min.

Goharrizi and Sepehri, (2010) also employed Fast Fourier transforms and Wavelet Transforms for detecting internal leakage in valve controlled hydraulic actuation system. They showed that by decomposing the original pressure signal, using either Wavelet or Fast Fourier transforms, the frequency component sensitive to internal leakage can be obtained. They then analyzed the root mean square of the processed pressure signal to predict internal leakage in the actuator for both open-loop and closed-loop systems. The results indicate that both approaches can detect internal leakage as low as 0.124 L/min without a need to explicitly include the model of the actuator or the leakage.

Also, it was found that for a Fourier Transform analysis to be effective, the signal must be stationary. On the contrary, wavelet transform has been shown to be more effective for signals with less degree of stationarity, though its effectiveness is dependent on the selection of the basis functions. Basis functions of wavelet transform are small waves located in different times. The basis functions are obtained using scaling, translation of a scaling function or wavelet functions. A poor selection of the basis function or mother wavelet may inversely degrade the performance (Huang and Hsieh, 1998).

There is a compromise between frequency and time resolutions when applying Fourier Transforms. A good realization in frequency domain may mean poor time representation or resolution and vice versa, so a compromise is always the solution. Also, Fourier Transforms has only frequency information represented while wavelet transforms have both frequency and time information represented. It is also important to note that the spectral information of wavelet transforms is not well localized in frequency rather it is

provided in terms of frequency bands. As such, the effectiveness of the wavelet transform is therefore dependent on variables such as the sampling frequency and the number of data points. A poor selection of any of these parameters may also lead to inaccuracy in measurements or poor performance (Umeh *et al.*, 2004).

By using autocorrelation and cross correlation of pressure signals May, (2012) detected internal leakages as low as 0.075 L/min (valve controlled actuation system). This is a significant milestone compared to leakages of 0.124 L/min detected using the Fourier transform, wavelet transform and Hilbert spectrum. He also found the cross correlation algorithm to be more effective in detecting actuator internal leakage compared to autocorrelation. He concluded that cross correlation of pressure signals performed well at wider range of window sizes and lag.

As recent technologies continually adopt hydraulic systems for heavy duty and risky tasks, the need for improving system performance and safety becomes essential. Consequently, advancing research work in the area of detecting much lower internal leakages becomes necessary. As such, in this thesis, internal leakages as low as 0.047 L/min are detected for the valve controlled actuation system and 0.98 L/min for the electrohydrostatic actuation system using fractal based approach, autocorrelation of pressure signal, cross correlation between pressure signals and cross correlation between piston displacement and control signal. The severity of leakage (0.047 L/min; valve controlled actuation system) detected in this research work has never been achieved in any literature. This result was obtained at different level of success for all algorithms used. Finally, the most preferred or effective method is recommended.

1.4 Research Objectives

Following the need to develop more effective methods for internal leakage detection, and the need to detect lower internal leakages. The proposed objectives of this research are to

1. validate that autocorrelation and cross correlation of pressure signals are employable for actuator internal leakage detection leakage in a valve controlled actuation system as well as electrohydrostatic actuation system,
2. employ the ratio of metric lengths concept for actuator internal leakage detection in valve controlled actuation system as well as electrohydrostatic actuation system,
3. employ cross correlation between piston displacement and control signal for actuator internal leakage detection in a valve controlled in a valve controlled actuation system as well as electrohydrostatic actuation system and,
4. investigate the responsiveness and effectiveness of these algorithms to the severity of internal leakage simulated.

1.5 Thesis Statement

Autocorrelation and cross correlation of pressure signals has been used to diagnose internal leakage in valve controlled hydraulic actuation system. This thesis will determine if it can also be employed for internal leakage diagnosis in electrohydrostatic actuation systems. This thesis will also try to investigate if cross correlation of piston displacement and control signal is employable for internal leakage diagnosis in valve controlled actuation systems as well as electrohydrostatic actuation systems. Also, this thesis will investigate if the ratio of the metric lengths of the same time sequence is employable for internal leakage diagnosis. Finally, for all methods considered, the minimum leakage detectable and conditions for high performance will be determined.

1.6 Thesis Outline

The outline of this thesis is as follows: Chapter 2 describes the valve controlled hydraulic actuation system and the experimental setup. Chapter 3 discusses the electrohydrostatic actuation system and the experimental setup, Chapter 4 describes the methodologies employed in preparing the signals and also for detecting internal leakage. Chapter 5 discusses the results associated with the valve controlled actuation system. Chapter 6 discusses the results associated with the electrohydrostatic actuation system and Chapter 7 provides a general summary of this research work, future work and its contributions to the body of knowledge.

CHAPTER 2

VALVE CONTROLLED ACTUATION SYSTEM

2 VALVE CONTROLLED ACTUATION SYSTEM

2.1 Description of the system

Valve controlled actuation systems uses flapper nozzles or jet pipe devices to position the servo valve. It provides the final control in a closed-loop valve controlled hydraulic actuation system by regulating the rate and direction of the hydraulic fluid flow to the actuator. The servo valve ports the fluid delivered by the hydraulic motor and pump system to the appropriate side of the actuator. Servo valves are used when it is essential to establish an accurate position control. An example of such is the control of a primary flight control surface. This position control is achieved using a closed-loop system comprising of a controller, servo valve, and feedback system.

Figure 2-1 illustrates the operating principle of a valve controlled hydraulic actuation system. The servo valve **1** receives a control signal from the controller **2** (High speed computer). It converts the control signal to a physical movement of the internal spool thereby enabling the porting of hydraulic fluids to the desired chamber **3 or 4** and the exhaust fluid returns to the tank **5**. The polarity of the control signal determines the direction of the spool and its amplitude determines how far the spools **7** (Spools alternately block and open channels in the hydraulic system) will move. The amplitude of the control signal reduces to zero at the end of each execution. This reduction brings the spool to the null or no flow position (Default position of the spools). The part labeled **7** is the point where the internal leakage is simulated between the hydraulic chambers. A needle valve **8** in line with a ball valve **9** is adjusted gradually to induce the leak. The rate of adjustment determines the magnitude of leak introduced. The magnitude of leak introduced is read by the flow meter **10**. Pressure sensors are used to measure the chamber pressures and encoders are used to read the actuator position.

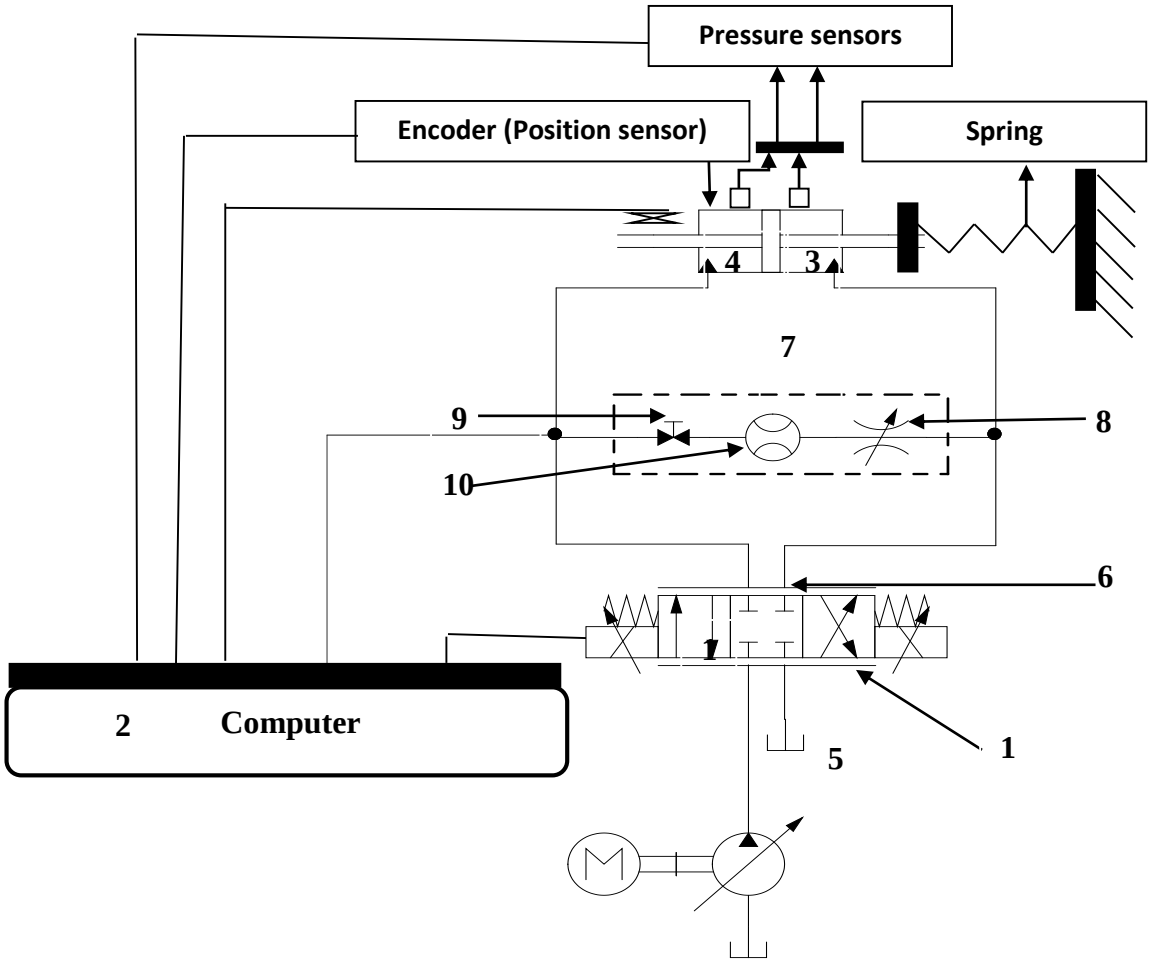

Figure 2-1: Schematics of valve controlled actuation system

2.2 Experimental set-up

The experimental setup as shown in Fig. 2-2 consists of a power supply unit, hydraulic pump, actuator, DAQ card, servo valve and a high speed computer. The actuator system is a double rod type having a 38.1-mm bore, 25.4-mm rods, and a 610-mm stroke. It is powered by a motor-driven hydraulic pump which operates at a nominal pressure of 2500 psi (17.2 MPa) and controlled by Moog D765 servo valve which has a flow capacity of 34 L/min at 3045 psi (21 MPa) input pressure.

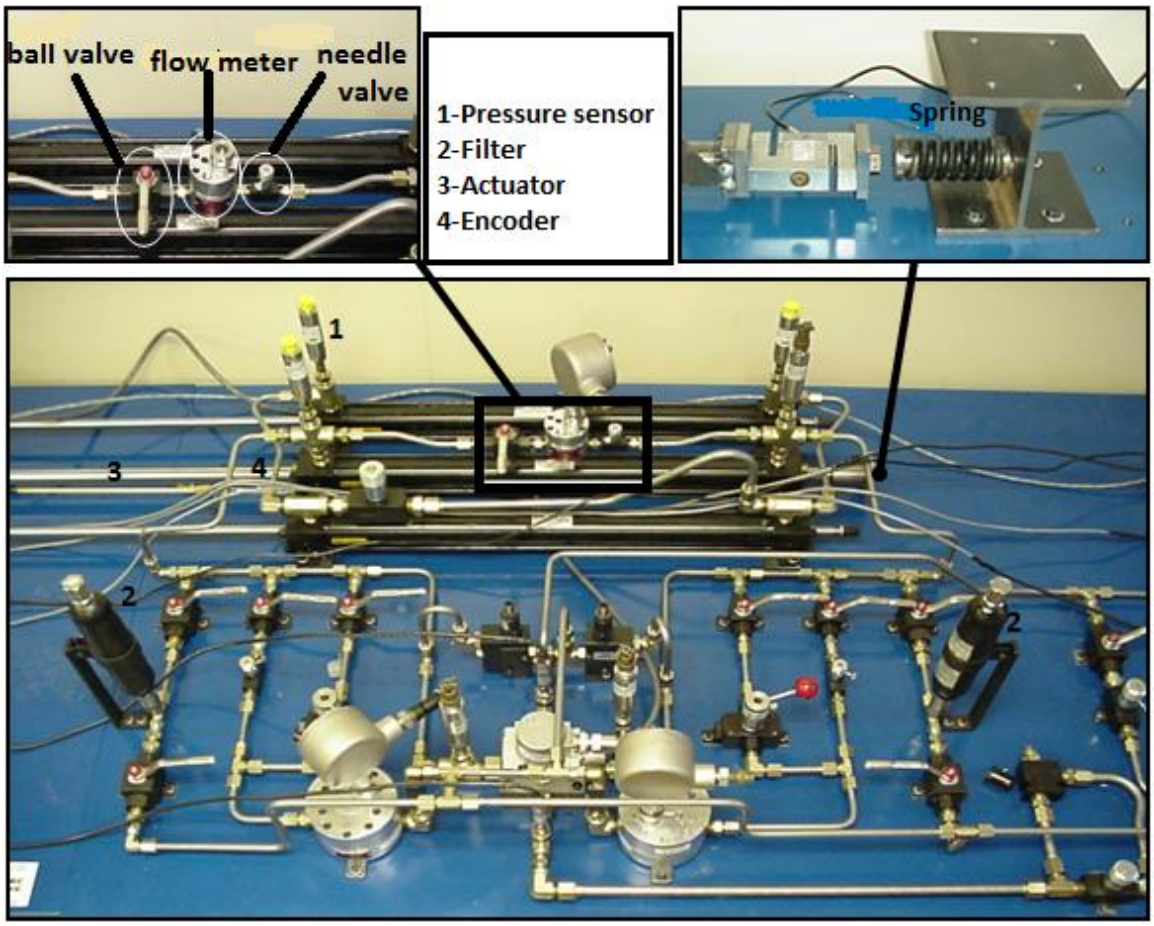

Figure 2-2: Typical experimental setup for valve controlled actuation system

The Moog D765 servo valve receives analog control signals from a high-speed computer furnished with a data acquisition board (DAQ board). It controls fluid pumped by the pump from the tank to the appropriate port of the actuator resulting to a displacement of the actuator. The actuator's displacement is read by a rotary optical encoder and sent to the DAQ board through a Metra byte M5312 quadrature incremental encoder card Keithley with an accuracy of 0.03 mm linear displacement. Hydraulic fluid is bypassed across the actuator piston. The adjustment of a needle valve connecting the two chambers allows for the experimental simulation of the internal leakage fault. The size of the simulated leak is adjusted by changing the orifice size of a needle valve that is in line with the ball valve. Changing the orifice size of the needle valve modifies the size of the simulated leak. The flow through the needle valve is monitored by a positive displacement flow meter (JVA-

20KL by AW) having a range from 0.047-7.57 liters per minute (L/min) with ±0.5% accuracy.

Hydraulic pumps are used to convert mechanical power into hydraulic energy. The hydraulic pump is driven by a motor and has a nominal operating pressure of 2500 psi (17.2 MPa). It is capable of pushing large amounts of oil through hydraulic cylinder.

The position of the actuator is measured using an encoder. The encoder is interfaced such that the actuator position is available to the PC. The D765 control valve, by means of integrated electronics allows the analog outputs of the DAS16F board, operating as a voltage source to drive the control valve.

Pressure sensors are used to capture the pressure readings. They are situated at the hydraulic chambers and connected to the DAQ card. The transducer has a range of 3000 Psig, an input supply of 5-20 VDC and an output supply of 0-5 VDC. The flow meter (20 gpm) is used to measure the flow rate of the simulated internal leakage. The flow meter is installed between the needle and throttle valve used for artificially introducing the leakage to the system.

DAQ, known as data acquisition, is the process of sampling signals that measure real physical conditions and converting the resulting samples into digital numeric values that can be analyzed by a PC. The components of data acquisition systems include:

1) Sensors that convert physical variables to signals (electrical).
2) Signal conditioning system that enhances the conversion of the sensor outputs to digital values.
3) Analog-to-digital converters, which converts the output of the signal conditioning system to digital values.

These components are DAS16F input–output board, 2-axis M5312 quadrature incremental encoder card, 21 MPa (3000 psi) pressure transducers, a 22 kN (5000 lb) load cell and 76 L/min positive displacement flow meters (20 gpm). The hydraulic actuator is interfaced to

the PC using the DAS16F input–output board and the encoder card. The DAS16F boards are used to digitize the outputs of all analog readings obtained from the following sensors, pressure transducers, load cell and positive displacement flow meters.

2.3 System Model

Figure 2-3 shows schematics of typical valve controlled actuator used in deriving the governing equations.

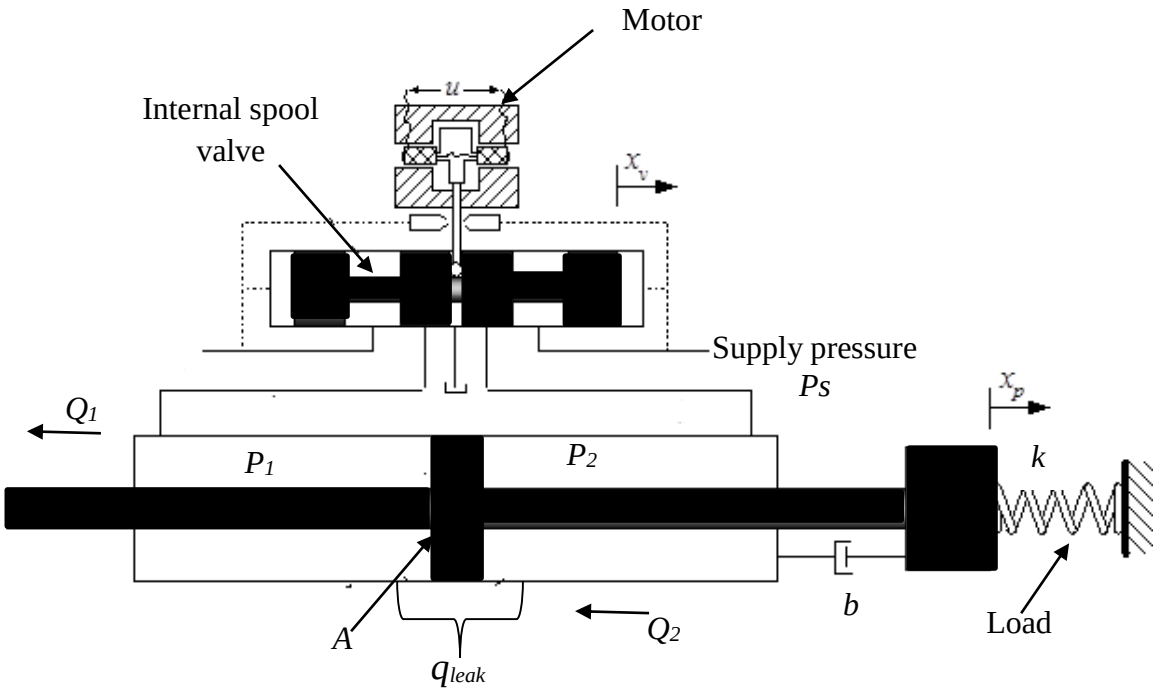

Figure 2-3: Schematics of typical valve controlled actuation system

The equations that describe the dynamics between control valve input u and the piston position x_p can be formed as in (Merritt, 1967) or (Goharrizi and Sepehri, 2010).

$$\dot{x}_p = v_p$$

$$\dot{x}_v = v_v$$

$$\dot{v}_p = \frac{1}{m}(AP_1 - AP_2 - dv_p)$$

$$P_1 = \frac{\beta}{(V+Ax_p)}\left(Q_1 - Q_l - Av_p\right) \qquad (2\text{-}1)$$

$$P_2 = \frac{\beta}{(V-Ax_p)}\left(-Q_2 + Q_l + Av_p\right)$$

$$\dot{v}_v = -w_v^2 x_v - 2\xi w_v v_v + k_v w_v^2 u)$$

Referring to Equation 2-1, the system states are actuator position x_p, actuator velocity v_p, line pressures P_1 and P_2, valve spool displacement and velocity $\{x_v, v_v\}$. Parameters m and d are the mass of the load and the effective viscous damping of the actuator, respectively. A is the annulus area of the actuator, β refers to the effective bulk modulus of the hydraulic fluid and V is the volume of the hydraulic fluid contained on both sides of the actuator when it is centered. Q_l (q_{leak}) refers to the flow rate of the internal leakage. The valve spool dynamics are expressed as a second-order lag; where k_v is the valve spool position gain and w_v and ξ represent the servo valve natural frequency and damping ratio, respectively. For a valve with a critically-lapped spool and having matched and symmetrical orifices, flows Q_1 and Q_2 through the valve follow the turbulent orifice equation. The nonlinear governing equations can be written in the following form (Karpenko and Sepehri, 2010).

$$Q_1 = K_V w x_V \sqrt{\frac{P_S}{2} + \text{sgn}(x_V)(\frac{P_S}{2} - P_1)}$$
$$Q_2 = K_V w x_V \sqrt{\frac{P_S}{2} + \text{sgn}(x_V)(P_2 - \frac{P_S}{2})} \quad (2\text{-}2)$$

Where the supply pressure is denoted by P_s, K_v is the valve flow gain, and w is the area gradient. The function sgn(x) is the sign function and defined as:

$$sgn(x) = \begin{cases} +1 & x > 0 \\ 0 & x = 0 \\ -1 & x < 0 \end{cases} \quad (2\text{-}3)$$

Leakage is a kind of nonideality that cannot be modeled exactly (Garimella and Yao, 2005). Here, if the actuator internal leakage is assumed to be turbulent, the following relationship can be written (Karpenko and Sepehri, 2010).

$$Q_l = k_l \sqrt{|P_1 - P_2|}\,\text{sgn}(P_1 - P_2) \quad (2\text{-}4)$$

Alternatively, if the leak is considered laminar, the following equation holds as in (Merritt, 1967).

$$Q_l = k_l (P_1 - P_2) \quad (2\text{-}5)$$

where Q_l is the leakage flow rate, k_l is the leakage coefficients whose values depend on the magnitude of the leakage. Q_l is zero for an actuator under normal operating condition. However, when a leak occurs due to wearing of the hydraulic seals, the dynamic performance of the system is affected. This is because the entire flow is no longer available to move the actuator against the load.

Furthermore, for an equal area actuator driven by a symmetrical and matched valve, the pressure in one cylinder half rises above $P_s/2$ while the pressure in other cylinder half

decreases below $P_s/2$ by roughly the same amount. Thus, for an extending stroke, the individual cylinder pressures are $P_1 \approx 1/2(P_s+P_L)$ and $P_2 \approx 1/2(P_s-P_L)$. Where, $P_L=P_1-P_2$ is the load pressure. Due to the relationship between P_1 and P_2, $K_{1f} \approx K_{2f} = K_f$ and $K_{1p} \approx K_{2p} = K_p$ (Merritt, 1967; Karpenko and Sepehri, 2005). The transfer functions relating pressures ΔP_1 and ΔP_2 to spool valve displacement, Δx_v, can now be found as:

$$\frac{\Delta P_1(s)}{\Delta X_v(s)} = \frac{0.5K_f(ms+d)\omega_h^2/A^2}{s^2+2\zeta_h\omega_h s+\omega_h^2} \tag{2-6}$$

$$\frac{\Delta P_1(s)}{\Delta X_v(s)} = \frac{0.5K_f(ms+d)\omega_h^2/A^2}{s^2+2\zeta_h\omega_h s+\omega_h^2} \tag{2-7}$$

Where $\omega_h = \sqrt{\frac{2\beta A^2}{mV}}$ is the hydraulic natural frequency, $\zeta_h = \frac{dV\omega_h}{4\beta A^2} + \frac{m(K_l+0.5K_p)\omega_h}{2A^2}$ is the hydraulic damping and $K_l = \frac{K_i}{\sqrt{|P_{10}-P_{20}|}}$ For normal operating conditions, $K_i = 0$.

For the actuator with internal leakage $K_i = 5.83\times10^{-8}\text{m}^3/\sqrt{\text{Pa}}.\text{s}$ is chosen. The values of all parameters used for this section can be found in Table 2-1.

Table 2-1: Parameters for valve controlled hydraulic actuation system

Parameter	Symbol	Value
Supply pressure	P_s	17.2 MPa
Combined mass of piston and rod	M	12.3 Kg
Viscous damping coefficient	D	250 Ns/m
Actuator stroke	L	0.6 m
Piston area	A	633 mm2
Volume of fluid in either side of actuator	V	234 cm3
Valve orifice area gradient	ω	20.75 mm2/mm
Valve spool position gain	k_v	0.0406 mm/V
Valve flow gain	K_v	0.0292 $m^{3/2}/kg^{1/2}$
Valve natural frequency	w_v	150 Hz
Valve damping ratio	ε	0.7
Fluid bulk modulus	β	689 MPa

CHAPTER 3

ELECTROHYDROSTATIC ACTUATION SYSTEM

3 ELECTROHYDROSTATIC ACTUATION SYSTEM

3.1 Description of the System

Electrohydrostatic actuation systems (EHA) work base on hydrostatic transmission. The flow of hydraulic oil into the cylinder is made possible with the help of an electric motor connected to the pump. The electric motor drives the pump and the pump controls the flow. In hydrostatic transmission, the returning fluid from the actuator (motor or cylinder) is returned directly to the pump inlet as compared to valve controlled actuation system where it returns to the tank. One advantage of the EHA system is high efficiency due to the absence of valves (Chinniah, 2004).

Hydrostatic transmissions have been used as options to valve controlled actuation systems when the need for position accuracy is not very strict. (Thakur, 2011). Figure 3-1 illustrates a typical schematic of an electrohydrostatic system.

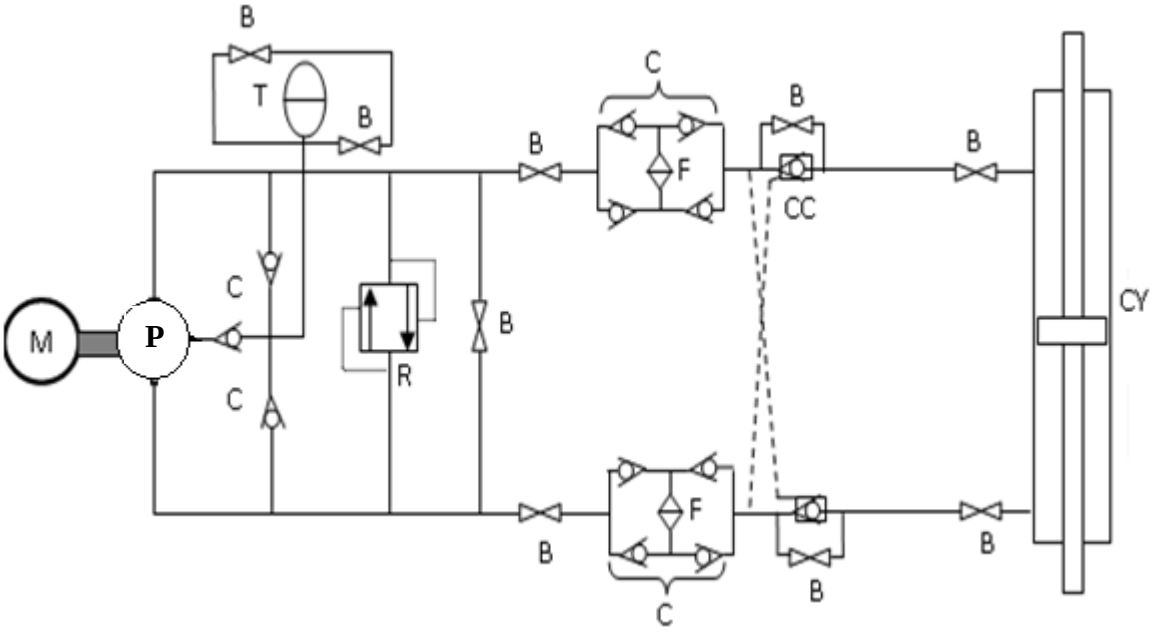

Figure 3-1: Typical schematics of an electrohydrostatics actuation system (EHA).

As shown in Fig. 3-1, the electric motor **M** rotates clockwise or counterclockwise depending on the signal it receives. It drives the pump **P** in either direction, leading to pressure build up at the port connected to the accumulator. The rise in pressure deactivates

the check valve **C** enabling the flow of fluid from the accumulator **T** into the pump**.** The fluid flows to one side of the hydraulic actuator **CY** through filter **F**, check valves **C**, pilot operated valves **CC** and gate valves **B** installed on the lines. The fluid returns from the other side of the hydraulic actuator **CY.** The returning fluid flows through the same set of devices but on the other line back to the pump inlet. The installation of filters, pilot operated valves, check valves and gate valves on both sides of the lines allow the flow of oil to enter and exit the filters and to be circulated throughout the rest of the system. Filters help to remove dirt and impurities from the fluid which aids in maintaining a high level of performance and efficiency. Check and pilot operated valves are used to control the direction of flow. Gate valves **B** have been installed in several part of the circuit to shut-off or to permit flow.

The pump flow rate and cylinder speed is controlled by the motor speed which is dependent on the input control signal. When a flowing hydraulic fluid encounters a resistance such as a hydraulic piston, its fluid pressure increases, resulting to a pressure difference in the piston chamber. This pressure difference in the piston chambers results in exertion of force and consequently movement of the piston.

3.2 Experimental Setup

Figure 3.2 shows the experimental test rig (EHA) used for performing all tests. The components include the electric motor, accumulator, pump, pressure sensors, position sensors, cross over relief valve, double rod acting cylinder, high speed computer, DAQ system and spring load.

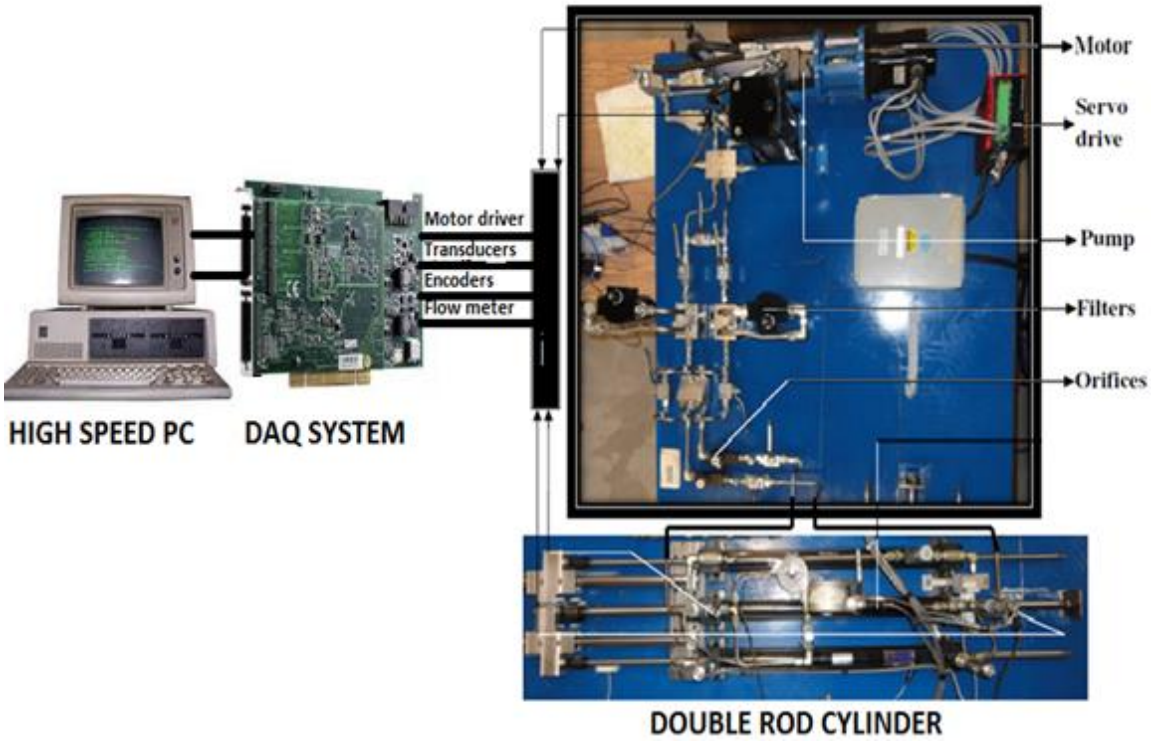

Figure 3-2: Experimental set-up (EHA)

Fixed Displacement Pump and Accumulator

The fixed displacement pump is a bi-directional pump. It is able to pump fluid in both counterclockwise and clockwise directions depending on the direction of rotation of the motor coupled to it. The direction of rotation of the motor depends on the input voltage. The pump and the motor are coupled by a flexible Oldham coupler which causes them to rotate together. It is equipped with inlet and outlet holes which let the flow of the oil back and forth depending on whether the rotor is moving in a clockwise or counter-clockwise direction. The maximum pressure and speed attainable by the pump are 5000 psi and 400 rpm respectively. It has a fixed displacement of 4.9 cm^3/rev and the piston's position accuracy is dependent on the pump volumetric displacement. It is connected to the accumulator which depends on the pressure generated by the pump to ensure oil supply to the entire system is maintained. The input-output ports are connected to the actuator ports through steel tubing and the case drain line is connected to the inner accumulator circuit through a check valve. An accumulator is a device that stores the energy (Potential energy) of an incompressible fluid subjected under pressure. A bladder type accumulator which has

an elastic barrier between the oil and the gas is used in the EHA. The accumulator is also used to prevent oil cavitations by pressurizing the forward and return lines to its preset pressure. It also prevents the introduction of air in the system and serves as a source of oil for the system (Habibi and Goldenburg, 2000).

Servo Motor and Drive

The electrical motor used for driving the EHA pump in this test rig is the M-4650**.** It receives its signal from the servo drive in terms of amplified voltage and it requires a minimum of 220V AC to operate. The M-4650 is a brushless, permanent magnet rotary servo motor which uses a sealed and a high precision encoder to ensure reliable results and operation. It is connected to an SSt-6000 RCX servo drive and its stators are mechanically locked and chemically bonded to eliminate slippage.

The SSt-6000-RCX servo drive is equipped with electrical operational features which aids the encoder positioning. It is equipped with a controller port which receives control signal from the DAQ via a wire. This wire is divided into two cables, which are the analog and the encoder cables. The analog output port is responsible for sending the voltage signal which emanates from the program. The servo driver receives the voltage signal and appropriately runs the motor. The encoder port describes the position of the motor rotation in terms of 20,000 quad counts per revolution of the rotor.

Data Acquisition and Sensors

The data acquisition system used is the Quanser Q8. It is a versatile and powerful tool for measuring and controlling an extensive range of input and output signals. This device allows for the flexibility to connect up to eight I/O analog ports, eight encoders and thirty two digital I/O ports within one terminal board. It serves as the major interface between the computer, servo drive and sensors. The specifications of the Quanser Q8 terminal board includes high speed sampling up to 350 kHz, simultaneous sampling of A/D, high resolution - 14-bit inputs, easy synchronization of multiple Q8 boards, extensive I/O and Pulse Width Modulation (PWM) outputs on-board.

The experimental test rig has five sensors consisting of one position sensor and four pressure sensors. The pressure sensors are installed at four different locations; two are connected to the inlet and outlet of the pump flow, and the other two are installed on each side of the cylinder to measure pressure changes. The maximum limit of each pressure sensor is 3000 psi. The position sensor is situated to encode the movement of the hydraulic actuator.

3.3 System Model

Figure 3-4 shows the simplified schematic for the experimental electrohydrostatic actuation test setup.

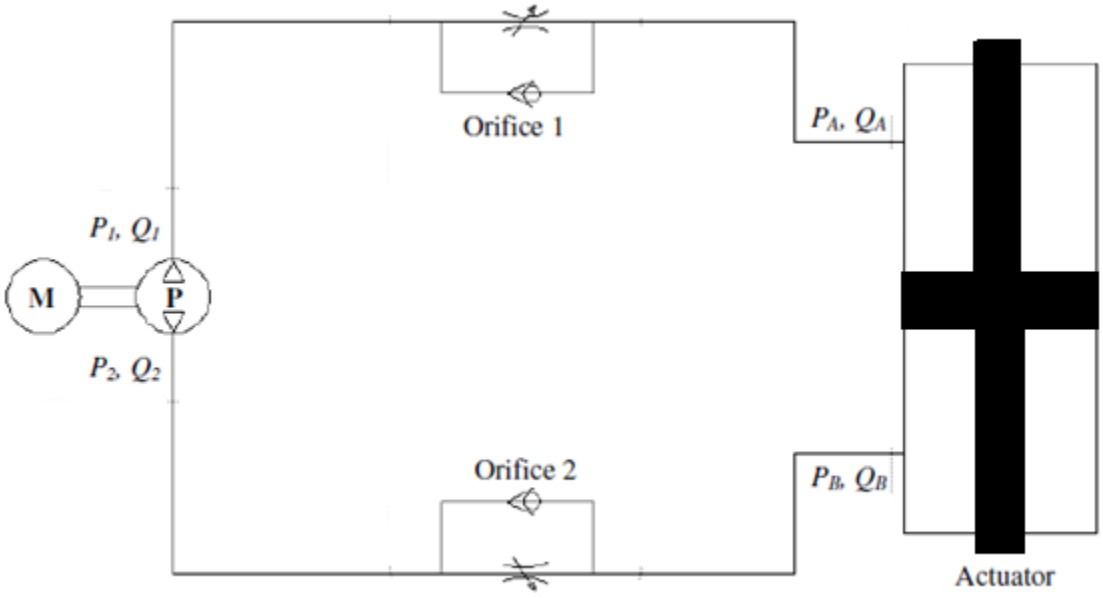

Figure 3-3: Typical schematics of the EHA system

The following mathematical equations represent the flow from the pump **P** with respect to a fixed displacement and the rotation of the motor **M** with respect to the load pressure on the motor shaft (Thakur, 2011)

$$V = k_p(\omega_d - \omega) + K_i i \tag{3-1}$$

$$i = i + h(\omega_d - \omega) \tag{3-2}$$

$$\frac{di}{dt} = \frac{V}{L_c} - \frac{R_c}{L_c} i - \frac{C_e}{L_c} \omega \tag{3-3}$$

$$\frac{d\omega}{dt} = \frac{C_m}{J_M} i - \frac{B_M}{J_M} \omega - \frac{q_b P_f}{2\pi J_M} \tag{3-4}$$

$$P_f = P_1 - P_2 \tag{3-5}$$

$$Q_1 = Q_2 = \frac{q_b}{2\pi} \omega \tag{3-6}$$

Equation 3-1 and 3-2 represents the proportional and integral control for a closed-loop motor. The current produced by the operation of the electric motor is expressed with respect to time in differential form as $\frac{di}{dt}$, similarly, $\frac{dw}{dt}$ reflects the rotation of the electric motor. V is the input voltage for the electric motor. Inductance and resistance of the motor is shown as L_c and R_c respectively; C_e is denoted as back electromotive force while C_m is the electromagnetism torque constant. The sum of the damping coefficient and the moment of inertia of the motor and pump is expressed as B_m and J_m respectively while P_f defines the load pressure on the pump. When hydraulic fluid from the accumulator runs into the pump and flows through any of the output ports, it is mentioned as Q_1 or Q_2 (equation 3-6), q_b

represents the fixed displacement of fluid from the pump while the rotation of the motor designated as *w*.

The EHA is equipped with two orifices. Each orifice allows for free flow in one direction and variable controlled flow in the opposite direction. The flow from the orifice has a huge impact on the pressure drop at the location P_A, P_B. The area of a cross-section of the orifice is less than the area of the line which allows for the flow of hydraulic fluid. This orifice feature is modeled with the help of the equations presented below by retaining all non-linear behaviors of the orifice in the equations.

$$A_{line} = {d_{line}}^2 \tag{3-7}$$

$$A_{ori} = kA_{line} \tag{3-8}$$

$$Q_A = C_{dori}\sqrt{\frac{2}{\rho}}\, A_{line}\sqrt{(P_1 - P_A)}\,;(P_1 > P_A) \tag{3-9}$$

$$Q_A = -C_{dori}\sqrt{\frac{2}{\rho}}\, A_{ori}\sqrt{(P_A - P_1)}\,;(P_1 \leq P_A) \tag{3-10}$$

$$Q_B = C_{dori}\sqrt{\frac{2}{\rho}}\, A_{line}\sqrt{(P_B - P_2)}\,;(P_B > P_2) \tag{3-11}$$

$$Q_B = -C_{dori}\sqrt{\frac{2}{\rho}}\, A_{ori}\sqrt{(P_2 - P_B)}\,;(P_2 \leq P_B) \tag{3-12}$$

where d_{line} and A_{line} represents the diameter and area of the line from which the fluid is flowing respectively. k varies depending on the ratio of the opening area for orifice A_{ori}. Q_A and Q_B denotes flow of fluid from the orifice in both directions of the test rig with C_{dori} expressing the drag coefficient of the orifice. ρ denote fluid density, P_A and P_B denotes pressure at both ends of the cylinder while P_1 and P_2 represents the inlet and outlet pressure at the pump (Thakur, 2011).

The double-acting hydraulic cylinder converts hydraulic energy into mechanical energy in the form of translational motion. The energy through hydraulic chambers helps in converting hydraulic energy into mechanical energy. Hydraulic fluid pumped under

pressure into one of the two cylinder chambers causes pressure difference between the chambers and forces the piston to move and exert force on the double-acting hydraulic cylinder rod.

Equations defining the pressures at the inlet and outlet of the pump and cylinders, displacement, velocity and acceleration of the rod, are presented with the help of state space equations

$$\frac{dx}{dt} = v \tag{3-13}$$

$$\frac{dv}{dt} = a \tag{3-14}$$

$$a = \frac{1}{M_{eq}}(P_A A_A - P_B A_B - F_l) \tag{3-15}$$

$$\frac{dP_1}{dt} = \frac{K_{oil}}{V_1}(Q_1 - Q_A) \tag{3-16}$$

$$\frac{dP_2}{dt} = \frac{K_{oil}}{V_2}(Q_B - Q_1) \tag{3-17}$$

$$\frac{dP_A}{dt} = \frac{K_{oil}}{V_A}(Q_A - A_A v) \tag{3-18}$$

$$\frac{dP_B}{dt} = \frac{K_{oil}}{V_B}(-Q_B + A_B v) \tag{3-19}$$

where $\frac{dx}{dt}$ represents the velocity of the cylinder rod and *x* is the displacement of the rod with maximum displacement of 60 cm. $\frac{dv}{dt}$ stands for the acceleration of the rod which further includes the total mass of the system M_{eq}. The pressure calculations of both

chambers (P_A P_B) are directly related to their areas A_A and A_B .The volume of both sides of the cylinder is represented as V_1, V_2, V_A and. V_B. The load at the actuator is shown as F_l. However, it is set to zero in this analysis (Thakur, 2011). The values of all parameters used for this section can be found in Table 3-1.

Table 3-1: General specifications of the EHA

Parameter	Symbol	Value
Pre load force at piston	F_{pr}	25 N
Combined mass of piston and rod	M_{eq}	12.3 kg
Viscous damping coefficient	F_v	300 Ns/m
Actuator stroke	L	0.6 m
Piston area	A_A, A_B	633 mm^2
Volume of fluid in either side of actuator	V	234 mm^2
Sum of damping coefficient of motor and pump	B_M	0.0004855N/m(rad/s)
Velocity threshold	V_{th}	0.01 m/s
Displacement of the pump	q_b	$4.9x10^{-6}$ m^3/rev
Fluid bulk modulus	β	689 MPa
Resistance of motor	R_c	0.73
Inductance of motor	L_c	3.5510^{-3} Henry
Back electromotive force constant	C_e	0.6963 V/(rad/s)
Sum of moment of inertia of motor and pump	J_m	0.000874 Kg m^2
Electromagnetism torque constant	C_m	0.6963 Nm/A
Fluid Density	ρ	847 Kg/m^3
Drag coefficient of orifice	C_d	0.92
Area of line	A_{line}	3.85mm^2
Diameter of line	d_{line}	7 mm

CHAPTER 4

METHODOLOGY

4 METHODOLOGY

This chapter describes signal processing based methodologies adopted in analyzing the signals and consequently detecting internal leakage faults in the valve controlled hydraulic actuator as well as the electrohydrostatic actuation system (EHA). Signal processing based approaches adopted for both systems include autocorrelation, cross correlation and ratio of metric lengths.

4.1 Autocorrelation

Autocorrelation is referred to as the correlation of a time series with its own past and future values. In other words, it is the cross-correlation of a signal with itself. The signal is shifted in time (past and future values) by an amount referred to as lag and then compared. A lag value is the distance between sets of data being compared. A lag of 20 for example would compare data points separated by 20 data points. Assuming N is the total number of data points being considered, the lag can vary from 1 to N -1.

Autocorrelation can be used to detect singularity and repeating patterns within a signal. Examples include a periodic signal obscured by noise (Bowerman and O'Connell, 1979; Box *et al.*, 1994). It can also be used for predictions. An autocorrelated time series is predictable probabilistically, because future values depend on present and past values. Autocorrelation coefficient is usually normalized; it ranges from -1 to 1. If a signal is highly correlated then the result of evaluating it using autocorrelation will be very high. A high autocorrelation would mean a value close or equal to 1. If however the signal is random, the value will be closer to zero. If the result is negative then this means that there is a negative correlation between the data points.

Assuming N is the size of the equally spaced data set for a time series analysis $X(t)$, then

$$ac_\tau = \frac{\sum_{j=1}^{N-\tau}(x_j - \bar{x})(x_{j+\tau} - \bar{x})}{\sum_{j=1}^{N}(x_j - \bar{x})^2} \qquad (4.1)$$

Where x_j refers to the j^{th} element from the data set. $\bar{x}$ is the mean value of the data set. τ , the lag term which determines how far apart the data points which are being compared are. The numerator of equation (4.1) is same as the covariance of x and x with a delay τ while the denominator is the variance of x .The autocorrelation function is applied to the pressure signal, producing a single coefficient for each pressure window. These values are then plotted as a time series view to show how the autocorrelation coefficients change over the course of an experiment (May, 2012).

4.2 Cross Correlation

Cross correlation can be used to estimate the degree to which two time series are correlated. It can also be used to measure the similarity of two signals or time series. A time lag is usually applied to one of the signal before analysis. Cross correlation is similar to autocorrelation in that, autocorrelation can be described as the cross correlation of a signal with itself, cross correlation function compares a block of data from one signal with a time shifted version of another signal. This shift is referred to as lag. It is presently applied in pattern recognition, template matching, neurophysiology, image processing, electron tomographic averaging, and single particle analysis.

Cross correlation coefficients are normalized in such a way that their values lie between −1 and +1. This is because the similarity between two high amplitude signals cannot be obtained by merely comparing the amplitude of their cross correlation. The correlation of two high amplitude signals will likely produce big numbers. A normalized version is thus adopted or preferred. The cross correlation of a pair of jointly wide sense stationary process can be determined by averaging the product of samples measured from one time series and samples measured from another time series. Finally, at all step subtracting the mean and dividing by the standard deviation.

Let X_i and Y_i represent a pair of time series that are jointly wide sense stationary (Section 4.6). The cross-correlation function of the series is given as

$$cc_\tau = \left(\frac{1}{N}\right)\frac{\sum_{j=1}^{N-\tau}\left(y_j - \bar{y}\right)\left(x_{j+\tau} - \bar{x}\right)}{\sqrt{\left(\sigma_x^2\right)\left(\sigma_y^2\right)}} \qquad (4.2)$$

Where *N* is the size of the data set or window size of the time series x_j and y_j, j refer to j^{th} element from the two data sets; $\bar{x}$ and $\bar{y}$ are the mean values of the data sets, τ (lag term) is an integer value for a time series analysis which determines how far apart the data points which are being compared are. The numerator of equation (4.2) is equivalent to the covariance of y and x with a delay τ while the denominator is the product of the standard deviation of x and y.The cross correlation function requires that the N data points be equally spaced in time.

From the function, the correlation coefficients are obtained. Coefficient values close to one indicate the two input signals are highly correlated and suggests a relationship between the two signals. This implies that as one increases, the other also increases with a similar rate. Coefficients close to minus one indicate that there is a relationship between the two signals, however they are inversely correlated meaning that as one signal increases, the other signal decreases. Values near zero suggest that there is little or no correlation between the two signals. By increasing the lag value, the function compares windows from the two data sets at increasingly further intervals. This may give rise to highly correlated coefficients depending on the nature of the signal or data set but a lag value of zero will give rise to a peak.

4.3 Ratio of Metric Lengths Concept

4.3.1 Introduction

A ratio of metric lengths of the same time sequence (also known as fractal number by some researchers) have been employed in several literatures for fault detection. This algorithm measures or describes the degree of irregularity and complexity in a signal and represents it with a number.

This technique has been recommended as an option for analyzing time-varying signals where most methods have not achieved the desired efficiency, precision, speed or accuracy (Huang and Hsieh, 2000). It has also been employed for quantizing chaotic behaviors of high impedance faults (Mamishev *et al.*, 1996)

Mamishev et al. (1996) employed the ratio of metric lengths of the same time sequence for characterizing chaotic behavior of high impedance faults. Impedance faults represent one of the most difficult protection problems in power distribution systems today. This is because the effective impedance incessantly changes resulting to a very chaotic fault current magnitude. This algorithm involves calculation of ratio of metric lengths measurements, pattern recognition and fault detection. They also showed the ability of the algorithm to succesfully differentiate between faults and other transients in power system.

Huang and Hsieh (1998) also employed the ratio of metric lengths of the same time series for detecting power quality disturbances. The ratio of metric length computation was embedded within the detection procedure. With this algorithm, they were able to closely monitor non stationary disturbances in the signal. They also tested the algorithm on various disturbances, including voltage sag, momentary interruption, harmonic distortion, voltage swell and oscillatory transient. The results have shown the feasibility of the algorithm for visualization of power system faults.

Zhiyong and Weilin (2006) also employed the ratio of metric lengths of the same time sequence and phase reconstruction for analyzing disturbance signals by treating them as non-linear time series. Eight disturbances were selected and annalyzed. Ratio of metric

lengths measurements were applied to detect the disturbances and phase reconstruction was employed to clasify them. Conclusively, they show the algorithm was effective.

Finally, Umeh *et al.* (2004) employed the ratio of metric lengths of the same time sequence for characterizing the problem of harmonics which are generated by widely dispersed non-linear loads. They annalyzed the harmonic current waveform generated from typical non-linear loads such as laser jet printer, oscilloscope, personal computer and fluorescent lights. The result showed the algorithm was effective in characterizing harmonic problems and can be employed towards the development of a harmonic recognition system.

Seeing that the ratio of metric lengths of the same time series have been successfully employed in power systems fault diagnosis, in this research, ratio of metric lengths of the same time sequence will be employed for internal leakage detection in valve controlled actuation systems as well as electrohydrostatic actuation systems.

4.3.2 Ratio of Metric Lengths Computation

A ratio of metric lengths of the same time sequence is used to quantize or characterize the behavior of our system. This ratio is also known as fractal number by some researchers (Mamishev *et al.*, 1996; Huang and Hseih, 1998; Umeh *et al.*, 2004; Li and Wu, 2006).

Given a time series X_n, which contains n number of data points, the fractal number (ratio of metric lengths) F_m , of the m^{th} data set S_m which contains N number of data points is defined as:

$$F_m = \frac{\sum_{j=1}^{N-l} \left\| x_{j+k} - x_j \right\|}{\sum_{j=1}^{N-l} \left\| x_{j+l} - x_j \right\|} \tag{4.3}$$

where k and l are small integers known as sampling step size which define the time interval between neighboring data points and $l > k$. The symbol F_m has been chosen to distinguish it from other representations. Different norms can be assumed, however, a

conventional Euclidean norm has been chosen due to its simplicity. This representation is suitable for different values of k and l which results in different ratios of the metric lengths of the same time sequence. The algorithm was found to be more effective when the ratio of k and l was not an integer. In this situation, not all data points from the l-sampled subset belong to the k-step sampled subset. (Shyh-Jier, 2001; Mamishev *et al.*, 1996).

Euclidean Norm

On an n-dimensional Euclidean space R^n, the intuitive notion of the length of the vector $x = (x_1, x_2,.., x_n)$ can be represented by the formula

$$\|x\| = \sqrt{x_1^2 + x_2^2 + x_3^2 + \cdots x_n^2} \tag{4.4}$$

Some advantages of the proposed method include

1) It is efficient in monitoring and observing the signal dynamics in time domain.. For periods where the process changes erratically, the proposed algorithm can locate the sections of interest for a better visualization and assessment of signal characteristics.
2) The algorithm allows the simultaneous presentation of both *Fm* and time information and is suitable for different sampling rates.
3) The approach can be successfully used for isolation of other faults such as faults due to external leakage and friction. This analysis has been performed but not reported in this research as is not the focus of this work.

This algorithm has also been tested on various hydraulic disturbances such as external leakage and friction. The algorithm presented is processed using the windowing procedure described in the following section.

4.4 Windowing Method

The algorithms (autocorrelation, cross correlation and ratio of metric lengths) are implemented using the windowing method described. To analyze the data and to run the algorithm, the signals are broken into fragments or segments called windows. A window could be seen as a mathematical function that is zero-valued outside a chosen interval. It is

used in time domain to analyze the periodic behavior of the signal in short duration. Gao *et al.,* (2005) showed that in order to extract reliable and complete information from the decomposed signals, each window must carry a sufficient length of data. A large sized window will contain more data points than a small sized window.

Different lag and overlap is applied in the analysis. The length of the overlap with respect to the window size must be carefully selected as a small overlap increases the computation cost and the nature of the windowed signal may not be sufficiently affected by the new data zone. A very large overlap increases the detection delay as one needs to wait longer to update the relevant index. Overlapping of windows is used so that if there is any effect of cutting the data off, or an effect of the analysis procedure on the end of window then the overlapping of windows will make this evident in viewing the time series (Goharrizi, 2011).

The result from each window was saved and plotted against time to reveal the behavior in time domain. The next step decreases the window size and the same analysis is performed on the smaller windows, again saving the result of each window and plotting the analysis as a time series, giving a finer view of the analysis. The windows are continually decreased in size until their size becomes too small to continue.
The windowing process is shown in Fig. 4-1.

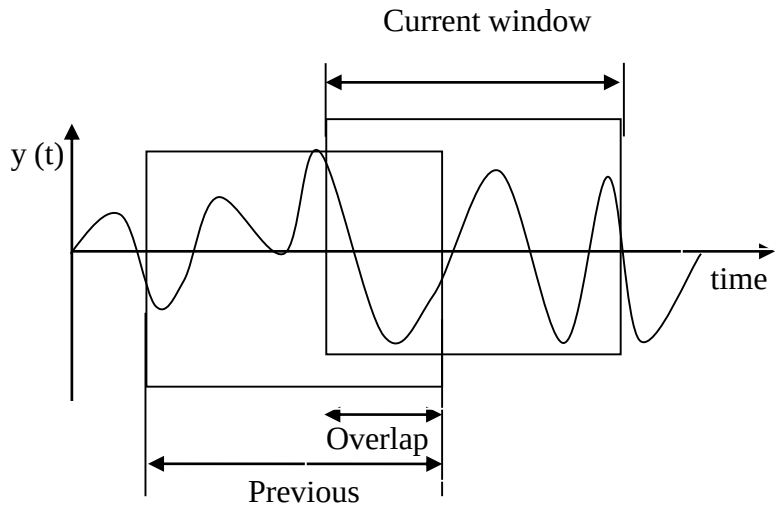

Figure 4-1: Illustration of windowing procedure

The analysis starts by varying the lag while the window size and overlap is held constant. The effect of the lag is observed and a high performing one is chosen and used for further analysis. The next step varies the window size while the overlap and preferred lag is held constant. A high performing window size is chosen and finally the preferred window size and preferred lag is held constant while the overlap is varied. The preferred overlap is chosen.

The choice of lag, window size or overlap is determined using the performance criteria discussed below. The performance of the algorithms is evaluated by visually inspecting the processed signal and by calculating the change in the mean RMS (root mean square) values between the leaking and non-leaking times of the experiment. Visual inspection denotes observing the processed signal for variations, number of spikes or abrupt changes in mean. The root mean square of both the leaking and non-leaking times of the processed signal is determined, the mean of the determined root mean square values is calculated and finally, the percentage change in mean between the leaking and non-leaking is obtained. The higher the percentage change the better the result. A good detection would show a greater percentage change (Between the mean RMS values of the leaking and non-leaking states of the processed signal).

4.5 Experimental Procedure (valve controlled actuation system)

This section introduces the nature of signals analyzed in this research. The description of the signals and insights into them is presented. The response of the system as a leak (fault) is introduced at about 200 seconds is also considered.

The sampling technique, calibration of the instrument and validation of the system model have been extensively discussed in the following Ph.D. research works, Karpenko, (2008). Also, the detailed description and derivation of the quantitative feedback controller (QFT) used for this test have been reported by (Karpenko and Sepehri, 2005; Karpenko, 2008).

Signal Preparation

+Before the acquired signals are analyzed, they are reviewed and a stationarity test (Section 4.7) conducted on them as any analysis conducted on a non-stationary process is not helpful (May, 2012). The stationarity of the signals was verified using statistical moments (Section 4.7).

The experiment performed for this research uses a pseudorandom input signal and under a load emulating a spring to simulate the normal working of a hydraulic actuator. Some of the tests were also conducted under no-load condition. Figure 4-2 shows typical signals employed at different stages of the analysis. The signals include control signal, pressure signals, internal leakage, desired and actual piston displacement. Again, these signals have been shown to provide a general insight into them.

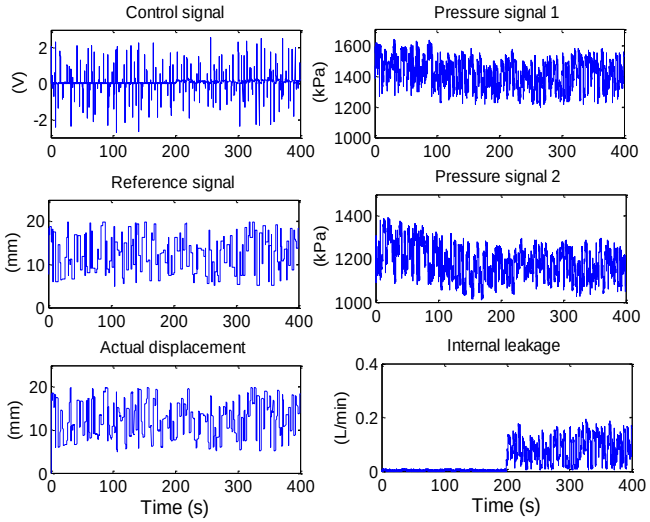

Figure 4-2: Typical system results

Figure 4-3 shows typical desired displacement, actual displacement and the control signal. The desired piston displacement is the pseudorandom reference input signal and the actual piston displacement is read by encoders installed at the piston area. The pseudorandom input signal is characterized with a series of desired step inputs having amplitudes between 2 mm to18 mm and under duration of 400 seconds. The control signal tracks the reference signal. It actuates the solenoids which control the valve position and this consequently

controls the motion of the piston. A positive control signal would result in an extension of the piston and a negative control signal would result in a retraction of the piston.

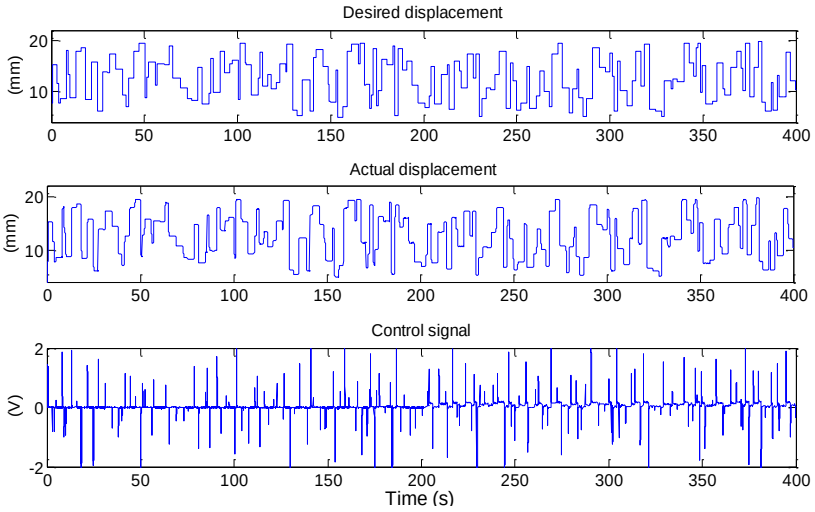

Figure 4-3: Desired displacement, actual displacement and control signal.

Figure 4-4 illustrates both pressure signals in the hydraulic chambers and the internal leakage simulated. Examining the plot, it is seen that as the pressure on one side of the piston increases the pressure on the other side decreases at the same rate as almost a perfectly mirrored image of the other. The internal leakage in the range of 0.047-0.5 L/min was simulated. The rate of leakage introduced is determined or measured using a flow meter. The experiment was performed at no leak condition for 200 seconds and in the last 200 seconds leakage was introduced.

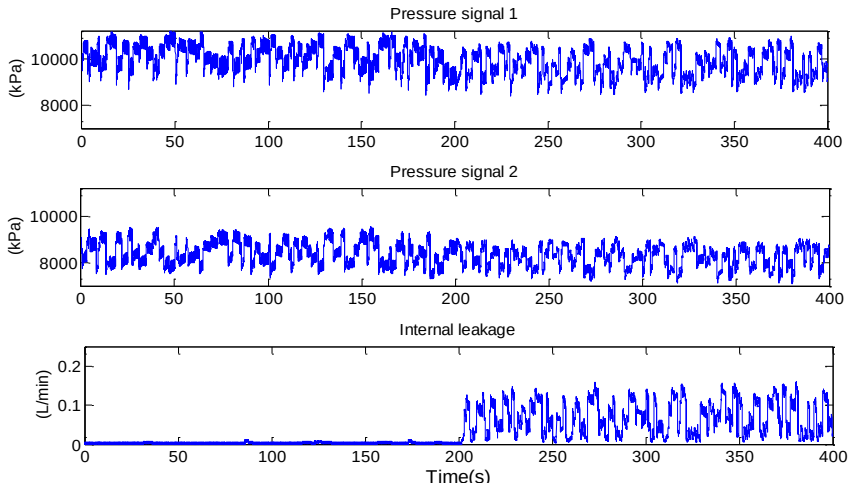

Figure 4-4: Pressure signals 1 and 2 and internal leakage

System Response to Internal Leakage

For most of the signals, the effect of the leakage is minimal as seen from their dynamics before and after 200 seconds. Figure 4-5 shows a closed-up view of the internal leakage. Before 200 seconds the leak is 0 L/min but after 200 seconds the leak varies. To determine the value of leak simulated, the mean of the leak after 200 seconds is calculated.

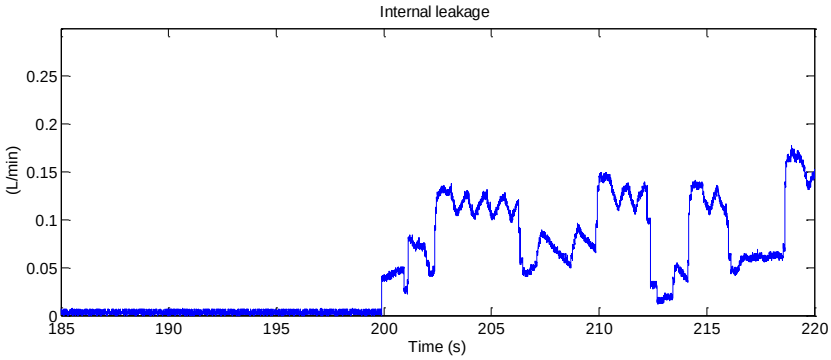

Figure 4-5: Internal leakage (Close-up view; 185s-220s).

Figure 4-6 shows the reference and actual displacement of the piston before and after the leakage is introduced. Judging from the dynamics, the effect of the leak on the system is clearly minimal. This is possibly due to the efficacy of the QFT controller used.

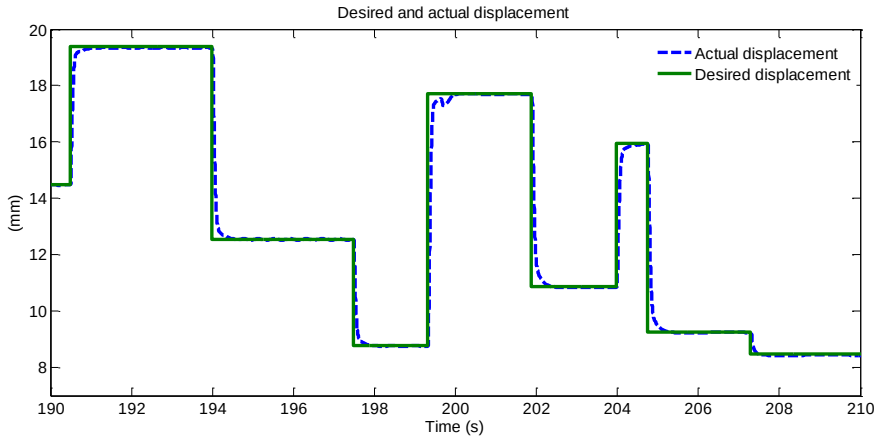

Figure 4-6: Desired and actual displacement (Closed-up view 190s)

Figure 4.7 shows a slight increase in the value of the control signal after 200 seconds. There is an increase in the variation and magnitude of the voltage spikes after 200 seconds. This is evident when the signal is observed for the whole time interval (Figure 4-3). Figure 4-8 shows the pressure signals meet each other at various times, this is due to the spring applying force on the actuator. The system at these points changes from a compression on the spring to an extension on the spring, hence the relative changes in magnitude of the pressure signals. The pressure signals however do show a slight change in their nature after the leak has occurred. These results are typical for all experiments performed regardless of the size of the leak introduced to the system.

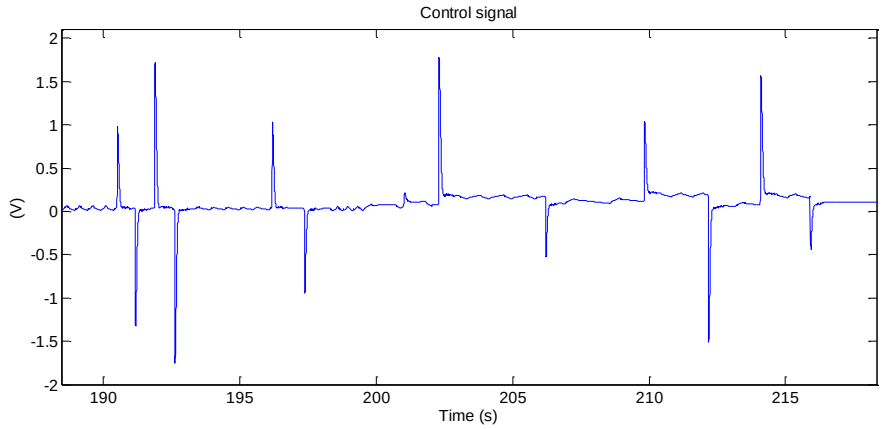

Figure 4-7: Close-up view of control signal (190s-205s)

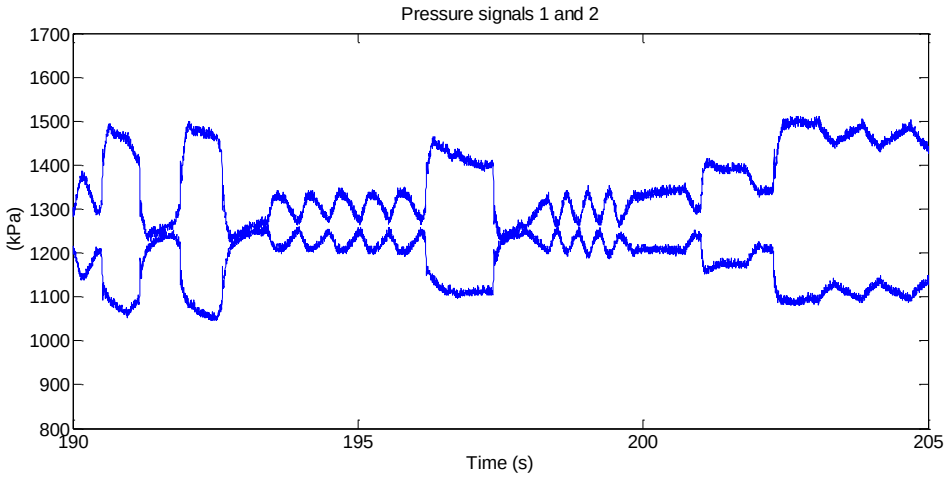

Figure 4-8: Close-up view of pressure signals 1 and 2 (190s-205s)

4.6 Experimental Procedure (electrohydrostatic actuation system)

This section introduces the nature of signals analyzed in this research. The description of the signals and insights into them is presented. The response of the system as a leak (fault) is introduced at about 90 seconds is also considered. The sampling technique, calibration of the instrument and validation of the system model have been reported by Thakur, (2011).

Signal Preparation

Before the acquired signals are analyzed, they are reviewed and a stationarity test (Section 4.7) conducted on them as any analysis conducted on a non-stationary process is not helpful (May, 2012). The stationarity of the signals was verified using statistical moments (Section 4.7).

The experiment performed in this section uses a sinusoidal input signal and under a load emulating a spring to simulate the normal working of a hydraulic actuator (EHA). Figure 4-9 show typical pressure signals and internal leakage. Examining this plot, it is observed that as the pressure on one side of the piston increases, the pressure at the other side decreases at the same rate. The duration of the experiment was 180 seconds wherein the first 90 seconds were performed without leakage and the final 90 seconds were performed under conditions of leak. Again, these signals have been shown to provide a general insight into them.

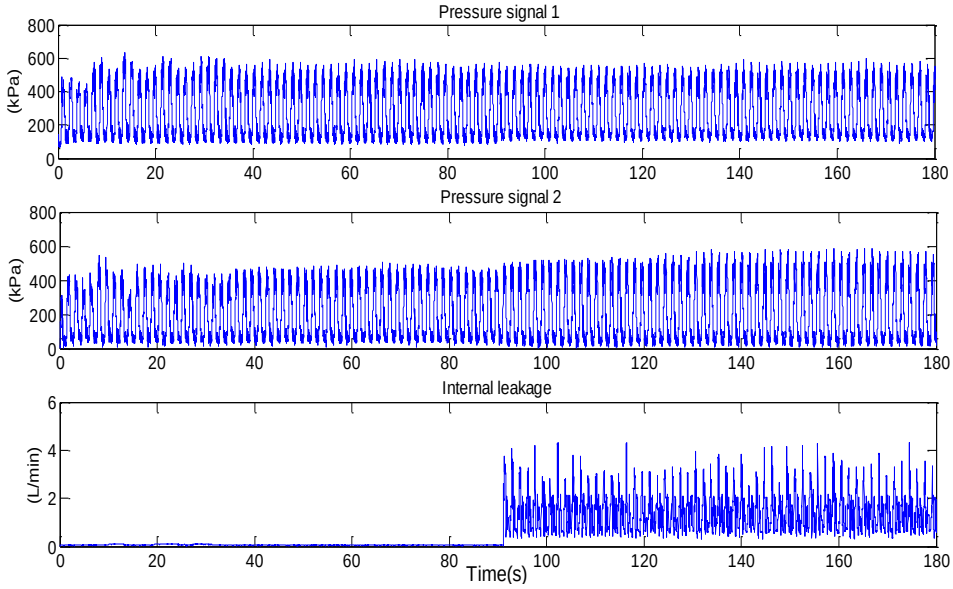

Figure 4-9: Pressure signals 1 and 2; internal leakage (EHA)

Figure 4-10 illustrates the input signal and piston displacement. The input voltage is a sinusoidal wave of amplitude 3 V and frequency 4rad/sec (3sin4t). The electrohydrostatic actuation system is triggered with the input of a sine wave. The displacement of the piston is shown for the entire 180 seconds. The plot of the piston displacement reduces at a constant rate due to the orifice and friction in the test rig. This reduction stops as soon as the leakage is introduced at the 90th second,

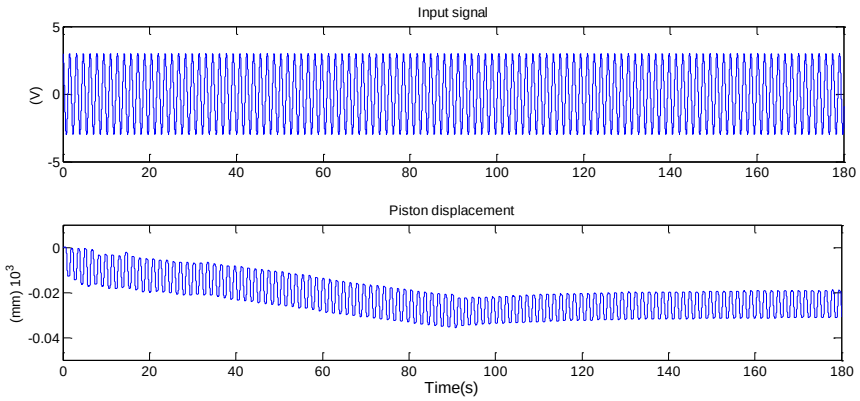

Figure 4-10: Input signal and piston displacement.

System Response to Internal Leakage

For most of the signals, the effect of the leakage is minimal as seen from their dynamics before and after 90 seconds. Figure 4-11 and 4-12 show close-up views of the pressure signals and internal leakage, input signal and piston displacement respectively. Before 90 seconds the leak is 0 L/min but after 90 seconds the leak varies. To determine the value of leak simulated, the average leak after 90 seconds is calculated. For these sets of experiments, the average simulated leak is in the range of 0.77 L/min-1.63 L/min.

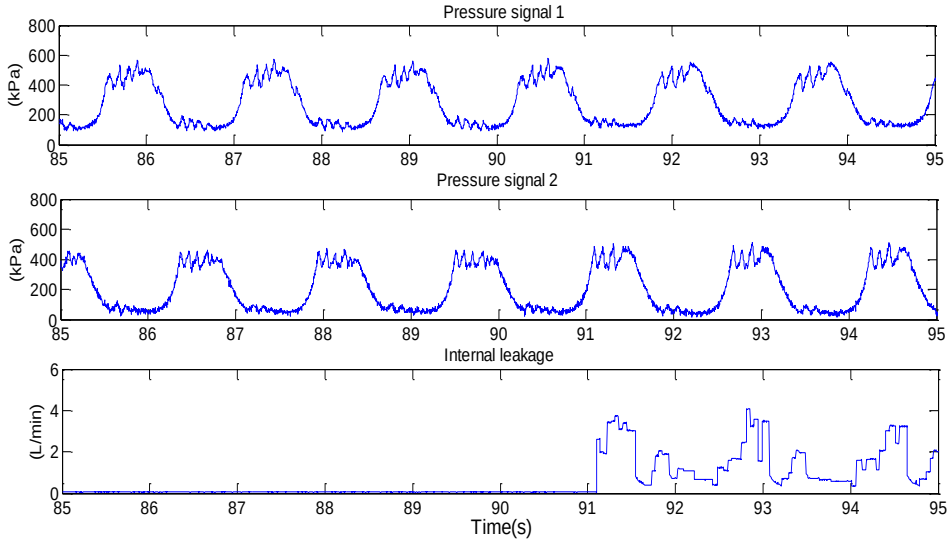

Figure 4-11: Close-up view; Pressure signals and internal leakage (85s-95s)

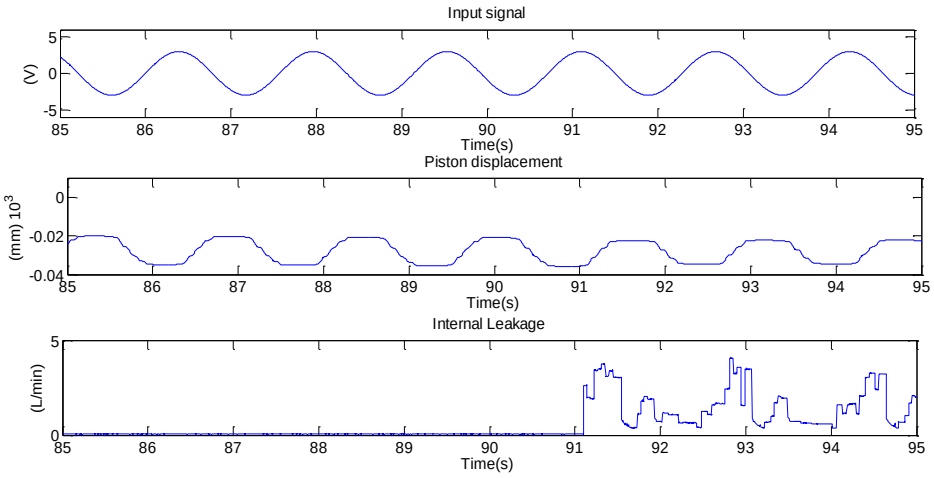

Figure 4-12: Close-up view; Input signal, piston displacement and internal leakage (85s-95s)

4.7 Stationarity Analysis

Analysis performed on a process without validating its stationarity is not helpful. This section illustrates the stationarity analysis performed on the input signals, pressure signals and the piston displacement signals associated to both the valve controlled actuation system and the electrohydrostatic actuation system. Statistical moments were employed for this test. The decision on whether to analyze a time series (signal) in levels or differences is made by investigating the stationarity of the signal.

Stationarity is defined as a quality of a process in which the statistical moments of the process do not change with time. Truly stationary processes have all higher-order moments constant, including the variance and mean (Challis and Kitney, 1991). There are two classes of stationarity: weak and strong stationarity. For a signal to be deemed strongly stationary, all its statistical moment must be unaffected by time. Strong stationarity is very difficult to prove, and is not required by most signal analysis processes. In fact, strongly stationary processes are never seen in practice and are discussed only for their mathematical properties (Challis and Kitney, 1991).

Weak stationarity, also known as weak sense stationarity (WSS) or covariance stationarity, requires that the first moment and covariance do not vary with time. There are different

degrees of stationarity, which are defined in orders to which the statistical moments are immune to the effect of time. For example, if a signal has a first order statistical moment unaffected by time but the second moment trends with time, then the signal would be called a first order weakly stationary signal (May, 2012). Mathematically, a sequence x_t is weakly stationary if the mean, variance and auto covariance do not grow over time.

STATISTICAL MOMENTS USED

M EAN

Mean is the arithmetic average of a set of values. Given a set of points $x_1, x_2 \ldots . x_n$ of a sample data X of length N. The Mean $\overline{X}$ is expressed as

$$\bar{X} = \frac{\sum_{j=1}^{N} X_j}{N} \tag{4.11}$$

VARIANCE

Variance is a measure of the dispersion of a set of data points around their average value. It can also be referred to as a mathematical expectation of the average squared deviations from the mean. Given a set of points $x_1, x_2 \ldots . x_n$ of a sample data X of length N. The variance σ^2 is mathematically expressed as

$$\sigma^2 = \frac{\sum_{j=1}^{N} \left(x_j - \bar{x}\right)^2}{N} \tag{4.12}$$

SKEWNESS

Skewness is a measure of the degree of asymmetry of a probability distribution. A distribution is said to be symmetric if the data points are similar throughout the data. In other words, skewness measures the degree to which the probability distribution of a real-valued random variable "leans" to one side of the mean and its value is either positive, negative or undefined. Qualitatively, if the left tail of the probability density function is

more pronounced than the right tail, the function is said to have negative skewness, however, if the converse is true, it has positive skewness and if the right and left tail are equal, then it has a zero skewness (Nwachukwu, 2012). Given a set of points $x_1, x_2 \ldots x_n$ of a sample data *X* of length *N*. The skewness is mathematically expressed as

$$Skewness = \frac{\sum_{j=1}^{N}\left(x_j - \bar{x}\right)^2}{(N-1)s^3} \tag{4.13}$$

Where $\bar{x}$ represents the mean, *s* is the standard deviation, and *N* is the number of data points.

KURTOSIS

Kurtosis measures the variability of a distribution. It describes the shape of a probability distribution. It measures whether the data are peaked or flat relative to a normal distribution (Nwachukwu, 2012). Given a set of points $x_1, x_2 \ldots x_n$ of a sample data *X* of length *N*. The kurtosis is mathematically expressed as

$$Kurtosis = \frac{\sum_{j=1}^{N}\left(x_j - \bar{x}\right)^4}{(N-1)s^4} \tag{4.14}$$

Where $\bar{x}$ represents the mean, *s* is the standard deviation, and *N* is the number of data points.

4.7.1 Stationarity Results (valve controlled actuation system)

Figure 4-13 and 4-14 show typical results obtained from performing a first, second, third and fourth moment analysis on pressure signals 1 and 2 using a window size of 400 data points and 50% overlap. Tests using other window sizes and overlaps were also performed though only results for (window size) 400 data points and 50% overlap are shown.

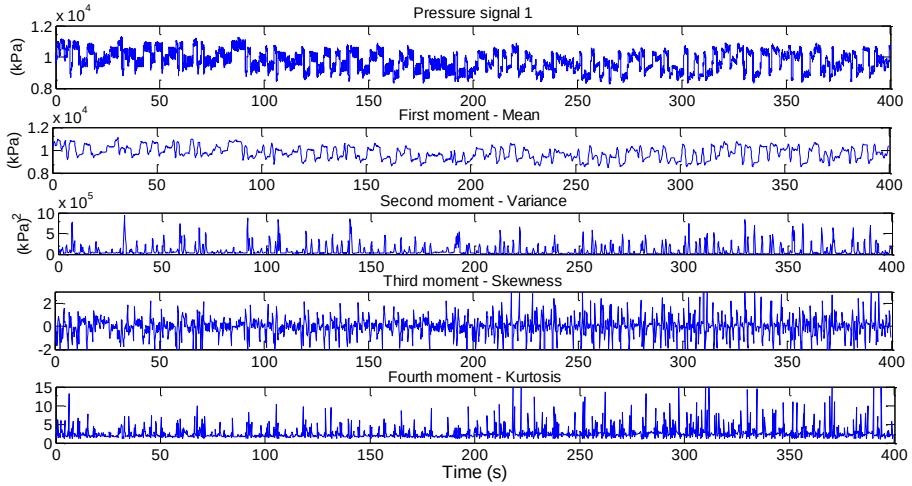

Figure 4-13: Stationarity test for pressure signal 1 using a window size of 400 data points and 50% overlap.

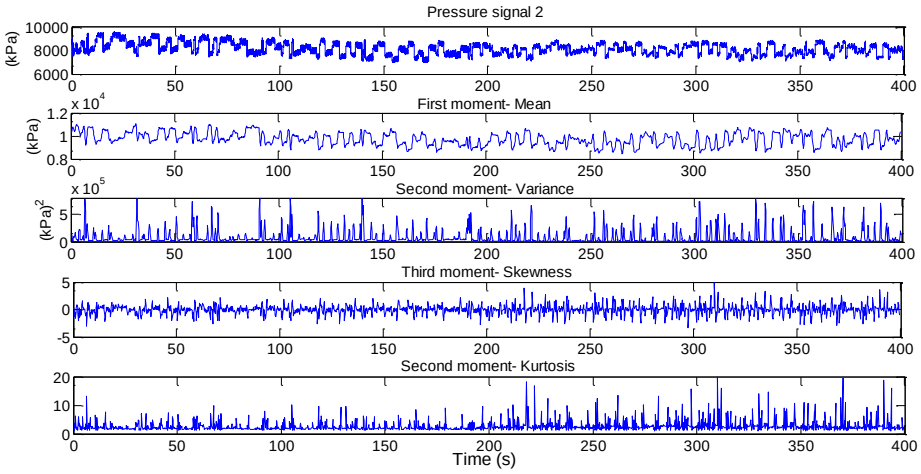

Figure 4-14: Stationarity test for pressure signal 2 using a window size of 400 data points and 50% overlap.

Figure 4-13 and Figure 4-14 show no obvious trend. The trend of a non-stationary series usually shows an upward, downward slope or jumps in level (Box, Jeikens and Reinsel, 1994; Paz and Pilar, 2003). Its trend or behavior can also be steep, exponential or approximately linear whereas a stationary series moves around a unique level in time. The first moment (mean) suggests stationarity of the signal as its mean appears reverting. A time series is non-stationary if it does not show a tendency of mean reversion (Box, Jeikens and Reinsel, 1994; Paz and Pilar, 2003). The finite variance (second moment)

clearly guarantees that the realization will never drift too far from its mean. The third and fourth moments also depict stationarity as there are virtually no jumps, upward or downward slope of the variance, skewness or kurtosis representation.

It is important to note that there is a change in the nature of the signal around 200 seconds. This is due to the introduction of a leak to the system. This change in the signal is suggested by viewing the number of spikes that are present in the skewness and kurtosis plots as well as their magnitudes. To validate that the signal changes was due to the introduction of the leak and not the effect of time, further experiments were run with leaks introduced at different times and the effect on the statistical moments was realized to coincide with the introduction of the leak and not with the effect of time.

Figure 4-15 and 4-16 show typical results obtained from performing a first, second, third and fourth moment analysis on piston displacement and control signal. These plots were obtained using window sizes of 400 data points with 50% overlap between successive windows.

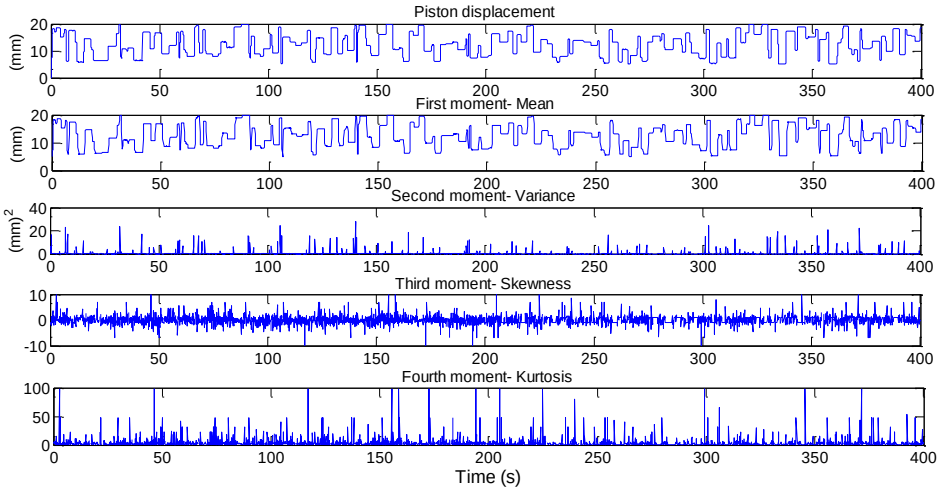

Figure 4-15: Stationarity test for piston displacement using a window size of 400 data points and 50% overlap.

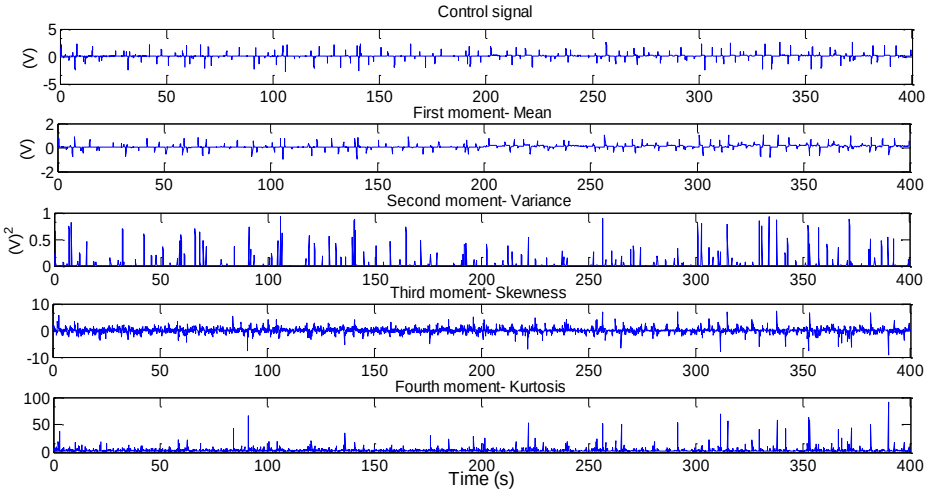

Figure 4-16: Stationarity test for control signal using a window size of 400 data points and 50% overlap.

Figure 4-15 and Figure 4-16 show no obvious trends. The first moment (mean) suggests stationarity of the signal as a mean reversion is observed. A time series is non-stationary, if it does not show a tendency of mean reversion. The finite variance (second moment) guarantees that the process will never drift too far from its mean. The third and fourth moments also depict stationarity as there are virtually no jumps, upward or downward slope of the variance, skewness or kurtosis representation (Paz and Pilar, 2003)

A change in the nature of the signal is observed around 200 seconds. This is due to the introduction of a leak to the system. This change in the signal is suggested by viewing the number of spikes that are present in the skewness and kurtosis plots and their magnitudes. To validate that the signal changes was due to the introduction of the leak and not the effect of time, further experiments were run with leaks introduced at different times and the effect on the statistical moments was realized to coincide with the introduction of the leak and not with the effect of time.

4.7.2 Stationarity Results (electrohydrostatic actuation system)

Figure 4-17, 4-18, 4-19 and 4-20 show typical results obtained from performing a first, second, third and fourth moment analysis on pressure signal 1, pressure signal 2, piston displacement and input signal respectively using the EHA . These plots were obtained using window sizes of 400 data points with 50% overlap between successive windows. Tests using other window sizes and overlaps were also performed though only results for (window size) 400 data points and 50% overlap are shown.

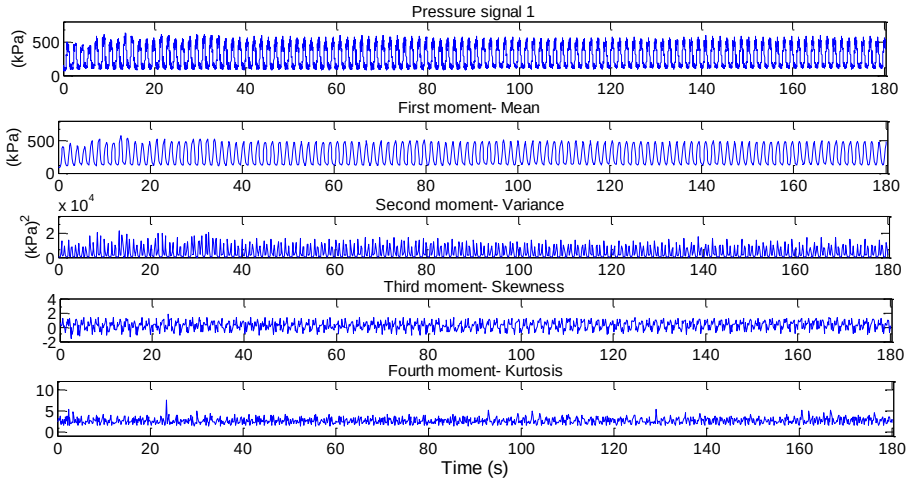

Figure 4-17: Stationarity test for pressure signal 1, using a window size of 400 data points and an overlap of 50% (EHA).

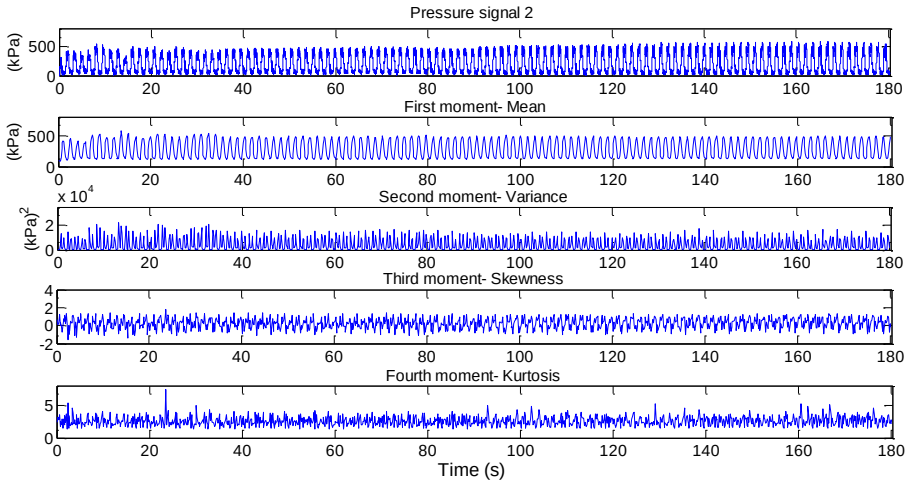

Figure 4-18: Stationarity test for pressure signal 2 using a window size of 400 data points and an overlap of 50% (EHA).

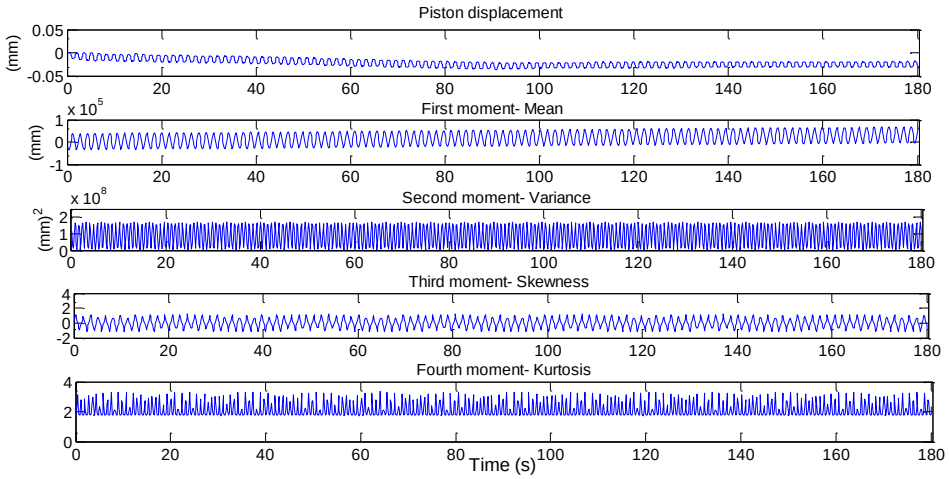

Figure 4-19: Stationarity test for piston displacement using a window size of 400 data points and an overlap of 50% (EHA).

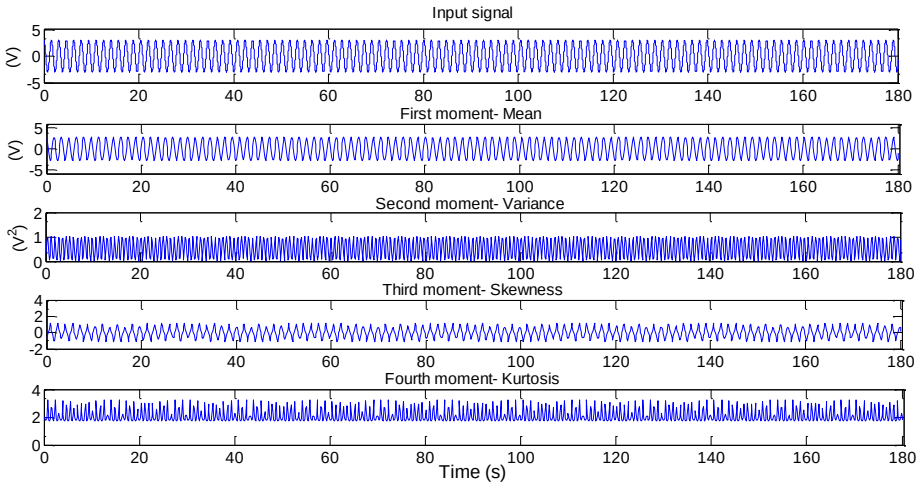

Figure 4-20: Stationarity test for input signal using a window size of 400 data points and an overlap of 50% (EHA).

Figure 4-17, 4-18, 4-19 and 4-20 show no obvious trend. The path of a non-stationary series shows an upward or downward slope or jumps in level. Its trend or behavior can also be steep, exponential or approximately linear whereas a stationary series moves around a unique level in time. The first moment (mean) suggests stationarity of the signal as its mean appears reverting. A time series is non-stationary, if it does not show a tendency of mean reversion. The finite variance (second moment) clearly guarantees that the realization will never drift too far from its mean. The third and fourth moments also depict stationarity as there are virtually no jumps, upward or downward slope of the skewness or kurtosis representation.

4.7.3 Summary

The three signal processing based techniques have been discussed and their applications have also been considered. Autocorrelation can be used on either pressure signal 1 or 2, cross correlation is used on both pressure signal 1 & 2 and also between control signal and piston displacement. Ratio of metric lengths is used on pressure signals 1 or 2. Windows ranging from 600 data points to 50 data points were used with overlaps from 0% to 50% for multiple experiments (VCA:73 experiments and EHA:34 experiments) with different severity of leaks and inputs.

From the statistical analysis performed on all experiment, the first four statistical moments appear to be unrelated to time regardless of the size of the window, or amount of overlap. The absence of trends in any of these plots suggests stationarity. It is safe to conclude that the signals produced from the test rig are stationary to perform the analysis. The results are discussed in the next chapter.

CHAPTER 5

EXPERIMENTAL RESULTS

VALVE CONTROLLED ACTUATION SYSTEM

5 EXPERIMENTAL RESULTS

5.1 Internal Leakage Detection (Valve Controlled Actuation System)

This section discusses the results of implementing all three detection methods (described in Chapter 4) on a valve controlled actuation system. It also highlight the effect of varying the window size, lag and overlap on the results. Three case studies considered:

1) Case study 1: A valve controlled actuator is excited with a pseudorandom input signal (amplitude: 8 mm to 20 mm) under a no-load condition. After 200 seconds of operation, a medium internal leakage having a mean value of 0.10 L/min is introduced and the system is allowed to run for a total of 400 seconds.

2) Case study 2: A valve controlled actuator is excited with a pseudorandom input signal (amplitude: 5 mm to 17 mm) under a no-load condition. After 200 seconds of operation, a small internal leakage having a mean value of 0.047 L/min is introduced and the system is allowed to run for a total of 400 seconds.

3) Case study 3: A valve controlled actuator is excited with a pseudorandom input signal (amplitude: 2 mm to 20 mm) under load and no-load conditions for different tests. The system is allowed to operate for different ranges of time. Some of the tests were operated for 300, 400 and 600 seconds. Internal leakage in the range of 0.047 L/min to 0.5 L/min is introduced at about half of the total test time. This case study is used to evaluate the sensitivity or responsiveness of the algorithms to different levels of internal leakage.

Case Study 1

The response of the system to a medium internal leakage is considered. An insight into the signals is reviewed next. Figures 5-1, 5-2 and 5-3 show close-up views of the set of signals under medium internal leakage (0.10 L/min) conditions.

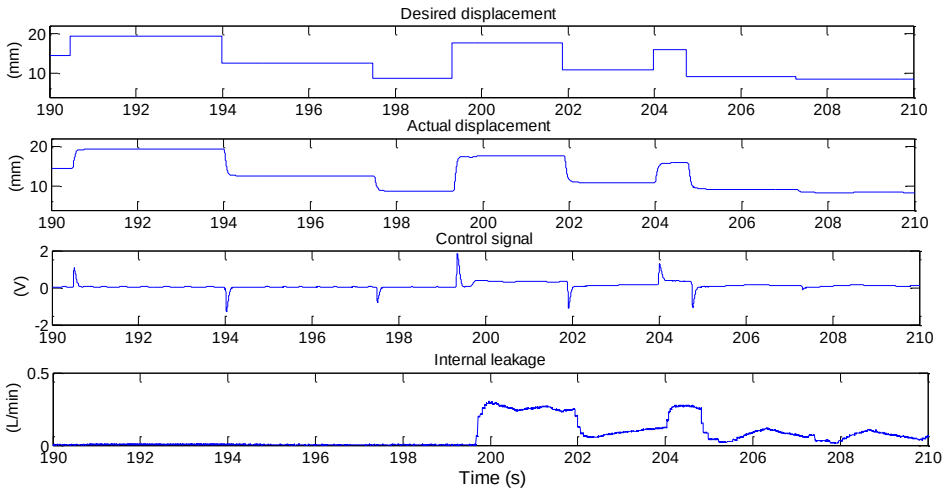

Figure 5-1: Desired displacement, actual displacement, control signal and medium mean internal leakage of 0.10 L/min (Close-up view: 190s-210s)

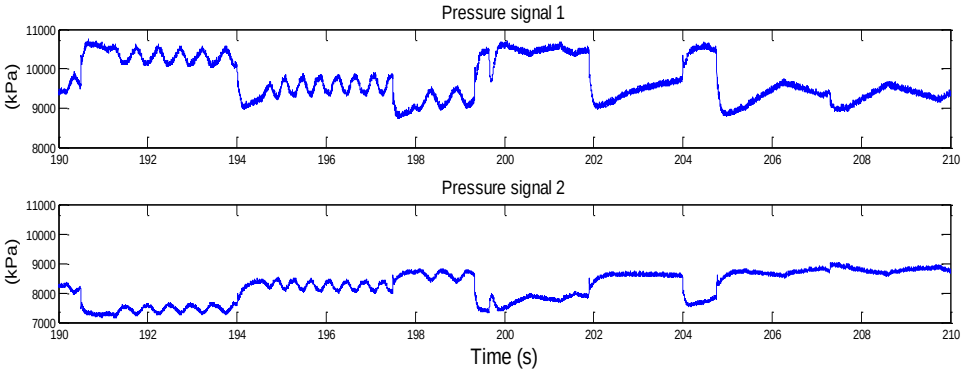

Figure 5-2: Typical pressure signals 1 and 2 (kPa), medium leak of 0.10 L/min, (Close-up view: 190s-210s).

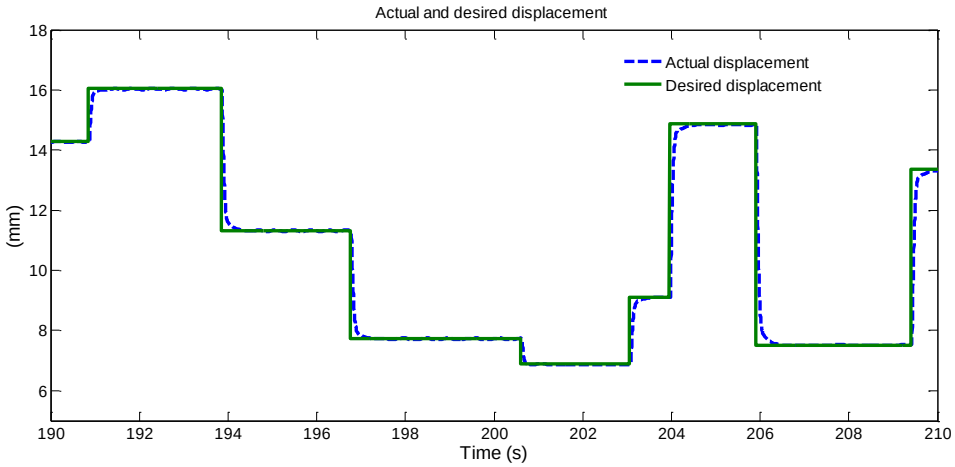

Figure 5-3: Desired and actual displacement (mm) (Close-up view: 190s-210s)

Figures 5-1, 5-2 and 5-3 provide an insight into the responses. From Figs. 5-1, the positional response of the actuator and control signal shows no significant difference between the healthy state (before 200 seconds) and unhealthy state (after 200 seconds). Similarly, the desired position response and actual displacement show no significant difference (Figure 5-3). The actuator appeared to have followed the desired sufficiently well enough.

Conversely, the pressure response show slight changes after the leakage was introduced. This may be due to the efficacy of the QFT controller employed, as it was designed to be robust to the parameters of the system and also to leakage.

Case Study 2

The response of the system to a small internal leakage is considered. An insight into the signals is reviewed next. Figures 5-4, 5-5 and 5-6 show close-up views of the set of signals under medium internal leakage (0.047 L/min) conditions. Figure 5-4, 5-5 and 5-6 show close-up views of the set of signals under smallest internal leakage (0.047 L/min) conditions

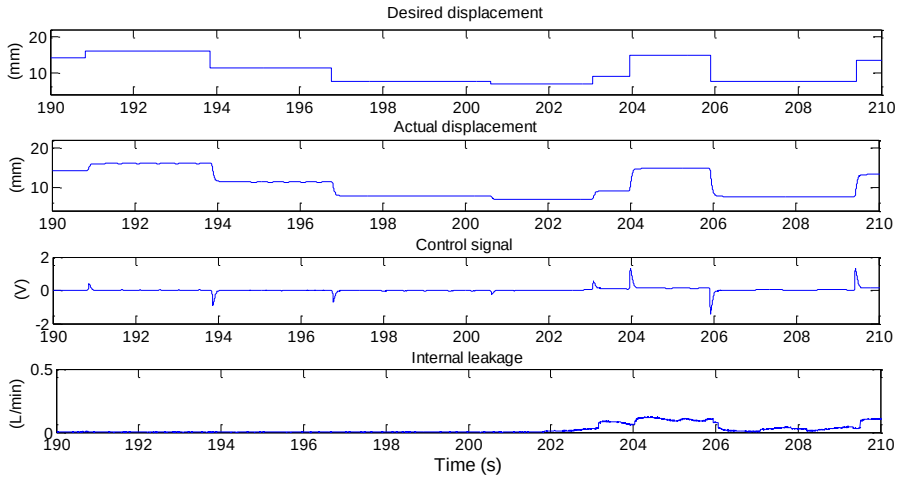

Figure 5-4: Desired displacement, actual displacement, control signal and internal leakage (smallest leak of 0.047 L/min), (Close-up view: 190s-210s).

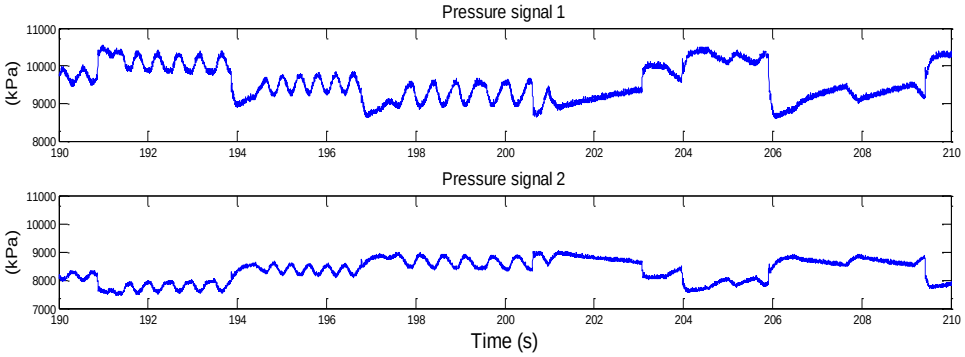

Figure 5-5: Typical pressure signals 1 and 2 (small leak of 0.047 L/min), (Close-up view: 190s-210s)

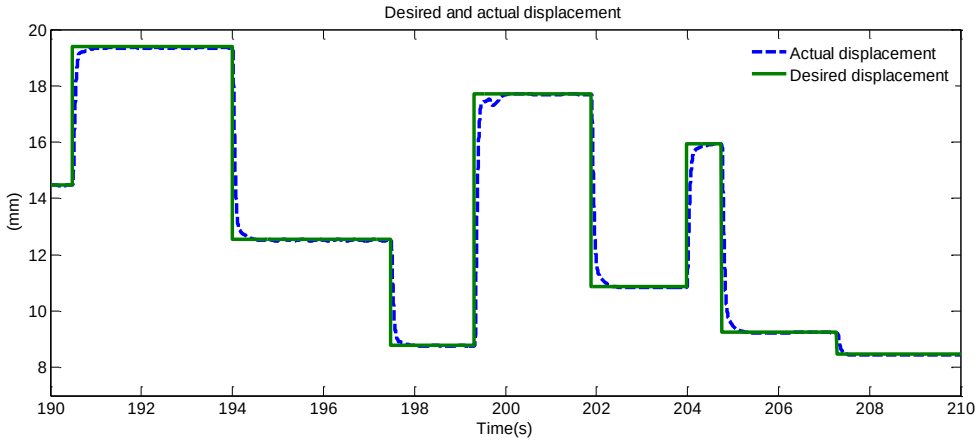

Figure 5-6: Typical Actual and desired displacement (small leak of 0.047 L/min), (Close-up view: 190s-210s).

Figures 5-4, 5-5 and 5-6 provide an insight into the signals and also illustrate the performance of the QFT controller. The controller performed well in tracking the desired displacement despite the introduction of leak at 200 seconds although there are slight delays in tracking the edges of the desired displacement.

Looking at the responses for both medium and small leak conditions, there are no significant differences between them as such, one can conclude that the controller's effort in counteracting the effect of leak severity on the system response is great. It is seen that for both medium and smallest leak conditions, the controller performance is acceptable

5.2 General Signal Processing Procedure.

The chart below illustrates the general steps procedure adopted in analyzing the signals and detection.

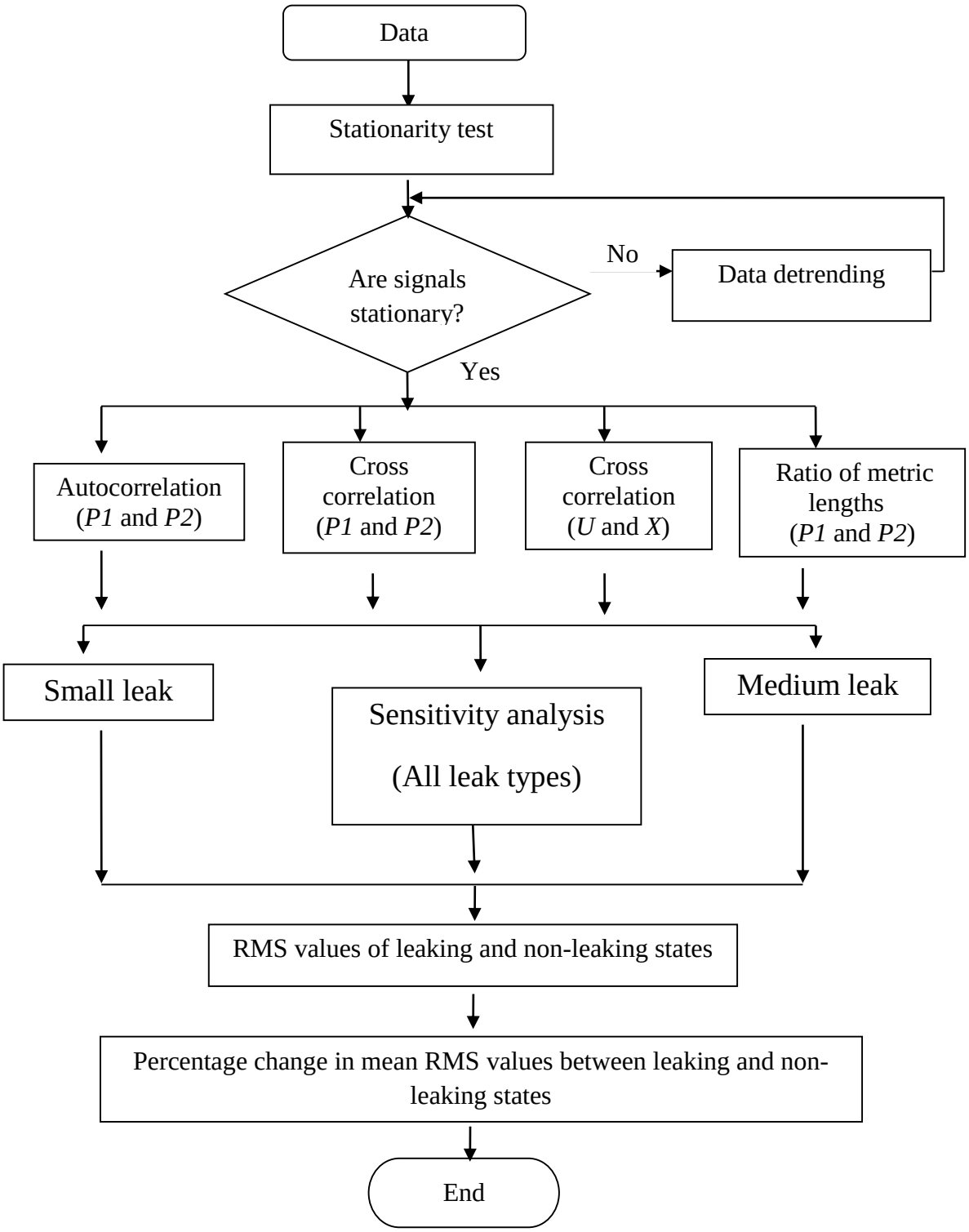

All parameters in the chart have been explained in Chapter 4 except for the root mean square (RMS) and mean of the root mean squares.

STEPS FOR CALCULATING THE ROOT MEAN SQUARE

1) Implementing the autocorration, cross correlation or the ratio of metric lengths concept, using the described signals (pressure signals 1 and 2, control signal and piston displacement) results in a time series of the coefficients or fractal numbers.
2) The ratio of metric lengths is divided into windows of equal number of data points
3) The root mean square (RMS) of each window is calculated and saved.

The RMS value of a continuous time series is the square root of the average of the squares of the original series. Given a set of n values $\{x_1, x_{2,} x_{3,} x_4 \ldots\ldots\ldots x_n\}$, The RMS value is given by

$$RMS = \sqrt{\frac{1}{n}\left(x_1^2 + x_2^2 + x_3^2 + \ldots\ldots\ldots\ldots\ldots x_n^2\right)} \qquad (5\text{-}1)$$

This results to a RMS value for each window.

4) The root mean squares are plotted in time domain to visualize how they change over the course of the experiment (Some of the RMS plots in time domain can be found at the appendix)
5) The RMS signal in time domain is divided into two equal windows (Leaking and non-leaking state) and the mean of each window is obtained.

Given a set of RMS values $\{RMS_1, RMS_{2,} RMS_{3,} \ldots\ldots\ldots RMS_n\}$, where *n* is the number of RMS values in each state (Leaking or non-leaking state), The Mean RMS value is given by

$$Mean_{RMS} = \frac{1}{n}\{RMS_1 + RMS_{2,} + \ldots\ldots\ldots RMS_n\} \qquad (5\text{-}2)$$

This results to a $Mean_{RMS}$ value for each state. The mean RMS for the leaking coefficients or ratio of metric lengths is designated as RMS_l while the mean RMS for the non-leaking coefficient is designated as RMS_{nl}.

6) The percentage change between the RMS_l and RMS_{nl} is obtained by the following

$$Percentage\ Change = \left(\frac{RMS_l - RMS_{nl}}{RMS_{nl}} \right) \times 100 \qquad (5\text{-}3)$$

5.3 Autocorrelation Results (valve controlled actuation system)

The autocorrelation function can be performed on either of the chamber pressure data. The autocorrelation function is applied to the pressure data, producing a single coefficient for each window. These values are then plotted in time to show the behavior or dynamics of the autocorrelation coefficients over the course of an experiment.

The windowing technique used is described in Section 4.5. It starts with assessing the effect of lag. This is achieved by varying the lag while the window size and overlap is held constant. The effect of the lag is observed and a high performing one is chosen and used for further analysis. The next step varies the window size while the overlap and preferred lag is held constant. A high performing window size is chosen and finally the preferred window size and preferred lag is held constant while the overlap is varied. The preferred overlap is chosen. The preferred lag, window size and overlap are used for detecting the smallest internal leakage (case study 2) and for performing the sensitivity analysis.

5.3.1 Effect of Lag

Figure 5-7 shows the result of an autocorrelation analysis of the pressure signal *P1* with a leak occurring at about 200 seconds using lag 1, 2 and 4, window size of 200 data points and an overlap of 5%. With reference to Figs. 5-7, there is a decrease in the autocorrelation coefficients at about 200 seconds for all three plots (lag 1, 2 and 4). This change coincides with the time the leak was introduced and suggests autocorrelation function is able to detect internal leakage faults.

The percentage change between the leaking and non-leaking coefficient increases as the lag is increased. This is determined using the steps illustrated in Section 5.2. In Table 5-1, the percentage change in mean RMS between the leaking and non-leaking coefficients is represented as a function of lag. The percentage change in mean RMS values increases as the lag is increased but converges to 45% for higher lags. A high percentage change would mean a better result.

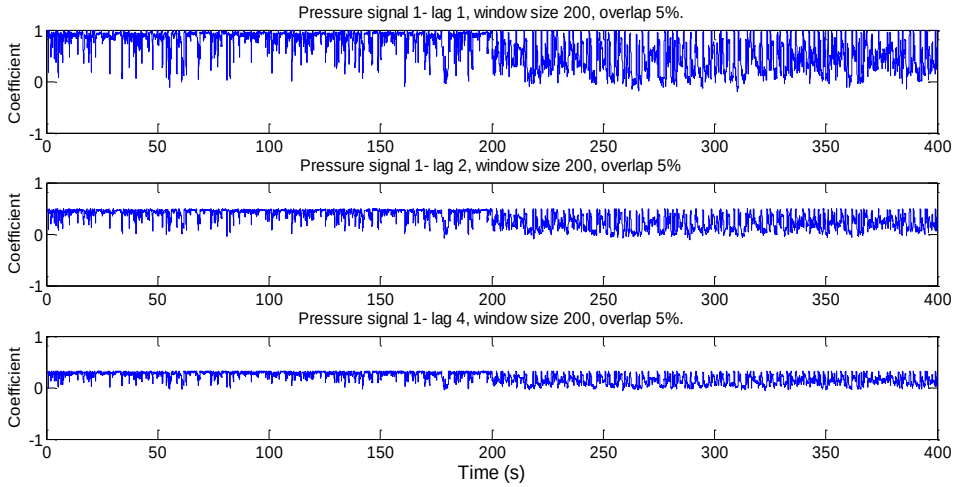

Figure 5-7: Effect of lag on autocorrelation coefficient for a mean leak of 0.10 L/min, using a window size of 200 data points and 5% overlap.

Table 5-1: Percentage change in mean RMS values as a function of lag.

Lag Value	Mean RMS before leak	Mean RMS after leak	(%)Change of Mean RMS
1	0.84864	0.48778	42.5218
2	0.41742	0.23625	43.4024
4	0.90702	0.15207	43.5898
8	0.75572	0.41812	44.6231
12	0.3488	0.19316	44.6706
18	0.20277	0.11166	44.9331

With reference to Table 5-1 and Figs. 5-7, lag 1 is preferred for subsequent analysis even though it has a percentage change of 42.5% and not the highest percentage in the table. This choice is motivated by assessing the nature of the signal (coefficient). The amplitude of the signal decreases as the lag increases. For further analysis, a signal with higher amplitude and energy is required to enhance visual appreciation of the signal. Also, the range of the percentage change is less than 3% (45%-42.5%) which implies that choosing any of the lags may not make much of a difference. If a signal with less amplitude or variation is required, then a higher lag would be preferable, conversely, a lower lag will be preferable.

5.3.2 Effect of Window Size

Here, the preferred lag (lag 1) is used while the window size is varied and the overlap is held constant. This will enable us to choose a high performing window size. Figure 5-8 shows the result of an autocorrelation analysis of pressure signal 1 with the introduction of leak at the 200^{th} second using window sizes of 200, 400 and 600 data points; lag 1 and 5% overlap.

With reference to Fig. 5-8, there is a significant decrease in the autocorrelation coefficients at about 200 seconds for all three plots (window size 200, 400 and 600). This change coincides with the time the leak was introduced and suggests autocorrelation function is able to detect internal leakage faults.

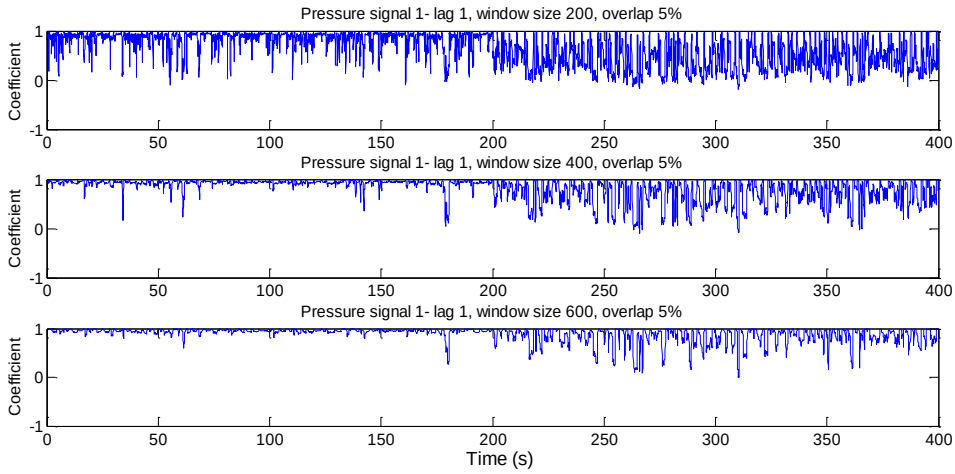

Figure 5-8: Effect of varying window size on autocorrelation coefficient with a mean leak of 0.10 L/min using lag 1 and 5% overlap

The effect of the window size on the autocorrelation coefficient is readily seen. As the window size is increased from 200 data points to 400 data points and to 800 data points, the signal becomes less noisy and the effective change on the autocorrelation coefficient increases, allowing for a clearer and easily readable result. This trend is apparent in higher and lower window sizes. In other words, the lower the window size, the noisier the signal becomes and the lesser the effective change becomes.

In Table 5-2, the percentage change in mean RMS values between the leaking and non-leaking coefficients is represented as a function of window size. A linear relationship exists between the window size and the percentage change in mean RMS values. As the window size increases, the percentage change decreases. A higher percentage would mean a better result as the higher the percentage change, the more likely the change would be noticeable. Analysis using window sizes in the range of 100 to 800 is shown though analysis for higher and lower window sizes were also performed (Not shown) and found to be consistent with the existing trend.

Table 5-2: Percentage change in mean RMS values as a function of window size

Window size	Mean RMS before leak	Mean RMS after leak	(%)Change of Mean RMS
100	0.6647	0.28257	57.489
200	0.84377	0.47187	41.23
300	0.90702	0.6322	30.2999
400	0.92958	0.72942	21.5326
600	0.84242	0.94908	11.2383
800	0.95987	0.89797	6.449

With reference to Table 5-2 and Fig. 5-8, window size of 200 is preferred for subsequent analysis even though it has a percentage change of 41.23% and not the highest percentage in the table. This choice is motivated by assessing the nature of the signal (coefficient). The amplitude and energy of the signal reduces as the window size is increased. For further analysis, a signal with higher amplitude and energy but less noise is required to enhance visual appreciation of the signal.

5.3.3 Effect of Overlap

Here, the preferred lag (lag 1) and window size (200 data points) is used while the overlap is varied. This is to enable us choose a high performing overlap. Figure 5-9 shows the result of an autocorrelation analysis of pressure signal 1 with the introduction of leak at the 200th second using overlaps of 5%, 25% and 50%; lag 1 and window size of 200 data points.

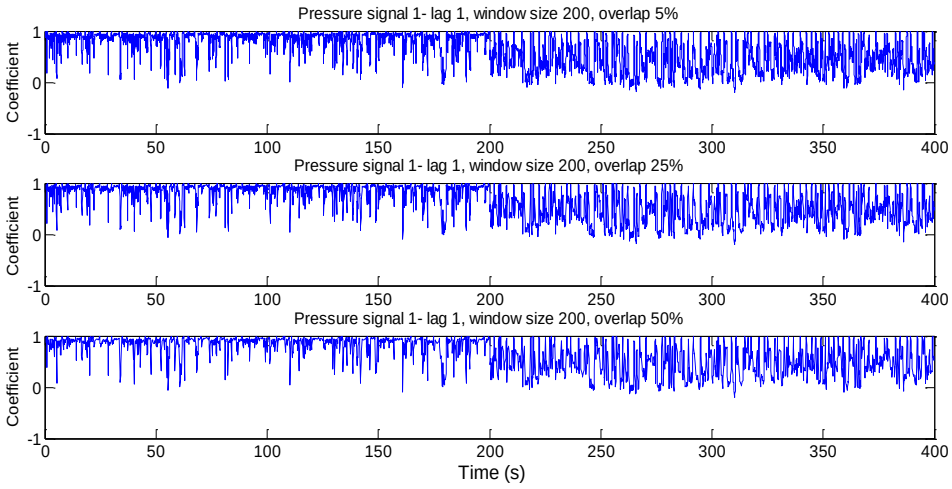

Figure 5-9: The effect of overlap on autocorrelation coefficient with a mean leak of 0.10 L/min using a window size of 200 data points and lag 1.

With reference to Fig. 5-9, there is a significant decrease in the autocorrelation coefficients at about 200 seconds for all three plots (Overlap: 5%, 25% and 50%). This change coincides with the time the leak was introduced and suggests autocorrelation function is able to detect internal leakage faults.

Overlaps of 5%, 25% and 50% is shown though analysis for higher and lower overlaps were also performed. Table 5-3 expresses the percentage change in mean RMS values between the leaking and non-leaking coefficients as a function of overlap. As the percentage overlap is increased, the percentage change in mean RMS values between the leaking and non-leaking coefficients decreases although visually, they appear the same.

Table 5-3: Percentage change in mean RMS values as a function of overlap

Overlap (%)	Mean RMS before leak	Mean RMS after leak	(%)Change of Mean RMS
5	0.84864	0.48778	42.5218
25	0.85794	0.52948	38.284
50	0.86201	0.54955	36.2478
75	0.86236	0.56443	34.5482

With reference to Table 5-3 and Fig. 5-9, an overlap of 5% is preferred for subsequent analysis considering that it has a percentage change of 42.52%; which is the highest in the table. This choice is motivated by assessing the nature of the signal (coefficient). At 5%, the amplitude and energy of all the plots are approximately the same. Based on this, choosing the highest percentage change is justifiable.

Case Study 2

5.3.4 Autocorrelation (small leak of 0.047 L/min)

The high performing lag, window size and overlap is now used for case study 2. It is employed for the smallest leak condition. Figure 5-10 shows the result of an autocorrelation analysis of pressure signals 1 and 2 with the introduction of a leak at the 200^{th} second using lag 1, window size of 200 data points and 5% overlap. With reference to Fig. 5-10, the results for pressure signal 1 and 2 are similar. This is probably because pressure signals 1 and 2 are chamber pressures. A change in pressure signal 1 is backed by a proportionate change in pressure signal 2.

In Table 5-4, the percentage change in mean RMS values between the leaking and non-leaking coefficients are shown. While a percentage change of 29.68 is obtained for pressure signal 1, a percentage change of 30.08 is obtained for pressure signal 2. Both changes are approximately equal and suggest the pressure signals are highly auto correlated. A high percentage change of about 30% for a leak of 0.047 L/min suggest the algorithm may likely detect leakages lower than 0.047 L/min.

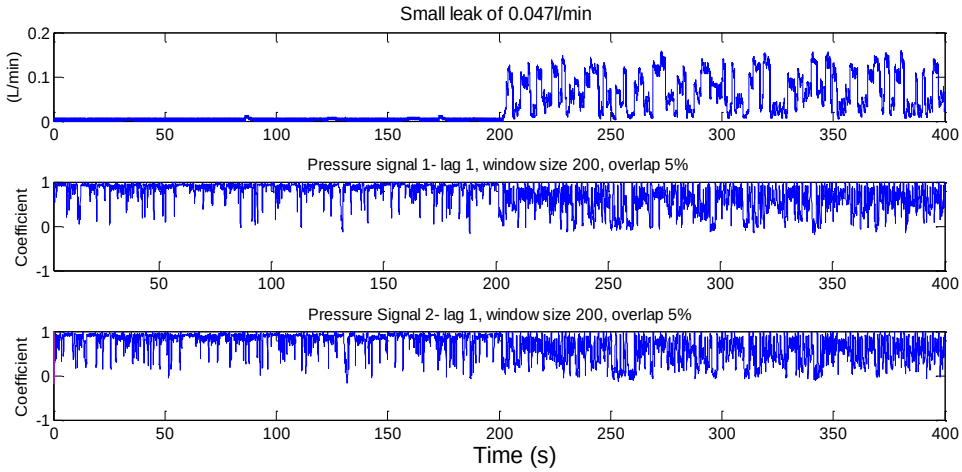

Figure 5-10: Autocorrelation results for pressure signals 1 and 2- mean small leak of 0.047 L/min using a window size of 200 data points, 5% overlap and lag 1.

Table 5-4: Percentage change in Mean RMS values as a function of small leak

Pressure signal	Mean RMS before leak	Mean RMS after leak	(%)Change of mean RMS
Pressure signal (*P1*)	0.86794	0.61028	29.6863
Pressure signal (*P2*)	0.83218	0.58183	30.0842

5.4 Results for Cross Correlation between Pressure Lines (valve controlled actuation system)

Cross correlation is used between pressure signals 1 and 2 shown in Fig. 5-5. As mentioned in chapter 4, both pressure signals are needed for implementing the cross correlation function. The cross correlation function is applied between both pressure data, producing a single coefficient for each window. These values are then plotted in time to show the behavior or dynamics of the cross correlation coefficients over the course of an experiment.

The windowing technique used is described in Section 4.5. It starts with assessing the effect of lag. This is achieved by varying the lag while the window size and overlap is held constant. The effect of the lag is observed and a high performing one is chosen and used for further analysis. The next step varies the window size while the overlap and preferred

lag is held constant. A high performing window size is chosen and finally the preferred window size and preferred lag is held constant while the overlap is varied. The preferred overlap is chosen. The preferred lag, window size and overlap are used for detecting the smallest internal leakage (case study 2) and for performing the sensitivity analysis.

5.4.1 Effect of Lag

Figure 5-11 show the result of the cross correlation analysis between pressure signals 1 and 2, with a leak occurring at about 200 seconds using lag 1, 4 and 10, window size of 200 data points and an overlap of 5%. By visual inspection or examination of the plots, all coefficients are within -1 and 1 which is due to normalization of the coefficients. There is a significant increase in the mean of the processed signal after 200 seconds for all three plots. This change coincides with the time the leak was introduced. Also, the variation or the number of spikes in the coefficients tends to decrease on the introduction of leak. These changes suggest pattern or feature for classification. Based on the above observations, one can conclude the algorithm is able to detect internal leakage.Increasing the lag from lag 1 to lag 4 and to lag 10, results to a slight reduction in the amplitudes of the non-leaking side of the signal (Before 200 seconds). The leaking side (after 200 seconds) also decreased slightly in amplitude and energy.

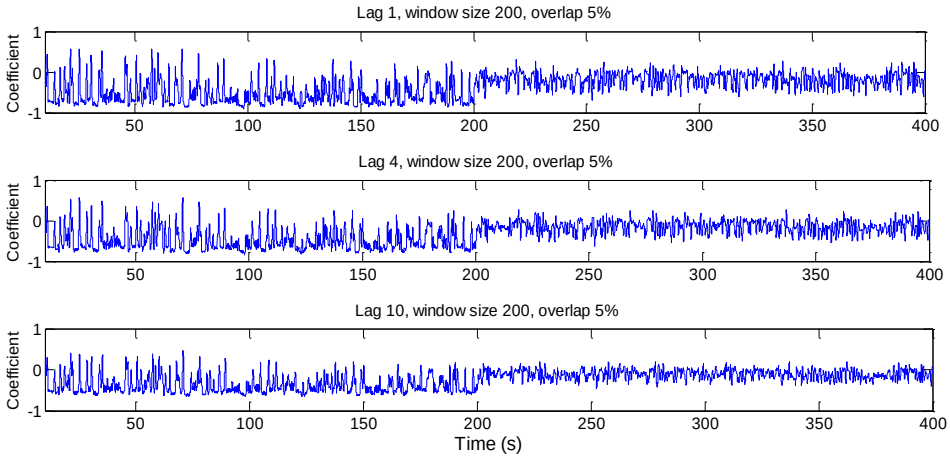

Figure 5-11: Cross Correlation of pressure signals 1 and 2- medium leak of 0.10 L/min- lag 1, lag 4, lag 10, window size 200, overlap 5%.

In Table 5-5, the percentage change in mean RMS values between the leaking and non-leaking coefficients is represented as a function of lag. As the lag increases, the percentage change increases. The percentage change for the shown lags (lag 1 to lag 10) is approximately within 65% and 67%. This implies, there is only a 2% difference as the lag varies from 1 to 10. This trend is apparent at higher lags up to 18 where the reverse begins to occur and the percentage change begins to reduce until lag 50 where the leaking and non-leaking coefficient becomes approximately equal and the percentage change in mean RMS values approaches zero. For Lags higher than 50, the mean coefficient of the leaking side becomes higher than those of the non-leaking sides. Following these considerations, lag 1 is chosen for subsequent analysis as increasing or decreasing the lag only creates a minimal change on the coefficient.

Table 5-5: Cross correlation coefficient as a function of lag.

Lag Value	Mean RMS before leak	Mean RMS after leak	(%)Change of Mean RMS
1	0.55308	0.194	64.9233
4	0.49802	0.16989	65.8859
8	0.42675	0.14403	66.2495
10	0.38874	0.12764	67.1665

5.4.2 Effect of Window Size

In this section, the preferred lag (lag 1) is used while the window size is varied. This is to enable us chose a high performing window size. Figure 5-12 show the result of the cross correlation analysis between pressure signals 1 and 2, with a leak occurring at about 200 seconds using window sizes of 100, 200, 400 data points, lag 1 and an overlap of 5%. The mean of the coefficients increases after 200 seconds. This mean change coincides with the time the leak was introduced to the test rig suggesting detection. More so, as the window size increases, the effective change between the leaking and non-leaking coefficients decreases.

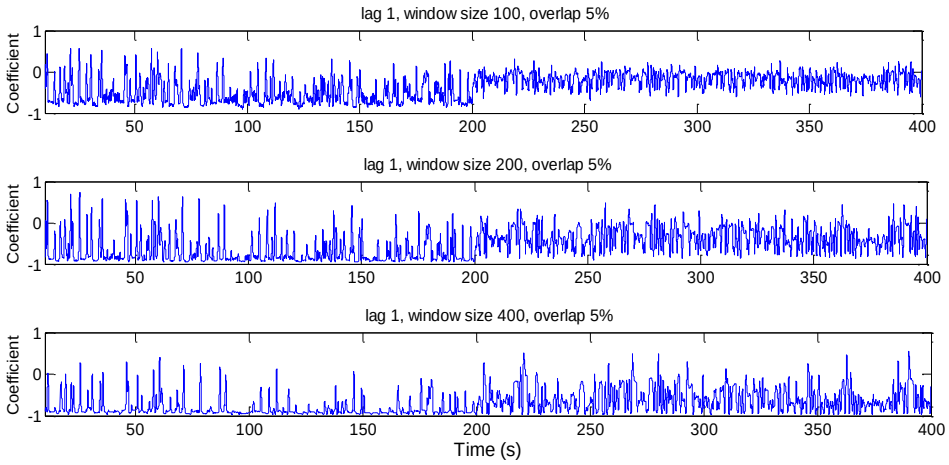

Figure 5-12: Correlation of pressure signals 1 and 2- medium leak of 0.10 L/min- lag 1, window size 100, 200, 400 and overlap 5%. As the window size increases, the percentage change in mean RMS values between the leaking and non-leaking coefficients decreases.

Window size of 100, 200 and 400 is shown although analyses for higher and lower window sizes were also performed. Table 5-6 expresses the percentage change in mean RMS values between the leaking and non-leaking coefficients as a function of window size. A linear relationship exists between the window size and the percentage change in mean RMS values. As the window size increases, the percentage change decreases. A window size of 100 data points resulted to a percentage change of 64.9% and a window size of 800 data point results to a change of 8.8%. This implies that using a smaller window size will aid the detection process though window sizes below 100 data points resulted to more noisy signals. Following these considerations, a window size of 100 data points is chosen for subsequent analysis.

Table 5-6: Percentage change in mean RMS values as a function of window size

Window size	Mean RMS before leak	Mean RMS after leak	(%)Change of Mean RMS
100	0.55308	0.194	64.9233
200	0.72248	0.36129	49.9926
400	0.82028	0.5928	27.7327
500	0.83743	0.65707	21.5326
600	0.85025	0.71425	15.995
800	0.86358	0.78726	8.8371

5.4.3 Effect of Overlap

The high performing lag and window size is used in this analysis to investigate the effect of overlap and obtain a high performing overlap. Figure 5-13 shows the result of the cross correlation analysis between the pressure signals 1 and with the introduction of leak at 200 seconds using overlaps of 5%, 25% and 50%; lag 1 and window size of 100 data points. The effect of the overlap on the cross correlation coefficient is readily seen as the mean of the coefficients significantly increases after 200 seconds. This mean change coincides with the time the leak was introduced to the test rig. A visual examination of the signal also reveals that as the overlap is increased from 5% through 50% and above, the signal becomes clearer and less noisy.

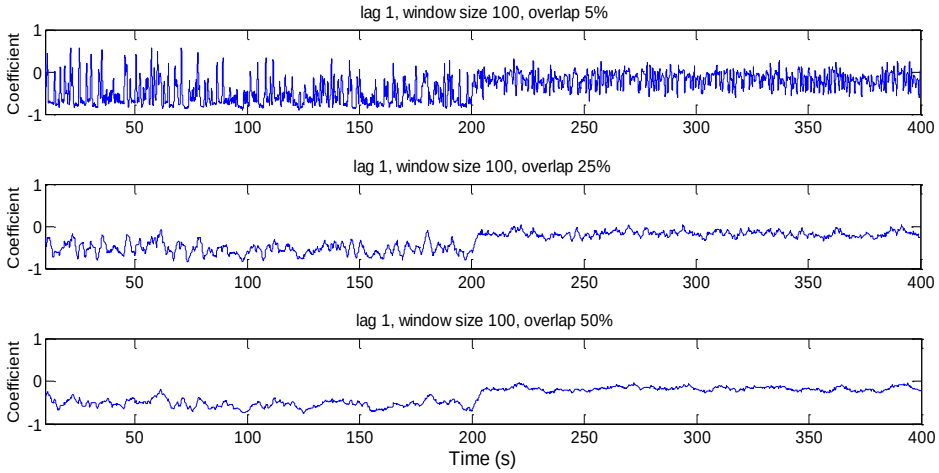

Figure 5-13: Cross correlation of pressure signals 1 and 2- Medium leak of 0.10 L/min; lag 1, window size 100, overlap 5%, 25%, 50%. Increasing the overlap, results to a clearer signal but has less effect on effective change between leaking and non-leaking coefficients

In Table 5-7, the percentage change in mean RMS values between the leaking and non-leaking coefficients is shown as a function of the overlap. As the overlap increases, the percentage change increases slightly. The percentage change for the shown overlaps (5%-75%) is approximately within 65% and 68%. This implies, there is only a 3% difference as the overlap varies from 5% to 75%. Hence, varying the overlap does not affect the detection process though increasing it would produce a clearer signal. Following these considerations, an overlap of 5% is chosen for subsequent analysis.

Table 5-7: Percentage change in mean RMS values as a function of the overlap

Overlap (%)	Mean RMS before leak	Mean RMS after leak	(%)Change of Mean RMS
5	0.55308	0.194	64.9233
25	0.53007	0.17848	66.3291
50	0.53106	0.17829	67.4275
75	0.54113	0.18923	67.5312

Case Study 2

5.4.4 Cross Correlation (small leak of 0.047 L/min)

The preferred lag, overlap and window size is used for the critical condition (case study 2). Figure 5-14 shows the result of the cross correlation analysis between pressure signals 1 and 2 with the introduction of leak at about 200 seconds using lag 1, window size of 100 data points and 5% overlap. The smallest leak of 0.047 L/min was simulated in the test rig. Visually the change is significant as the variation of the signal or spikes in the signal before the leak was introduced is higher compare to the variations or spikes after the leak was introduced and also a potential shift in the mean at about 200 seconds suggests the algorithm can detect leak as low as 0.047 L/min.

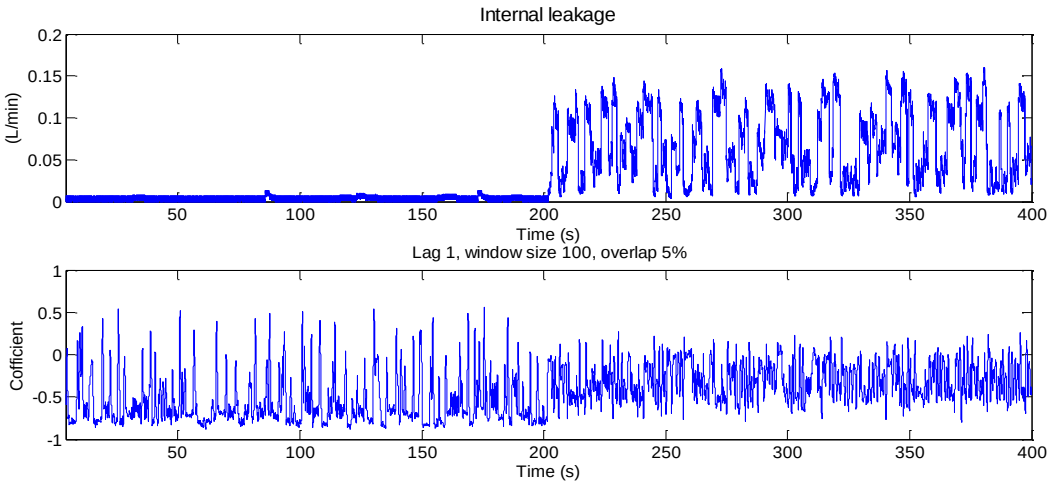

Figure 5-14: Cross correlation of pressure signals 1 and 2- small leak of 0.047 L/min; lag 1, window size 100, overlap 5%

Table 5-8 shows the percentage change in mean RMS values as a function of the smallest leak. A percentage change of 46.6% is obtained and implies the algorithm may successfully detect leakages smaller than 0.047 L/min.

Table 5-8: Percentage change in Mean RMS values as a function of small leak

Pressure signal	Mean RMS before leak	Mean RMS after leak	(%)Change of RMS
Pressure signal (*P1* and *P2*)	0.5851	0.31243	46.6027

5.5 Results for Cross Correlation between Control Signal and Piston Displacement

As illustrated in Chapter 4, two signals are needed for executing the cross correlation algorithm. In this section, control signal and piston displacement (Figure 4.6 and 4.7) is cross correlated. The cross correlation function is applied between both control signal and piston displacement data, producing a single coefficient for each window. These values are then plotted in time to show the behavior or dynamics of the cross correlation coefficients over the course of an experiment.

The windowing technique used is described in Section 4.5. It starts with assessing the effect of lag. This is achieved by varying the lag while the window size and overlap is held constant. The effect of the lag is observed and a high performing one is chosen and used for further analysis. The next step varies the window size while the overlap and preferred lag is held constant. A high performing window size is chosen and finally the preferred window size and preferred lag is held constant while the overlap is varied. The preferred overlap is chosen. The preferred lag, window size and overlap are used for detecting the smallest internal leakage (case study 2) and for performing the sensitivity analysis.

5.5.1 Effect of Lag

Figure 5-15 show the result of a cross correlation analysis between the control signal and piston displacement, with a leak occurring at about 200 seconds using lag 1, 20 and 30, window size of 200 data points and an overlap of 5%. By visual inspection or examination of the plots, all coefficients are within -1 and 0. Also, there is a significant increase in the mean of the processed signals at about 200 seconds and onwards. This change coincides with the time the leak was introduced suggesting detection. It is also observed that the signal gets less noisy as the lag increases.

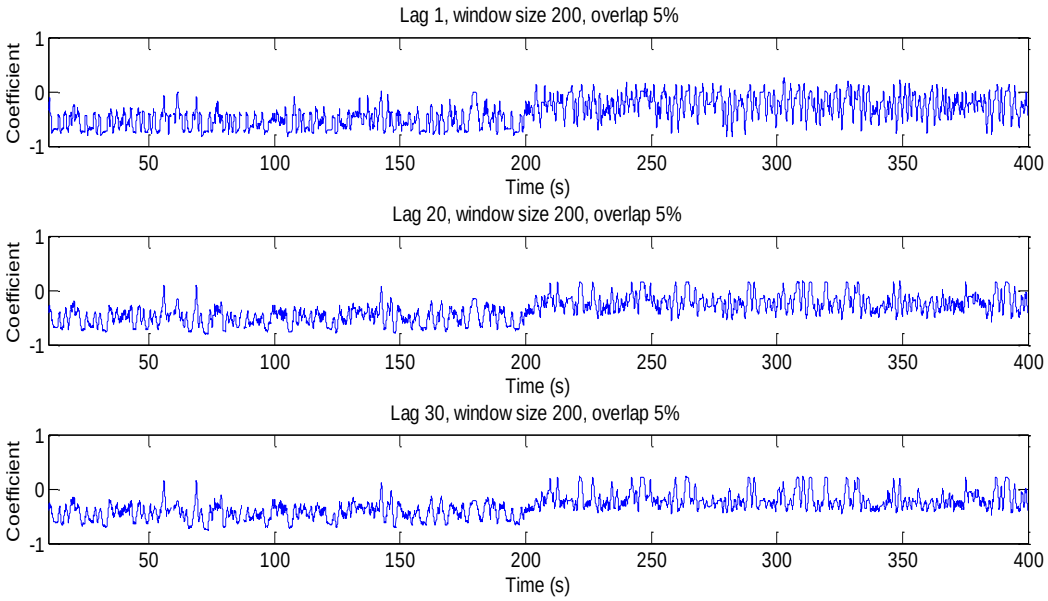

Figure 5-15: Effect of lag on cross correlation between control signal and piston displacement for a medium leak of 0.10 L/min, window size 200, and overlap 5%.

In Table 5-9, the percentage change in mean RMS values between the leaking and non-leaking coefficients is expressed as a function of lag. As the lag increases, the percentage change decreases though the effect is not significant. The percentage change from lag 1 to lag 30 is approximately within 55% and 48%. Following these, lag 1 is chosen for subsequent analysis. This phenomenon is apparent at higher lag values up to 60 when the leaking and non-leaking coefficient becomes approximately equal and the percentage change of mean RMS approaches zero.

Table 5-9: Percentage change in mean RMS values as a function of lag

Lag Value	Mean RMS before leak	Mean RMS after leak	(%)Change of Mean RMS
1	0.53511	0.24258	54.6671
15	0.52504	0.24347	53.6286
20	0.50145	0.24033	52.0728
25	0.47099	0.23497	50.1113
30	0.43613	0.22878	47.5438

5.5.2 Effect of Window Size

In this section, the high performing lag (lag 1) is used while the window size is varied. Figure 5-16 shows the result of the cross correlation analysis between control signal and piston displacement, with a leak occurring at about 200 seconds using window sizes of 100, 200, 400 data points, lag 1 and an overlap of 5%. The mean of the coefficients increases after 200 seconds. This mean change coincides with the time the leak was introduced to the test rig and suggests the detection of internal leakage.

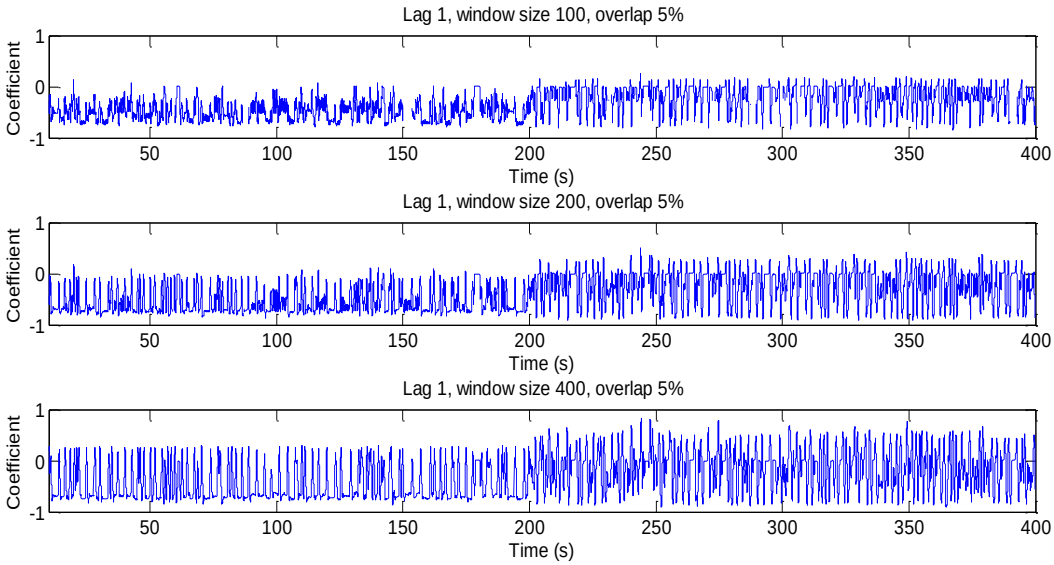

Figure 5-16: Effect of window size on cross correlation coefficient of control signal and piston displacement for a medium leak of 0.10 L/min, window size 100, 200, 400, Lag 1 and overlap 5%.

Window sizes of 100, 200 and 400 data points is shown though analyses for higher and lower window sizes were also performed. Visually, the variation in the coefficient increases as the window size is increased from 100 to 200 and to 400. This variation is apparent for both leaking and non-leaking sides of the signal. In Table 5-10, the percentage change in mean RMS values as a function of the window size is shown. As the window size increases, the percentage change in mean RMS values decreases. The lower the window size, the better the detection. However, a window size of 100 data points is chosen for subsequent analysis. This is to because the signal gets noisier and doesn't make any further sense as the window size increases.

Table 5-10: Percentage change in mean RMS values as a function of window size

Window size	Mean RMS before leak	Mean RMS after leak	(%)Change of Mean RMS
100	0.47124	0.22318	52.6398
200	0.5361	0.28111	47.5633
400	0.49834	0.32683	34.4167

5.5.3 Effect of Overlap

In this section, the preferred lag (lag 1) and window size (window size 100) is used while the overlap is varied to determine the high performing overlap. Figure 5-17 shows the result of the cross correlation analysis between the control signal and piston displacement, with the introduction of a leak at 200 seconds using overlaps of 5%, 10% and 25%; lag 1 and window size of 100 data points.

The mean of the coefficients significantly increases after 200 seconds. This mean change coincides with the time the leak was introduced to the test rig. A visual examination of the signal also reveals that, as the overlap is increased from 5% to 15% and above, the signals becomes clearer and less noisy.

In Table 5-11, the percentage change in mean RMS values between the leaking and non-leaking coefficient is presented as a function of the overlap. The percentage change in mean RMS values increases slightly as the overlap increases although the rate of increment is small. For the given overlap range (5% - 15%) the percent change varies from about 53% to 56%. A higher percentage would mean a better result. Analysis for higher overlaps was performed but the change is minimal and appears to converge to 60%. An overlap of 5% is chosen for subsequent analysis. This is so because any chosen overlap will not create much of a difference. The criteria for selection would depend on if a clearer signal is desired. For clearer and less noisy results, higher overlaps may be used.

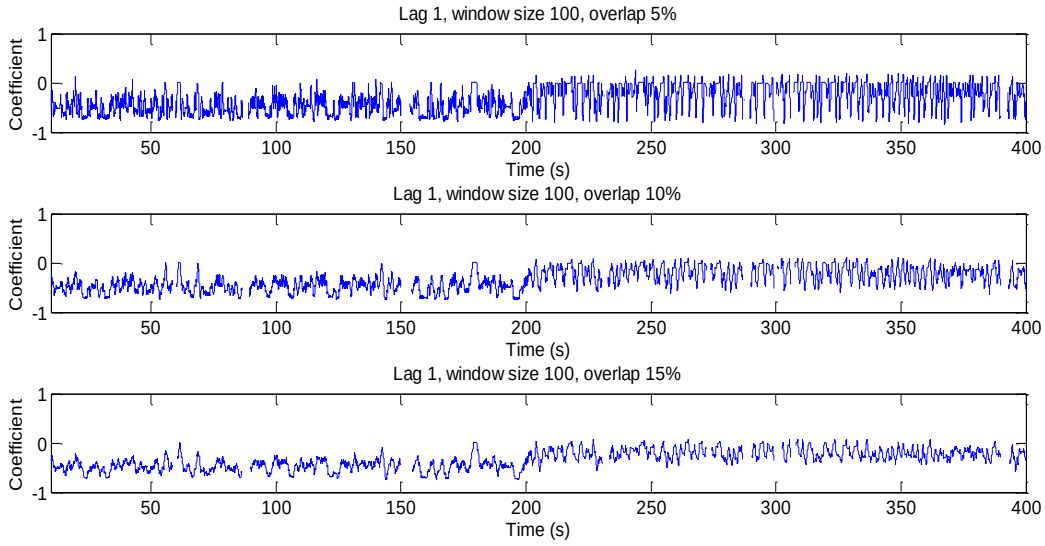

Figure 5-17: Effect of overlap on cross correlation coefficient of control signal and piston displacement for a medium leak of 0.10 L/min, window size 200, overlap 5%, 10%, 15% and lag 1.

Table 5-11: Percentage change in mean RMS values as a function of overlap.

Overlap (%)	Mean RMS before leak	Mean RMS after leak	(%)Change of Mean RMS
5	0.47124	0.22318	52.6398
10	0.47023	0.20969	55.4078
15	0.47023	0.20704	55.970
25	0.47152	0.20547	56.424
50	0.47439	0.20477	56.8345
75	0.47456	0.19978	57.9019

Case Study 2

5.5.4 Cross Correlation (small leak 0.047 L/min)

The preferred lag, window size and overlap is used for the smallest leak condition (case study 2). Figure 5-18 shows the result of the cross correlation analysis between control signal and piston displacement with the introduction of a leak at about 200 seconds using lag 1, window size of 100 data points and 5% overlap. The smallest leak of 0.047 L/min was simulated in the test rig. Visually, the change is significant as the mean of the signal increases after 200 seconds being the time the leak was introduced. Table 5-12 shows the percentage change in mean RMS values as a function of the smallest leak. A percentage change of 40.45% is obtained and implies the algorithm will successfully detect leakages smaller than 0.047 L/min.

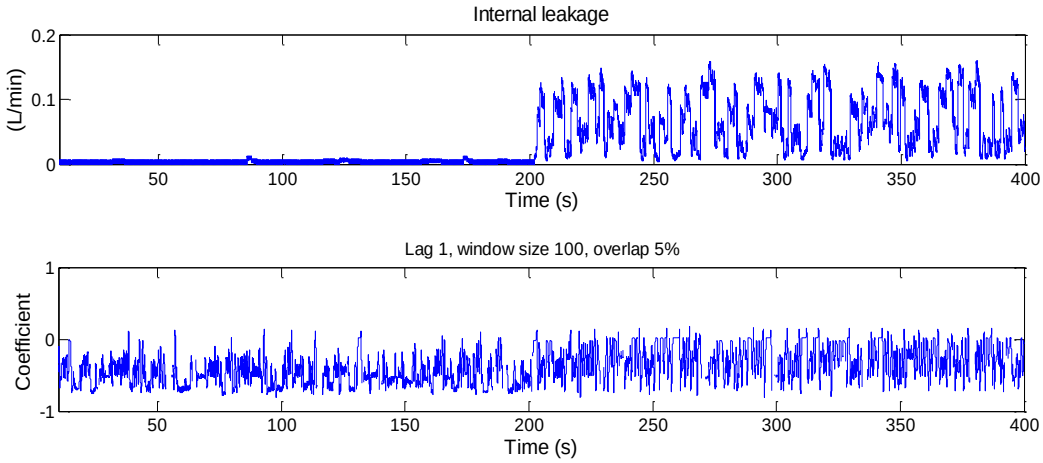

Figure 5-18: Cross correlation of piston displacement and control signal; small leak of 0.047 L/min; Lag 1, window size 100; overlap 5%.

Table 5-12: Percentage change in mean RMS values as function of small leak

Signal	Mean RMS before leak	Mean RMS after leak	(%)Change of RMS
Piston displacement (*X*) and control signal (*U*)	0.37923	0.2258	40.4587

5.6 Ratio of Metric Lengths Results (valve controlled actuation system)

Detecting internal leakage faults by calculating the ratio of the metric length of the same time sequence requires either of the chamber pressures (pressure signal 1 or pressure signal 2). As explained in Chapter 4, the ratio of metric lengths of the signal quantizes the complexity in the signal. It has the ability to detect patterns, trends and changes in a signal. The pressure signal is divided into windows and the algorithm is applied on it producing a single number for each window. These values are then plotted in time to show the behavior or dynamics of the ratio of metric lengths over the course of an experiment.

The windowing technique used is described in Section 4.5. It starts with assessing the effect of lag. This is achieved by varying the lag while the window size and overlap is held constant. The effect of the lag is observed and a high performing one is chosen and used for further analysis. The next step varies the window size while the overlap and preferred lag is held constant. A high performing window size is chosen and finally the preferred window size and preferred lag is held constant while the overlap is varied. The preferred overlap is chosen. The preferred lag, window size and overlap are used for detecting the smallest internal leakage (case study 2) and for performing the sensitivity analysis.

5.6.1 Effect of Lag

Figure 5-19 shows the results of the ratio of metric lengths computation using pressure signal 1 with a leak occurring at about 200 seconds using lag ratios of 83:3, 57:3 and 43:3; window size of 500 data points and an overlap of 5%. By visual examination of the plots, there is a significant increase in the mean of the processed signals after 200 seconds. Also, the processed signal becomes noisier after 200 seconds. These changes coincide with the time the leak was introduced.

In Table 5-13, the percentage change in mean RMS values between the leaking and non-leaking fractal numbers (ratios of metric lengths) is shown as a function of the lag ratio. As the lag ratio decreases, the percentage change in mean RMS values decreases. As such, the higher the lag ratio, the better the detection. The preferred lag ratio is 83:3 and would be used for subsequent analysis.

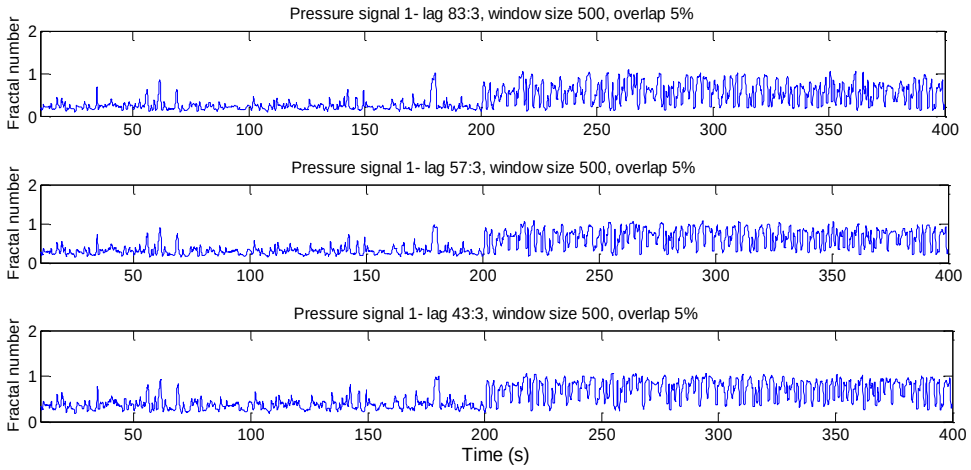

Figure 5-19: Effect of lag on ratio of metric lengths of pressure signal 1 for a medium leak of 0.10 L/min, window size 500, and overlap 5%. Lag 83:3, 57:3, and 43:3.

Table 5-13: Percentage change in mean RMS values as a function of lag.

Lag Value	Mean RMS before leak	Mean RMS after leak	%Change of Mean RMS
83:3	0.23777	0.56562	137.8815
57:3	0.30569	0.6558	114.5281
43:3	0.3727	0.71746	92.5011
28:3	0.49803	0.79586	59.8004
23:3	0.56322	0.83099	47.5434
16:3	0.68361	0.88104	28.8808

5.6.2 Effect of Window Size

In this section, the high performing lag ratio (83:3) is used while the window size is varied. Figure 5-20 shows the result of the ratio of metric lengths computation using pressure signal 1 with a leak occurring at about 200 seconds using window sizes of 100, 300, 500 data points, lag ratio 83:3 and an overlap of 5%. By visual examination of the plots, there is a significant increase in the mean of the processed signals after 200

seconds. More so, the number of spikes in the signal increases after 200 seconds. These changes coincide with the time the leak was introduced.

As the window size increases (100-300-500), the processed signals become clearer and less noisy but the effective change between the leaking and non-leaking ratio of metric lengths decreases. In Table 5-14, the percentage change in mean RMS values between the leaking and non-leaking ratio of metric lengths is shown. As the window size increases, the percentage change in mean RMS values increases until the window size is 500 where it reverses and starts decreasing. A window size of 500 data points is preferred for subsequent analysis. For a window size of 500 data points, the percentage change in mean RMS values is about 137%; a change very high compared to previous methods discussed.

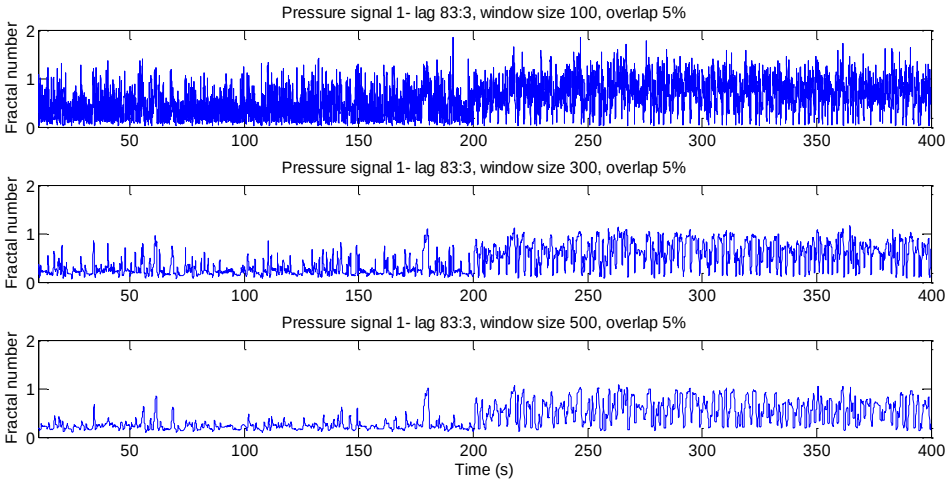

Figure 5-20: Ratio of metric lengths of pressure signal 1 for a medium leak of 0.10 L/min, window size 100, 300, 500, overlap 5%. Lag 83:3.

Table 5-14: Percentage changes in mean RMS values as a function of window size.

Window size	Mean RMS before leak	Mean RMS after leak	(%)Change of Mean RMS
100	0.38738	0.71532	84.653
300	0.26426	0.62306	135.7769
500	0.23777	0.56562	137.8815
800	0.22494	0.51032	126.8743
1000	0.2204	0.48529	120.1836
1200	0.2175	0.46497	113.7735

5.6.3 Effect of Overlap

In this section, the preferred lag (83:3) and window size (500 data points) is used while the overlap is varied to determine the high performing overlap. Figure 5-21 shows the results of the ratio of metric lengths computation using pressure signal 1with a leak occurring at about 200 seconds using overlaps of 5%, 25% and 50%; window size of 500 data points and a lag ratio of 83:3. By visual examination of the plots, there is a significant increase in the mean of the processed signals after 200 seconds. More so, the number of spikes in the signal increases after 200 seconds. These changes coincide with the time the leak was introduced. Also, as the overlap increases, the processed signals becomes clearer and less noisy. In Table 5-15, the percentage changes in mean RMS values between the leaking and non-leaking fractal numbers (ratios of metric lengths) are shown. As the overlap increases, the percentage change in mean RMS values decreases slightly. An overlap of 5% is employed for subsequent analysis as it has the highest percentage change of mean RMS values.

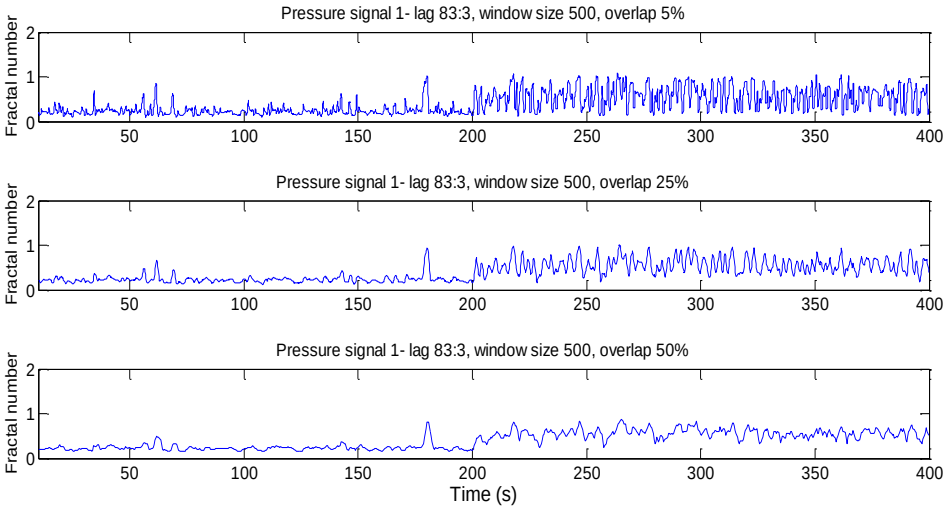

Figure 5-21: Effect of overlap on the ratio of metric lengths (fractal number) of pressure signal 1 for a medium leak of 0.10 L/min, window size 500, overlap 5%, 25% and 50%,

Table 5-5-15: Percentage change in mean RMS values as a function of overlap.

Overlap (%)	Mean RMS before leak	Mean RMS after leak	(%)Change of Mean RMS
5	0.23777	0.56562	137.8815
25	0.24031	0.56968	137.0634
50	0.24014	0.5617	133.9072

5.7 Ratio of Metric Lengths (small leak of 0.047 L/min)

The preferred lag, window size and overlap are used for detecting the smallest leak conditions (case study 2). Figure 5-22 shows the result of the ratio of metric lengths computation using both chamber pressure signals with the introduction of leak (0.047 L/min) at about 200 seconds using lag 83:3, window size of 500 data points and 5% overlap. By visual examination, the mean of the signal increases after 200 seconds, being the time the leak was introduced. The result depicts the algorithm is able to detect a small leak of 0.047 L/min. In Table 5-16, the percentage change in mean RMS values between the leaking and non-leaking ratio of metric lengths is shown. While a percentage change

of 97.2814% is obtained for pressure signal 1, a percentage change of 84.2918% is obtained for pressure signal 2. Both changes are close in range and suggest the pressure signals are highly auto-correlated.

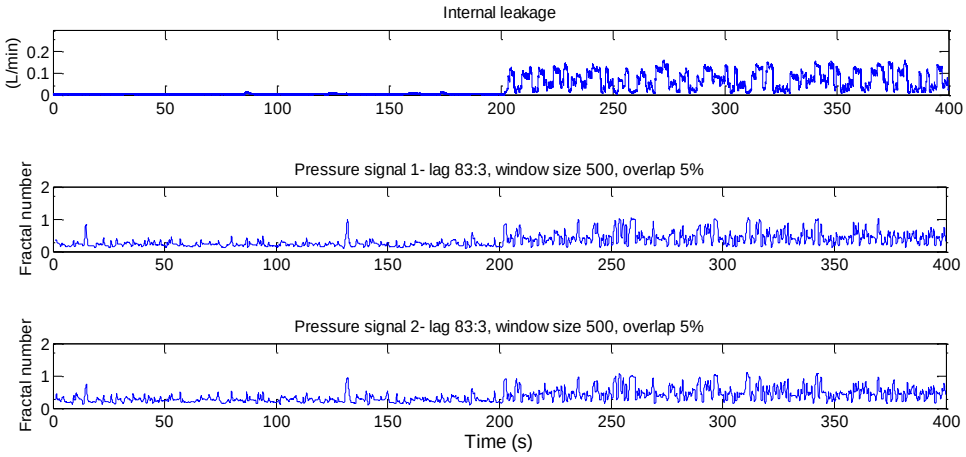

Figure 5-22: Ratio of metric lengths of pressure signals 1 and 2 for a small leak of 0.047 L/min, window size of 500 data points, overlap 5% and lag 83:3.

Table 5-16: Percentage change in mean RMS values as a function of small leak.

Pressure signal	Mean RMS before leak	Mean RMS after leak	(%)Change of Mean RMS
Pressure signal (*P1*)	0.22579	0.44544	97.2814
Pressure signal (*P2*)	0.26083	0.48069	84.2918

Case Study 3

5.8 Sensitivity Analysis (VCA)

The sensitivity analysis for various leaks (0.047 L/min-0.5 L/min) and load is performed using all three algorithms and shown in Figs. 5-23, 5-24, 5-25, 5-26, 5-27 and 5-28 for valve controlled actuation system.

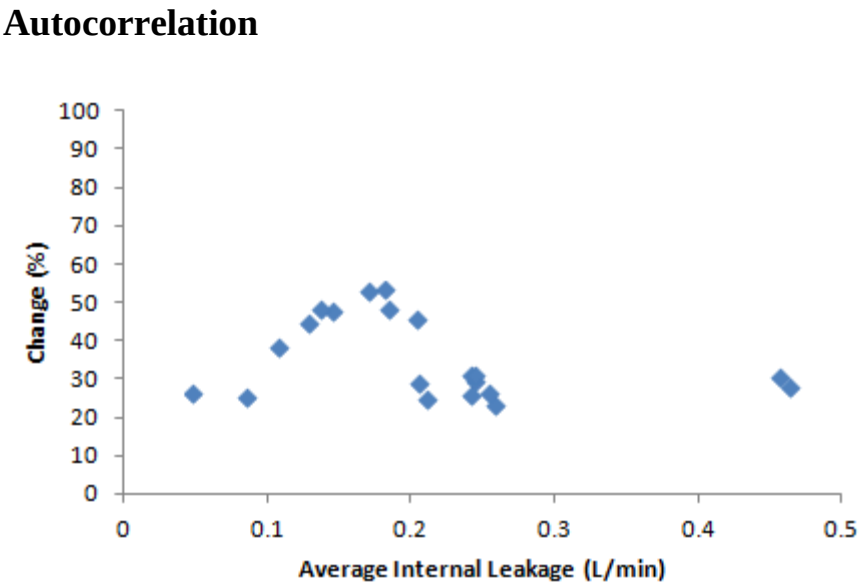

Figure 5-23: Sensitivity of autocorrelation coefficient of pressure signal 1 to the severity of leak simulated.

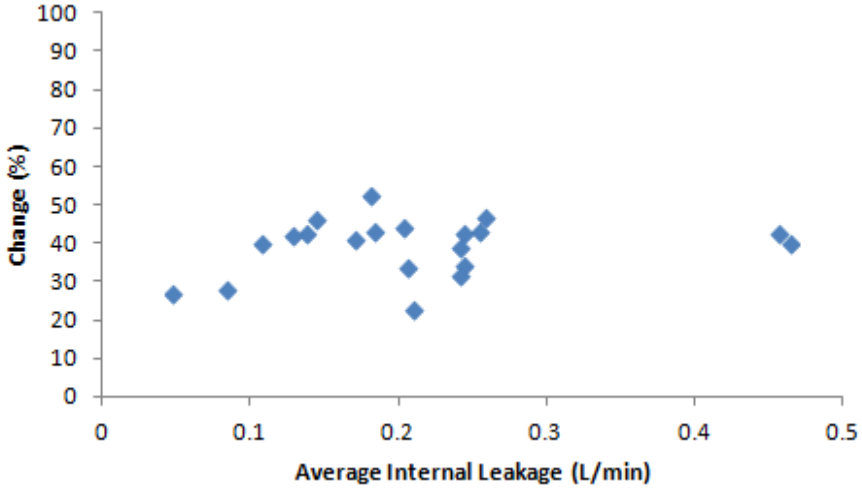

Figure 5-24: Sensitivity of autocorrelation coefficient of pressure signal 2 to the severity of leak simulated.

Cross correlation between Pressure Lines

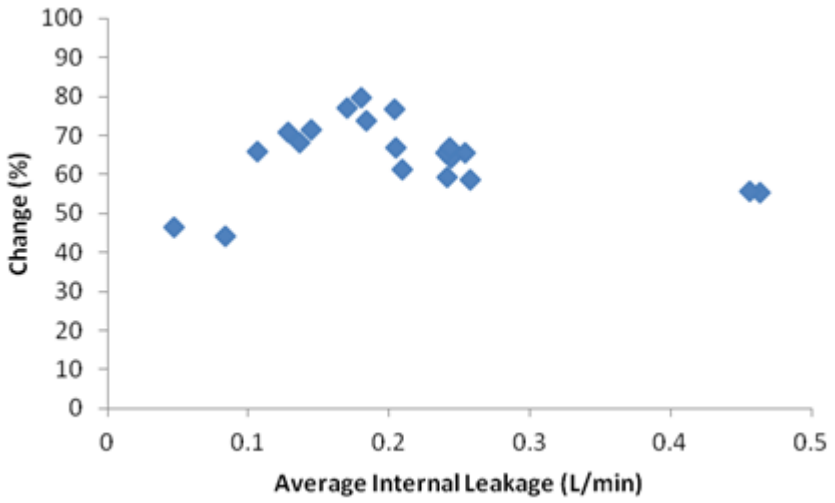

Figure 5-25: Sensitivity of the cross correlation coefficient to the severity of the leak introduced.

Cross Correlation between Control Signal and Piston Displacement

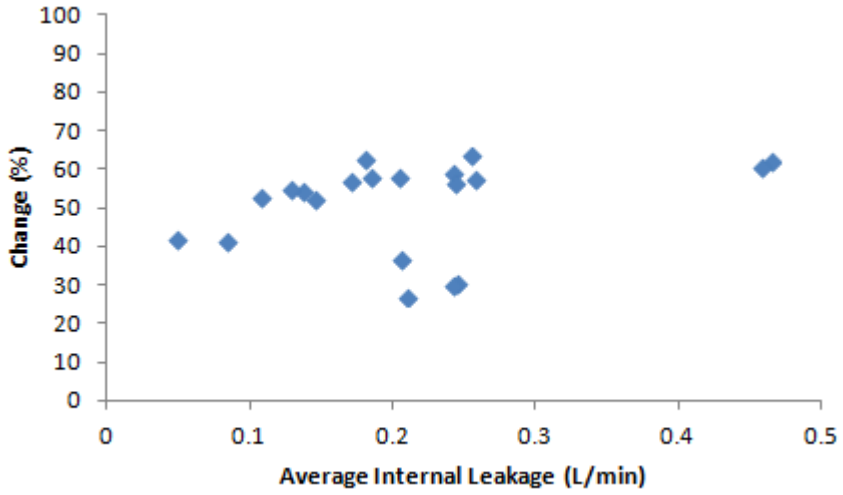

Figure 5-26: Sensitivity of cross correlation coefficient between control signal and piston displacement to the severity of leak simulated.

Ratio of metric lengths

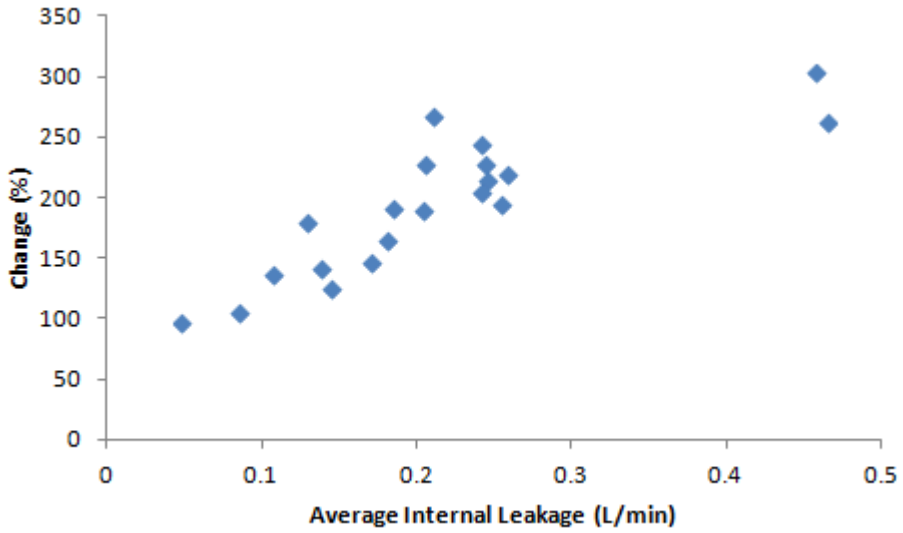

Figure 5-27: Sensitivity of ratio of metric lengths of pressure signal 1 to the severity of leak simulated.

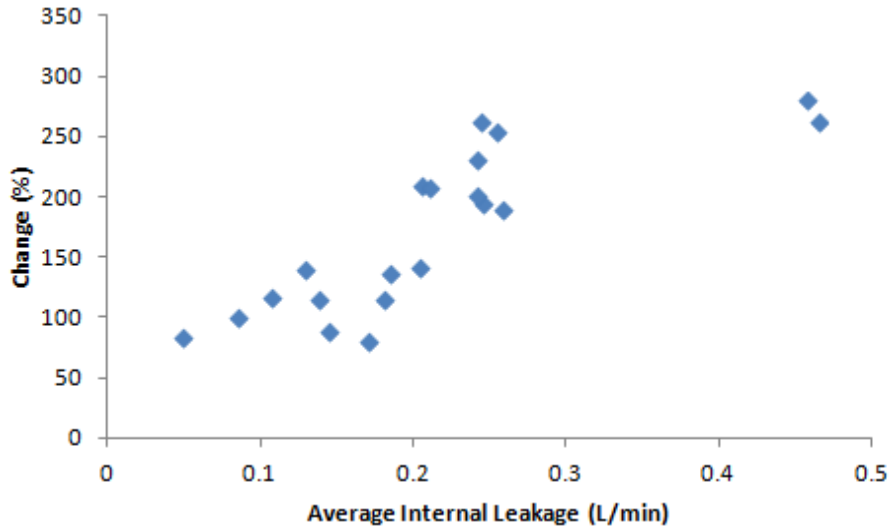

Figure 5-28: Sensitivity of ratio of metric lengths of pressure signal 2 to the severity of leak simulated.

Discussions

Considering the plots above, the following observations is made:

Either Pressure signal 1 or 2 can be successfully used with the autocorrelation function for detection purposes (Figures 5-23 and 5-24). As the severity of the leak increases from 0.047 L/min to about 0.55 L/min, the percentage change in mean RMS values between the leaking and non-leaking coefficient increases over time. This trend is also seen in the other algorithms (Figures. 5-25, 5-26, 5-27 and 5-28) but more significant when the ratio of metric lengths of pressure signal is employed.

For all the tests performed, autocorrelation of pressure signals shows a change in the range of 19%-50% (Figures 5-23 and 5-24), cross correlation of pressure signals shows a change in the range of 25%-75% (Figure 5-25)., cross correlation of piston displacement and control signal shows a change in the range of 25%-63% (Figure 5-26) and the ratio of metric lengths of pressure signals shows a change in the range of 84%-300% (Figures 5-27 and 5-28). Following these, one can say the ratio of metric lengths of pressure signals is more sensitive compared to the other methods. Its lower sensitivity range of about 84% shows it has the greater tendency to detect leakages lower than 0.047 L/min compared to its counterparts.

More so, the close range results obtained for autocorrelation of pressure signals 1 and 2 (Figures 5-23 and 5-24) and ratio of metric lengths of pressure signals 1 and 2 (Figures 5-27 and 5-28) suggests a correlation between the chamber pressures. Table 5-17 summarizes the sensitivity results.

Table 5-17: Summary: Valve Controlled Actuation System

Algorithms	Sensitivity range
Cross Correlation (Pressure signals)	25%-75%
Cross Correlation (Piston displacement and control signal)	20%-63%
Autocorrelation	19%-50%
Ratio of metric lengths concept	84%-300%

5.9 Summary

All three methods can be successfully used to diagnose faults due to internal leakage for the valve controlled actuation system. Valve controlled actuation system showed a percentage change in the range of 30%-300% for all test. Using this technique, internal leakages, in the range of 0.047-0.5 L/min, was detected regardless of the type of loading condition used.

Autocorrelation of pressure signal, cross correlation of pressure signals and cross correlation of piston displacement and control signal was found to perform well at window sizes in the range of 100-200 data points, overlap of 5% and lag 1. The ratio of metric lengths of pressure signals gets better as the lag ratio increases and window size decreases. It performs well at a window size of 500 data points and lag ratio of 83:3.

The autocorrelation and cross correlation coefficient decreases as internal leakage is introduced at about 200 seconds. This is believed to be due to the fact that internal leakage affects the dynamics of the signal. The randomness in the signal increases after the leakage is introduced and the signal becomes less correlated. Similarly, the ratio of metric lengths of the signal increases after the introduction of internal leakage to the system. This is due to the fact that the randomness in the signal increases at this time.

CHAPTER 6

RESULTS USING ELECTROHYDROSTATIC ACTUATION SYSTEM

6 RESULTS USING ELECTROHYDROSTATIC ACTUATION SYSTEM

Introduction

This section shows the results of implementing all three detection methods described in Chapter 4 on an electrohydrostatic actuation system. It also highlights the effect of varying the window size, lag and overlap on the processed signals.. Three case studies are considered.

1. Case study 1: An electrohydrostatic actuation system is excited with a sinusoidal input signal (amplitude: -3 V to 3 V) under a no-load condition. After 90 seconds of operation, a medium internal leakage having a mean value of 1.2 L/min is introduced and the system is allowed to run for a total of 180 seconds.

2. Case study 2: An electrohydrostatic actuation system is excited with a sinusoidal input signal (amplitude: -3 V to 3 V) under a no-load condition. After 90 seconds of operation, a small internal leakage having a mean value of 0.98 L/min is introduced and the system is allowed to run for a total of 180 seconds.

3. Case study 3: An electrohydrostatic actuation system is excited with a sinusoidal input signal (amplitude: -3 V to 3 V) under load and no-load conditions, for different severity of leaks. The system is allowed to run for a total of 180 seconds. Internal leakage in the range of 0.77 L/min to 1.63 L/min is introduced at about half of the total run time. This case study is used to evaluate the sensitivity or responsiveness of the algorithm to different levels of internal leakage.

6.1 Autocorrelation Results (EHA)

The autocorrelation function is performed on both chamber pressure data. The windowing technique described in Section 4.5 is used starting with assessing the effect of lag. This is achieved by varying the lag while the window size and overlap is held constant. The effect of the lag is observed and a high performing one is chosen and used for further analysis. The next step varies the window size while the overlap and preferred lag is held constant. A high performing window size is chosen and finally the preferred window size and

preferred lag is held constant while the overlap is varied. The preferred overlap is chosen. The preferred lag, window size and overlap are used for detecting the smallest internal leakage (case study 2) and for performing the sensitivity analysis.

6.1.1 Effect of Lag

The autocorrelation function is applied to the pressure data, producing a single coefficient for each window. These values are then plotted in time to show the behavior or dynamics of the autocorrelation coefficients over the course of an experiment. Figure 6-1 shows the result of an autocorrelation analysis on pressure signal 1, with a leak occurring at about 90 seconds using lag 1, 2 and 4, window size of 200 data points and an overlap of 10%. There is a decrease in the autocorrelation coefficients at about the 90^{th} second for lag 1, 2 and 4. This change coincides with the time the leak was introduced. Hence, the dynamics of the autocorrelation coefficients suggest autocorrelation function is able to perform fault detection. In Table 6-1, the percentage change in mean RMS values between the leaking and non-leaking coefficients is shown as a function of lag. As the lag increases, the percentage change in mean RMS values decreases. A higher percentage would mean a better detection process. As such, for subsequent analysis a lag of 1 is preferred.

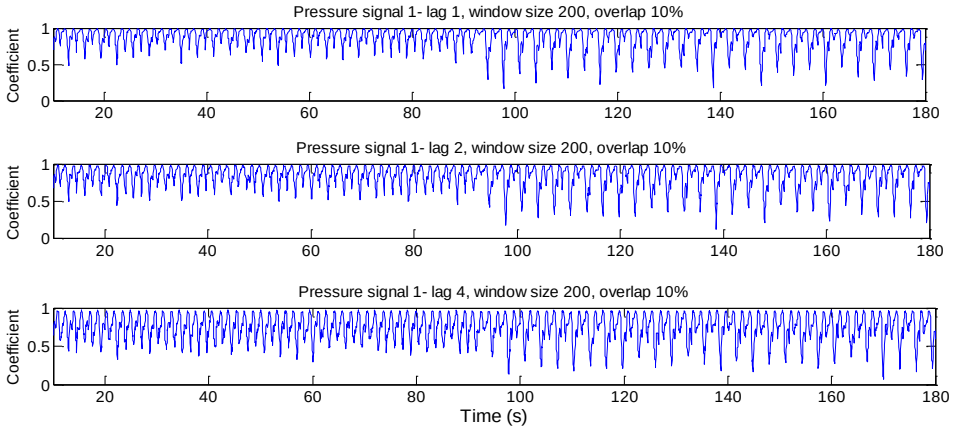

Figure 6-1: Effect of lag on autocorrelation coefficient for a mean leak of 1.2 L/min, window size of 200 data points and 10% overlap.

Table 6-1: Percentage change in mean RMS values as a function of lag.

Lag Value	Mean RMS before leak	Mean RMS after leak	(%)Change of Mean RMS
1	0.89187	0.8546	4.1782
2	0.85531	0.82532	3.5059
4	0.76656	0.75359	1.6931

6.1.2 Effect of Window Size

Here, the preferred lag (lag 1) is used while the window size is varied and the overlap is held constant. This is to enable us choose a high performing window size. Figure 6-2 shows the result of an autocorrelation analysis of pressure signal 1 with the introduction of a leak at the 90^{th} second using window sizes of 100, 200 and 300 data points; lag 1 and 10% overlap. By visual examination of the plots, there is a decrease in the coefficients after 90 seconds. More so, the number of spikes in the processed signal increases after 90 seconds. However, the signal becomes less noisy as the window size increases. These changes coincide with the time the leak was introduced. As the window size increases, the effective change between the leaking and non-leaking coefficients decreases.

In Table 6-2, the percentage change in mean RMS values between the leaking and non-leaking coefficients is shown as a function of window size. As the window size increases, the percentage change in mean RMS values decreases. A window size of 200 data points is preferred for subsequent analysis.

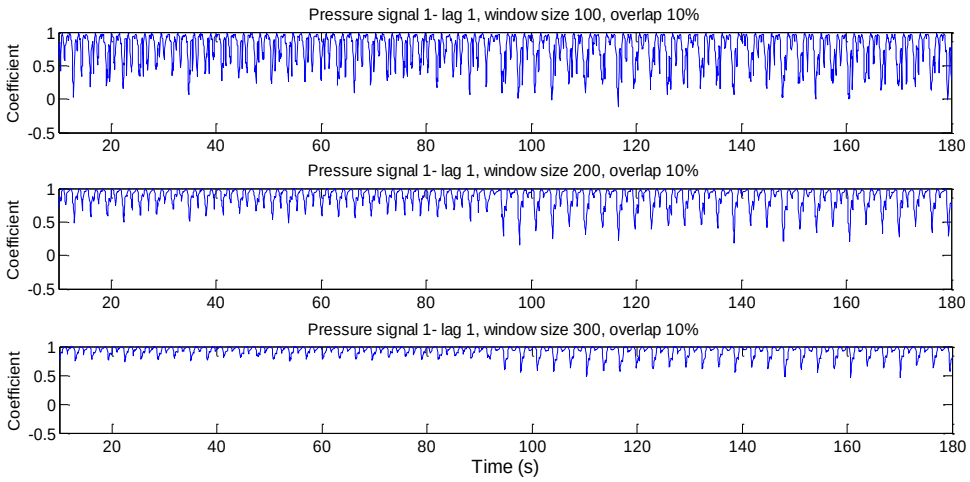

Figure 6-2: Effect of window size on autocorrelation coefficient of pressure signal 1, Medium leak of 1.2 L/min, using window sizes of 100, 200 and 300 data points, lag 1 and 10% overlap

Table 6-2: Percentage change in mean RMS as a function of window size

Window size	Mean RMS before leak	Mean RMS after leak	(%)Change of Mean RMS
100	0.79881	0.75596	5.3632
200	0.89187	0.8546	4.1782
300	0.94071	0.91445	2.7913

6.1.3 Effect of Overlap

The preferred lag (lag 1) and window size (200 data points) is used while the overlap is varied. This is to enable us choose a high performing overlap. Figure 6-3 shows the result of an autocorrelation analysis of pressure signal 1 with the introduction of leak at the 90th second using overlaps of 10%, 20% and 50%; lag 1 and window size of 100 data points.

By visual examination of the plots, there is a decrease in the mean of the processed signals after 90 seconds. More so, the number of spikes in the signal increases after 90 seconds. These changes coincide with the time the leak was introduced suggesting detection. In Table 6-3, the percentage change in mean RMS values between the leaking and non-

leaking coefficients is shown. As the overlap increases, the percentage change in mean RMS values decreases slightly. An overlap of 10% is preferred for subsequent analysis.

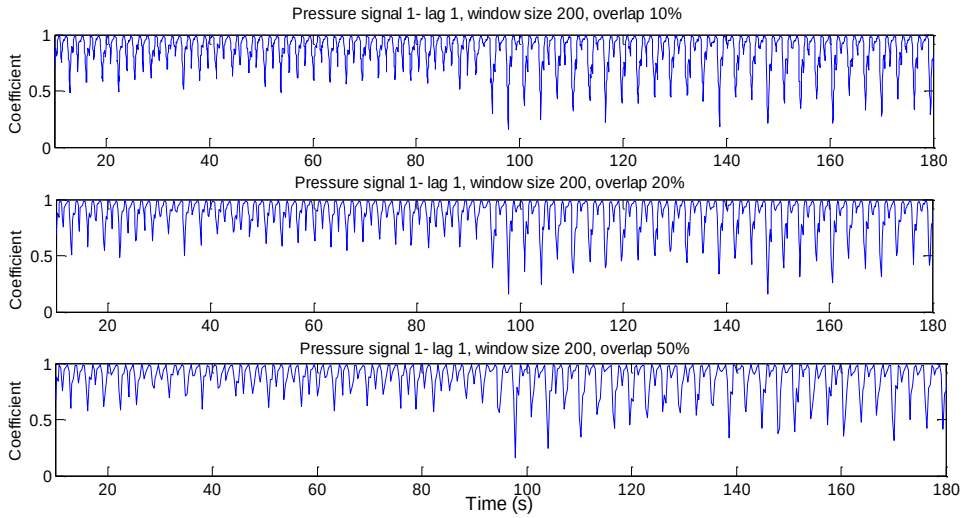

Figure 6-3: Effect of overlap on autocorrelation coefficient for pressure signal 1; Medium leak of 1.2 L/min, overlap of 10%, 20% and 50% using a window size of 200 data points and lag 1

Table 6-3: Percentage change in mean RMS as a function of overlap

Overlap (%)	Mean RMS before leak	Mean RMS after leak	%Change of Mean RMS
10	0.89187	0.8546	4.1782
25	0.8948	0.86186	3.6823
50	0.89571	0.86513	3.4143

Case Study 2

6.1.4 Autocorrelation (small leak of 0.98 L/min)

The high performing lag, window size and overlap is now used for case study 2. It is employed for detecting the smallest leak conditions. Figure 6-4 shows the result of an autocorrelation analysis of pressure signals 1 and 2 with the introduction of a leak at 90 seconds using lag 1, window size of 200 data points and 10% overlap. There is a change in the signal after 90s suggesting the occurrence of an event (detection). The results for pressure signal 1 and 2 are similar. This is because pressure signals 1 and 2 are chamber pressures. A change in pressure signal 1 is backed by a proportionate change in pressure signal 2. In Table 6-4, the percentage change in mean RMS values between leaking and non-leaking coefficient is shown. The percentage change in mean RMS for pressure signal 1 and 2 are 2.1% and 2.5% respectively. Lower leakages may not be detectable since the percentage changes are relatively low

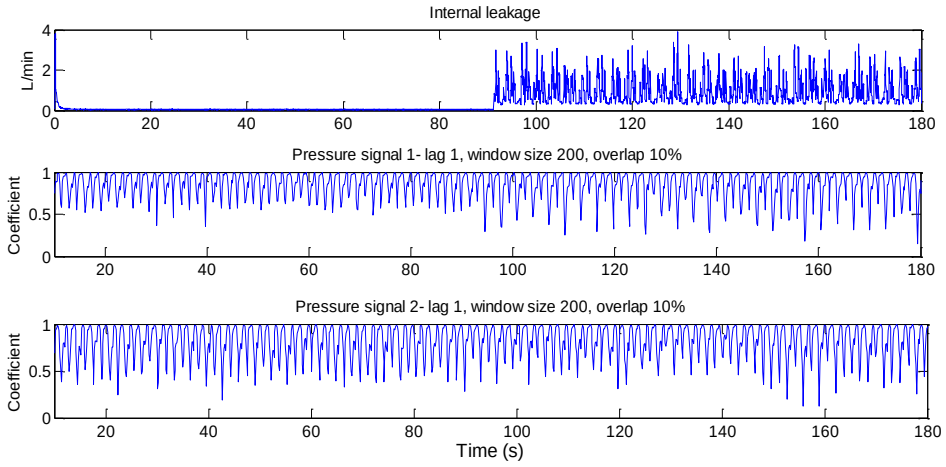

Figure 6-4: Autocorrelation for pressure signals 1 and 2; small leak of 0.98 L/min using a window size of 200 data points, 10% overlap and lag 1.

Table 6-4: Percentage change in mean RMS as a function of small leak

Pressure signal	Mean RMS before leak	Mean RMS after leak	(%)Change of Mean RMS
Pressure signal (P1)	0.87124	0.85269	2.1287
Pressure signal (P2)	0.82239	0.84373	2.5951

6.1.5 Sensitivity Analysis

Figure 6-5 shows the sensitivity analysis for the autocorrelation function. Several tests were performed using leakage of different severity. The sensitivity of the leak approximately increases as the severity of the leak increases. While there is no significant trend the sensitivity is between 0% and 11%. This implies that the maximum change obtainable for this range of leak (0.77 L/min-1.63 L/min) is 11%.

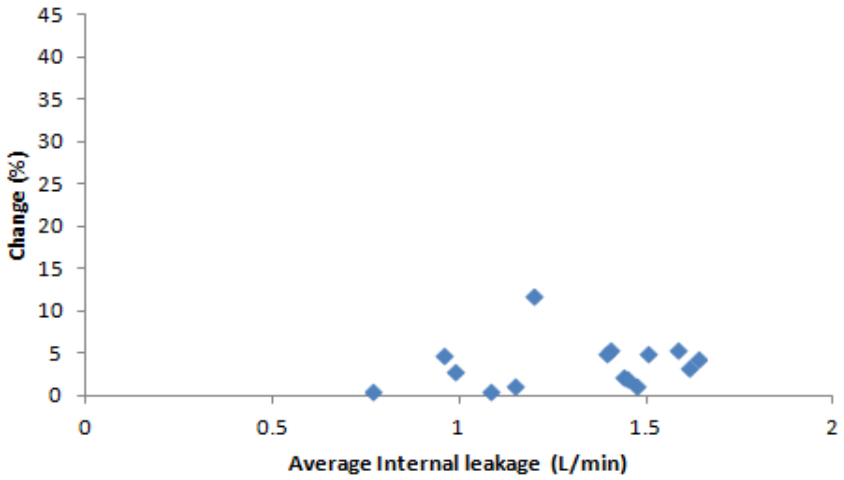

Figure 6-5: Sensitivity of autocorrelation coefficient (pressure signal 1 to the severity of internal leakage simulated.

6.2 Results for Cross Correlation between Pressure Signals (EHA)

Cross correlation is used between pressure signals 1 and 2 (Fig. 4-9). As mentioned in chapter 4, both pressure signals are needed for implementing the cross correlation function. The cross correlation function is applied between both pressure data, producing a single coefficient for each window. These values are then plotted in time to show the behavior or dynamics of the cross correlation coefficients over the course of an experiment.

The windowing technique used is described in Section 4.5. It starts with assessing the effect of lag. This is achieved by varying the lag while the window size and overlap is held constant. The effect of the lag is observed and a high performing one is chosen and used for further analysis. The next step varies the window size while the overlap and preferred lag is held constant. A high performing window size is chosen and finally the preferred window size and preferred lag is held constant while the overlap is varied. The preferred overlap is chosen. The preferred lag, window size and overlap are used for detecting the smallest internal leakage (case study 2) and for performing the sensitivity analysis. The choice of window size, lag and overlap is based on established balance between performance, flexibility and meaningfulness of results.

6.2.1 Effect of Lag

Figure 6-6 shows the result of a cross correlation analysis between pressure signals 1 and 2, with a leak occurring at about the 90^{th} second using lag 10, 12 and 16, window size of 100 data points and an overlap of 5%. By visual inspection or examination of the plots, all coefficients are within -0.5 and 0.5 which is due to normalization of the coefficients. Also, there is a significant change in the mean of the processed signals after 90 seconds. This change coincides with the time the leak was introduced. Hence, the algorithm has the ability to detect internal leakages.

In Table 6-5, the percentage change in mean RMS values between the leaking and non-leaking coefficients is shown as a function of lag. The percentage change in mean RMS value increases as the lag is increased. The percentage change (lag 1 to

lag 16) is approximately within 1% and 32%. A higher change would mean a better result. A lag of 16 is chosen for subsequent analysis.

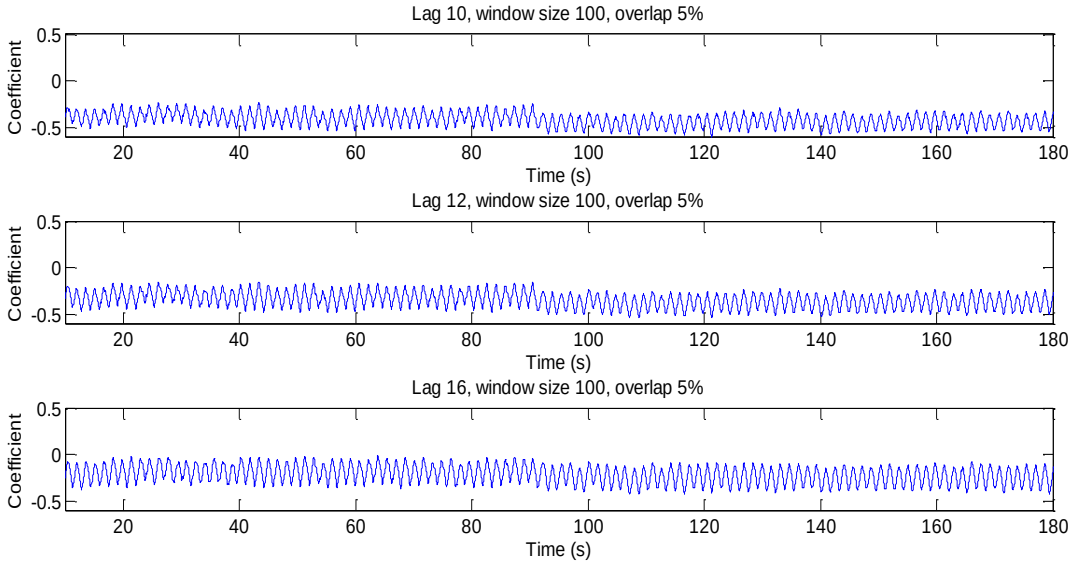

Figure 6-6: Effect of lag on cross correlation between pressure signals 1 and 2- medium leak of 1.2 L/min- lag 10, lag 12, lag 16, window size 100, and overlap 5%.

Table 6-5: Percentage change in mean RMS values as a function of lag

Lag Value	Mean RMS before leak	Mean RMS after leak	(%)Change of Mean RMS
1	0.70328	0.71247	1.3074
4	0.60815	0.6352	4.4487
8	0.46058	0.5131	11.4035
10	0.38528	0.44565	15.6973
12	0.31176	0.37891	21.5391
16	0.18733	0.24766	32.2022

6.2.2 Effect of Window Size

In this section, the preferred lag (lag of 16) is used while the window size is varied. This is to enable us chose a high performing window size. Figure 6-7 shows the result of the cross correlation analysis between pressure signals 1 and 2 with a leak occurring at about the 90th second using window sizes of 100, 200, and 300 data points, lag 16 and an overlap of 5%. By visual examination of the plots, there is a slight decrease in the mean of the processed signals after 90 seconds. More so, the signals are noisier before 90 seconds for all three plots shown. However as the window size increases, the processed signal becomes clearer but the effective change between the leaking and non-leaking coefficients decreases. These changes coincide with the time the leak was introduced suggesting the algorithm is able to detect internal leakages.

In Table 6-6, the percentage change in mean RMS values between leaking and non-leaking coefficient is shown. As the window size increases, the percentage change in mean RMS values decreases. A window size of 100 data points is preferred for subsequent analysis.

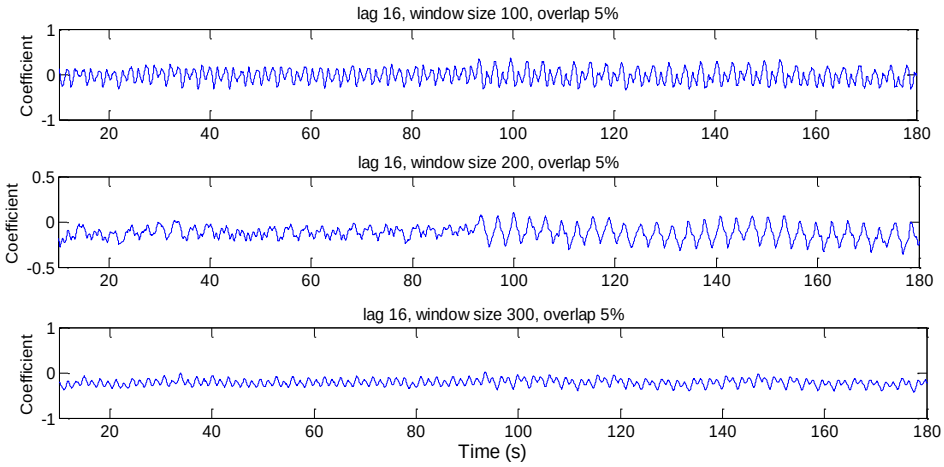

Figure 6-7: Effect of window size on cross correlation between pressure signals 1 and 2; medium leak of 1.2 L/min- lag 16, window size 100, 200, and 300; overlap 5%.

Table 6-6: Percentage change in mean RMS as a function of window size

Window size	Mean RMS before leak	Mean RMS after leak	(%)Change Mean RMS
100	0.11029	0.13786	24.9998
200	0.12397	0.13742	10.8471
300	0.22522	0.22226	1.3121

6.2.3 Effect of Overlap

The high performing lag (lag of 16) and window size (100 data points) is used in this analysis to investigate the effect of overlap and obtain a high performing overlap. Figure 6-8 shows the result of the cross correlation analysis between the pressure signals 1 and 2 with the introduction of leak at 90 seconds using overlaps of 5%, 8% and 10%; lag 16 and window size of 100 data points. The effect of the overlap on the cross correlation coefficient is readily seen as the mean of the coefficients slightly decreases after 90 seconds. This mean change coincides with the time the leak was introduced to the test rig. Also, a visual examination of the signal also reveals that as the overlap is increased from 5% through 15% and above, the signal becomes clearer and less noisy.

In Table 6-7, the percentage change in mean RMS values between leaking and non-leaking coefficients is shown. As the overlap increases, the percentage change in mean RMS values increases. This implies, as the overlap is increased, the detection becomes better. From this analysis, an overlap of 10% is chosen for subsequent analysis.

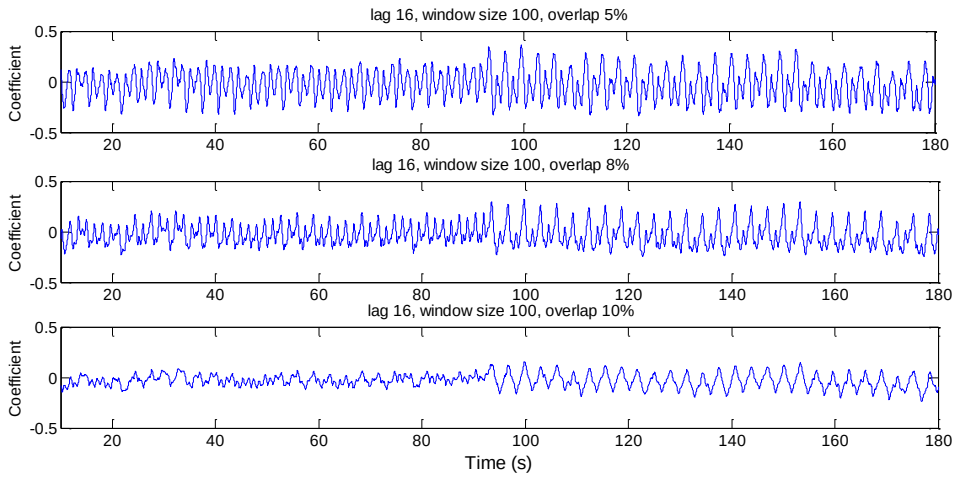

Figure 6-8: Effect of overlap on cross correlation between pressure signals 1 and 2- Medium leak of 1.2 L/min; lag 16, window size 100, overlap 5%, 8%, 10%.

Table 6-7: Percentage change in mean RMS values as a function of overlap.

Overlap (%)	Mean RMS before leak	Mean RMS after leak	(%)Change of Mean RMS
5	0.11029	0.13786	24.9998
8	0.083629	0.11067	32.3300
10	0.04851	0.073228	50.9555

Case Study 2

6.2.4 Cross Correlation (small leak of 0.98 L/min)

The preferred lag, overlap and window size is used for the critical condition (case study 2). Figure 6-9 shows the result of the cross correlation analysis between pressure signals 1 and 2 with the introduction of leak at about 90 seconds using lag 16, window size of 100 data points and 10% overlap. A small leak of 0.98 L/min was simulated in the test rig. Visually the change is significant as there is a decrease in the mean after 90 seconds. Also, the

variation of the signal is higher before the leak which suggests detection. Table 6-8 shows the percentage change in mean RMS value as a function of the small leak. From this result, a percentage change of 9.4 is observed for a leak of 0.98 L/min. This change implies the algorithm may not detect leakages lower than 0.98 L/min.

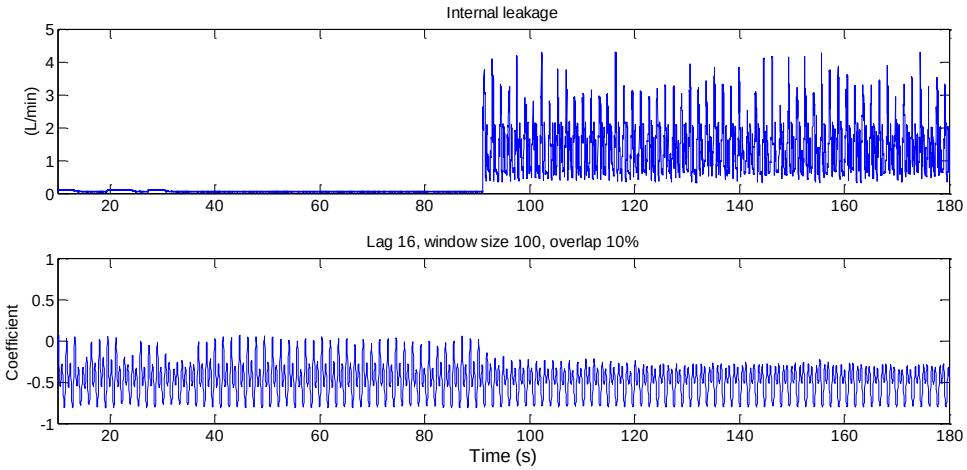

Figure 6-9: Cross correlation between pressure signals 1 and 2- small leak of 0.98 L/min; lag 16, window size 100, overlap 10%

Table 6-8: Percentage change in mean RMS values as a function of small leak.

Pressure signal	Mean RMS before leak	Mean RMS after leak	(%)Change of RMS
Pressure signal (*P1* and *P2*)	0.47029	0.51479	9.4623

6.2.5 Sensitivity Analysis

The sensitivity analysis for various leaks (0.77 L/min-1.63 L/min) and load is performed Figure 6-10 shows the sensitivity of the cross correlation analysis of pressure signals 1 and 2 to the severity of internal leakage simulated. While there is no consistent trend, the sensitivity is between 0% and 40%. This implies, the maximum change obtainable for the leakage range considered is 40%.

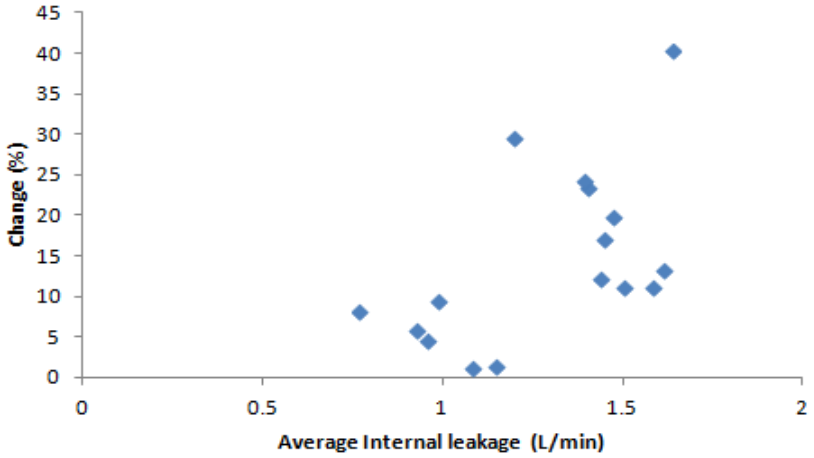

Figure 6-10: Sensitivity of the cross correlation between pressure signals 1 and 2 to the severity of leakage simulated.

6.3 Cross Correlation Results (piston displacement and input signal: EHA)

As illustrated in Chapter 4, two signals are needed for executing the cross correlation algorithm. The cross correlation function is applied between the control signal and piston displacement data, producing a single coefficient for each window. These values are then plotted in time to show the behavior or dynamics of the cross correlation coefficients over the course of an experiment.

The windowing technique used is described in Section 4.5. It starts with assessing the effect of lag. This is achieved by varying the lag while the window size and overlap is held constant. The effect of the lag is observed and a high performing one is chosen and used for further analysis. The next step varies the window size while the overlap and preferred lag is held constant. A high performing window size is chosen and finally the preferred window size and preferred lag is held constant while the overlap is varied. The preferred overlap is chosen. The preferred lag, window size and overlap are used for detecting the smallest internal leakage (case study 2) and for performing the sensitivity analysis.

6.3.1 Effect of Lag

Figure 6-11 shows the result of a cross correlation analysis between input signal and piston displacement, with a leak occurring at about 90 seconds using lag 1, 4 and 8, window size of 100 data points and an overlap of 5%. By visually examining the plots, all coefficients are within -1 and 1. Also, there is a very slight change in the mean of the processed signals after 90 seconds. This change coincides with the time the leak was introduced. Hence, the algorithm has the ability to detect internal leakages but with minimal level of success.

In Table 6-9, the percentage change in mean RMS values between the leaking and non-leaking coefficients is shown as a function of lag. The percentage change in mean RMS values increases as the lag is increased. The percentage change for lag 1 and lag 8 is approximately within 30% and 35% respectively. However, there appears to be no trend after lag 8. The percentage change in mean RMS values increases gradually until lag 8. A lag of 8 is chosen for subsequent analysis.

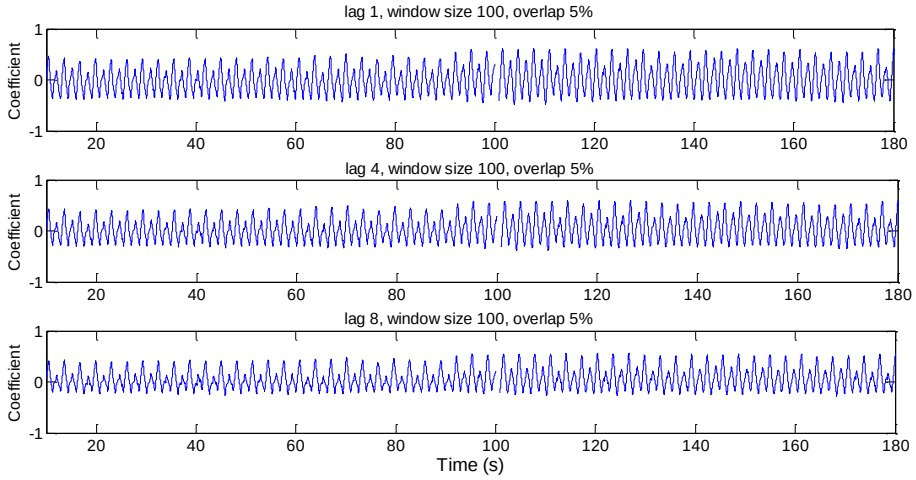

Figure 6-11: Effect of lag on cross correlation between input signal and piston displacement medium leak of 1.2 L/min- lag 1, lag 4, lag 8, window size 100, overlap 5%.

Table 6-9: Percentage change in mean RMS values as a function of lag

Lag Value	Mean RMS before leak	Mean RMS after leak	(%)Change of Mean RMS
1	0.18767	0.24396	29.9915
4	0.15819	0.2128	34.5185
8	0.1312	0.17741	35.2248

6.3.2 Effect of Window Size

Figure 6-12 shows the result of the cross correlation analysis between input signal and piston displacement with a leak occurring at about the 90^{th} second using window sizes of 100, 200, and 300 data points, lag 8 and an overlap of 5%. By visual examination of the plots, there is a slight increase in the mean of the processed signals after 90 seconds. More so, as the window size increases, the processed signal becomes more packed. These changes coincide with the time the leak was introduced suggesting the algorithm is able to detect internal leakages.

In Table 6-10, the percentage change in mean RMS values between leaking and non-leaking coefficient is shown. As the window size increases, the percentage change in mean RMS value decreases as the window size increases until the window size is 300 data points. It maintains an irregular pattern for higher window sizes suggesting the need to be precautious when making the choice of window size. For subsequent analysis a window size of 100 data points is chosen for subsequent analysis.

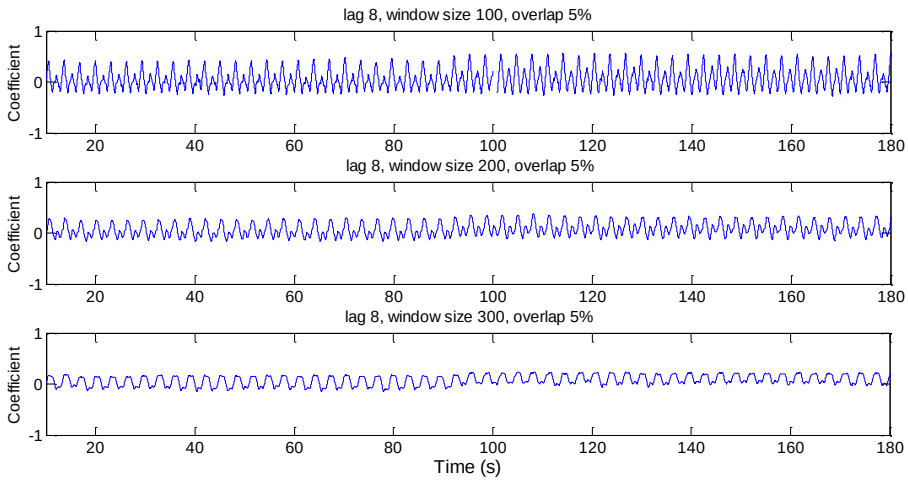

Figure 6-12: Effect of window size on the cross correlation between input signal and piston displacement; medium leak of 1.2 L/min- lag 8, window size 100, 200, 300, overlap 5%.

Table 6-10: Percentage change in mean RMS as a function of window size.

Window size	Mean RMS before leak	Mean RMS after leak	(%)Change of Mean RMS
100	0.1312	0.17741	35.2248
200	0.10518	0.128	21.6873
300	0.097109	0.11184	15.1736

6.3.3 Effect of Overlap

Figure 6-13 shows the result of the cross correlation analysis between the input signal and piston displacement with the introduction of leak at 90 seconds using overlaps of 5%, 10% and 15%; lag 8 and window size of 100 data points. A visual examination of the signal also reveals that as the overlap is increased from 5% through 15% and above, the signal becomes clearer and less noisy. The overlap has less visual effect on the cross correlation coefficient though the variation of the processed signal increased slightly after the 90th second. More so, the signal tends to be distorted for higher overlaps (overlap 10% and 15%) at approximately this same time. This discontinuity is due to the fact that the mean of the signals are not real numbers at that point.

In Table 6-11, the percentage change in mean RMS values between leaking and non-leaking coefficients is shown. As the overlap increases, the percentage change in mean RMS values increases until the overlap becomes 15%. An overlap of 5% is chosen for subsequent analysis though quantitatively, a higher change is obtained for overlap 15%. This is because the result for 5% overlap shows a better visual change and has more variation on the signals before and after the leak was introduced.

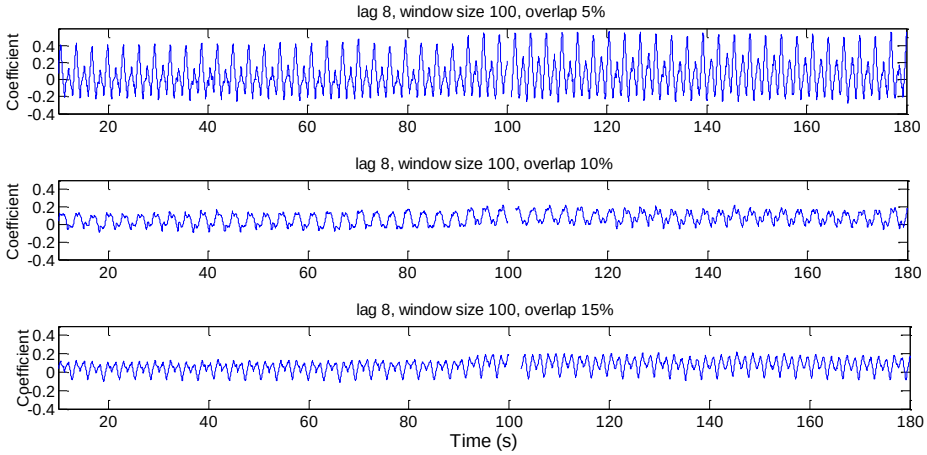

Figure 6-13: Effect of overlap on cross correlation between Input signal and piston displacement- Medium leak of 1.2 L/min; lag 8, window size 100, overlap 5%, 10%, 15%.

Table 6-11: Percentage change in mean RMS values as a function of overlap

Overlap (%)	Mean RMS before leak	Mean RMS after leak	(%)Change of Mean RMS
5	0.1312	0.17741	35.2248
10	0.06502	0.090066	38.5209
15	0.067871	0.10034	47.8345

6.3.4 Cross Correlation (small leak of 0.98 L/min)

The preferred lag, window size and overlap are used for the smallest leak condition (case study 2). Figure 6-14 shows the result of the cross correlation analysis between input signal and piston displacement with the introduction of a leak at about 90 seconds using lag 8, window size of 100 data points and 5% overlap. A small leak of 0.98 L/min was simulated in the test rig. Visually, there is a slight change in the signal after 90 seconds as there is a decrease in its mean after 90 seconds. Also the variation of the signal is higher before the leak which suggests detection. Table 6-12 shows the percentage change in mean RMS values as a function of the smallest leak. From this result, a percentage change of 31.9 is observed for a minimum leak of 0.98 L/min. This change implies the algorithm may not detect leakages lower than 0.98 L/min.

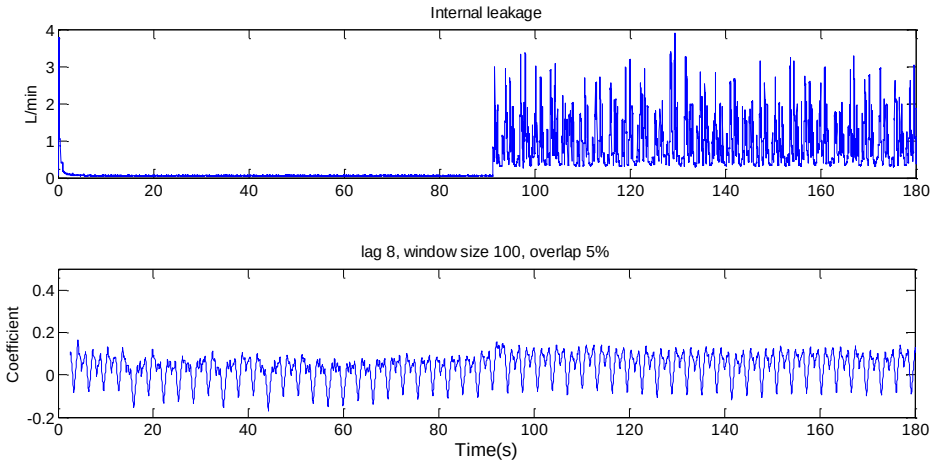

Figure 6-14: Cross correlation between piston displacement and input signal- small leak of 0.98 L/min; lag 8, window size 100, overlap 5%.

Table 6-12: Percentage change in mean RMS as a function of small leak

Signal	Mean RMS before leak	Mean RMS after leak	(%)Change of RMS
Input signal and Piston displacement (*U* and *X*)	0.057528	0.075907	31.9485

6.3.5 Sensitivity Analysis

The sensitivity analysis for varieties of leak (0.77 L/min-1.63 L/min) and load is performed. Figure 6-15 shows the sensitivity of the cross correlation analysis between input signal and piston displacement to the severity of internal leakage simulated. While there is no consistent trend, the sensitivity is between 0% and 35%. This implies, the maximum change obtainable for the leakage range is 35%.

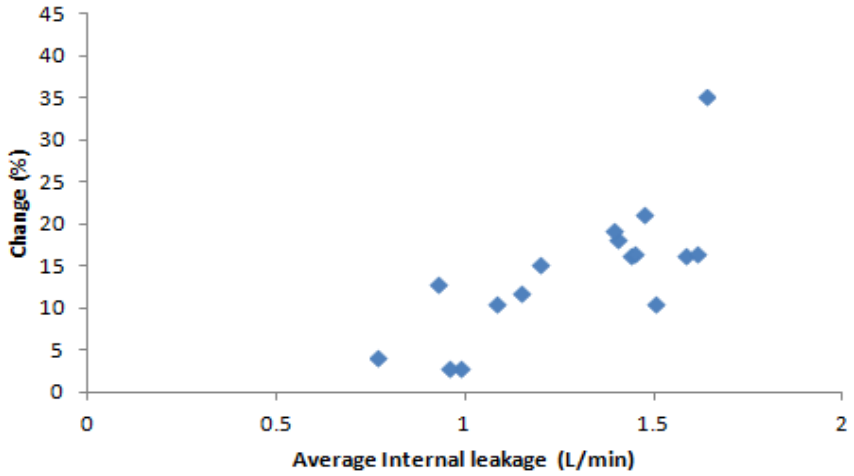

Figure 6-15: Sensitivity of cross correlation between piston displacement and input signal to the severity of internal leakage simulated.

6.4 Ratio of metric lengths (electrohydrostatic actuation system)

Detecting internal leakage faults by calculating the ratio of metric lengths requires either pressure signal 1 or pressure signal 2. As explained in Chapter 4, the ratio of metric lengths of the signal quantizes the complexity in the signal. It has the ability to detect patterns, trends and changes in a signal. The algorithm would be implemented using pressure signals 1 and 2. The pressure signal is divided into windows and the algorithm is applied producing a single number for each window. These values are then plotted in time to show the behavior or dynamics of the ratios of the metric lengths over the course of an experiment.

The windowing technique used is described in Section 4.5. It starts with assessing the effect of lag. This is achieved by varying the lag while the window size and overlap is held constant. The effect of the lag is observed and a high performing one is chosen and used for further analysis. The next step varies the window size while the overlap and preferred lag is held constant. A high performing window size is chosen and finally the preferred window size and preferred lag is held constant while the overlap is varied. The preferred overlap is chosen. The preferred lag, window size and overlap are used for detecting the smallest internal leakage (case study 2) and for performing the sensitivity analysis.

6.4.1 Effect of Lag

Figure 6-16 shows the result of the ratio of metric lengths computation using pressure signal 1 with a leak occurring at about 90 seconds using lag ratios of 43:3, 40:3 and 37:3; window size of 200 data points and an overlap of 5%. By visual examination of the plots, there is a significant increase in the amplitude of the processed signals after 90 seconds. More so, the number of spikes in the signal increases after 90 seconds. These changes coincide with the time the leak was introduced. Increasing the lag ratio improves the effective change but it leaves the processed signals packed.

In Table 6-13, the percentage change in mean RMS values between leaking and non-leaking fractal numbers is shown. As the lag ratio decreases, the percentage change in mean RMS values decreases slightly. This implies, the lag ratio affects the detection process. A lag ratio of 43:3 is preferred for subsequent analysis.

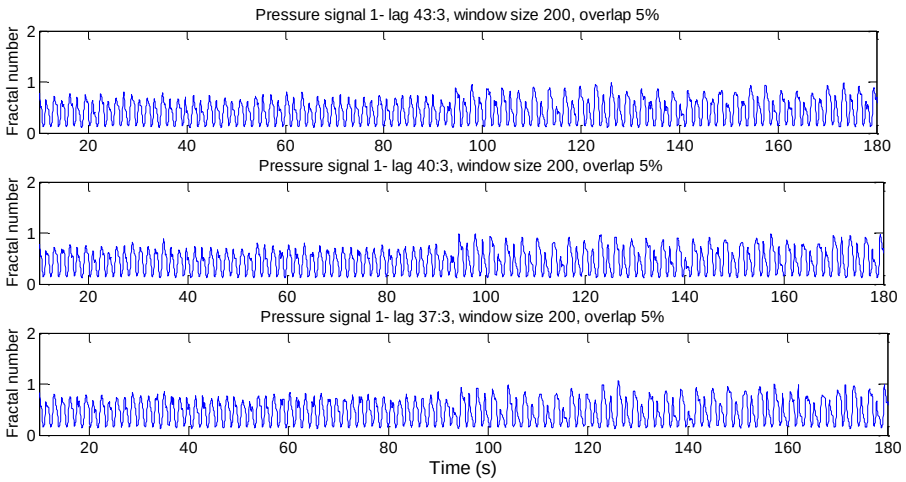

Figure 6-16: Effect of lag on the ratio of metric lengths (fractal number) of pressure signal 1 for a medium leak of 1.2 L/min, window size 200, Overlap 5%. Lag 43:3, 40:3 37:3.

Table 6-13: Percentage change in mean RMS values as a function of lag ratio

Lag Value	Mean RMS before leak	Mean RMS after leak	(%)Change of Mean RMS
43:3	0.47524	0.41752	13.8248
40:3	0.44128	0.48264	9.3726
37:3	0.46433	0.47866	3.0867

6.4.2 Effect of Window Size

Figure 6-17 shows the result of the ratio of metric lengths using pressure signal 1 with a leak occurring at about the 90th second using window sizes of 200, 300, 400 data points, lag ratio 43:3 and an overlap of 5%. By visual examination of the plots, there is a slight increase in the mean of the processed signals after 90 seconds. More so, the number of spikes in the signal increases after 90 seconds increases. These changes coincide with the time the leak was introduced and hence suggests detection. Also, as the window size increases, the processed signals become clearer and less noisy. The effective change between the leaking and non-leaking ratio of metric lengths increases slightly.

In Table 6-14, the percentage change in mean RMS values between leaking and non-leaking ratio of metric lengths (fractal number) is shown. As the window size increases, the percentage change in mean RMS values increases slightly. This implies, the window size affects the detection process slightly. Following a slight difference between the changes for the shown window sizes, a window size of 400 data points is chosen for subsequent analysis.

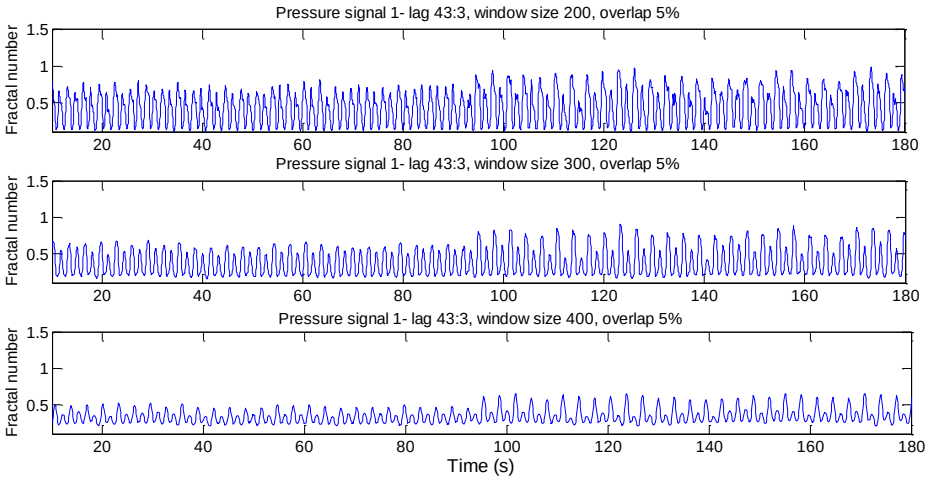

Figure 6-17: Effect of window size on the ratio of metric lengths (fractal number) of pressure signal 1 for a medium leak of 1.2 L/min, window size 200, 300, 400, overlap 5%, and lag 43:3.

Table 6-14: Percentage change in mean RMS values as a function of window size

Window size	Mean RMS before leak	Mean RMS after leak	(%)Change of Mean RMS
200	0.47524	0.41752	13.8248
300	0.36944	0.42177	14.1648
400	0.33121	0.37835	14.2334

6.4.3 Effect of Overlap

Figure 6-18 shows the result of the ratio of metric lengths computation using pressure signal 1 with a leak occurring at about the 90th second using window overlaps of 5%, 15%

and 25%; window size of 200 data points and a lag ratio of 43:3. By visual examination of the plots, there is a slight change in the appearance of the processed signals after 90 seconds. More so, the number of spikes in the signal increases after 90 seconds. These changes coincide with the time the leak was introduced and hence suggest detection. As the overlap increases the processed signals becomes clearer and less noisy but the effective change between the leaking and non-leaking ratios of metric lengths remains approximately constant.

In Table 6-15, the percentage change in mean RMS values between the leaking and non-leaking ratios of metric lengths is shown. As the overlap increases, the percentage change in mean RMS values is approximately constant; although there is a slight increase to 3 decimal places. This implies, the overlap has less influence on the detection process. Hence, an overlap of 5% is chosen for subsequent analysis.

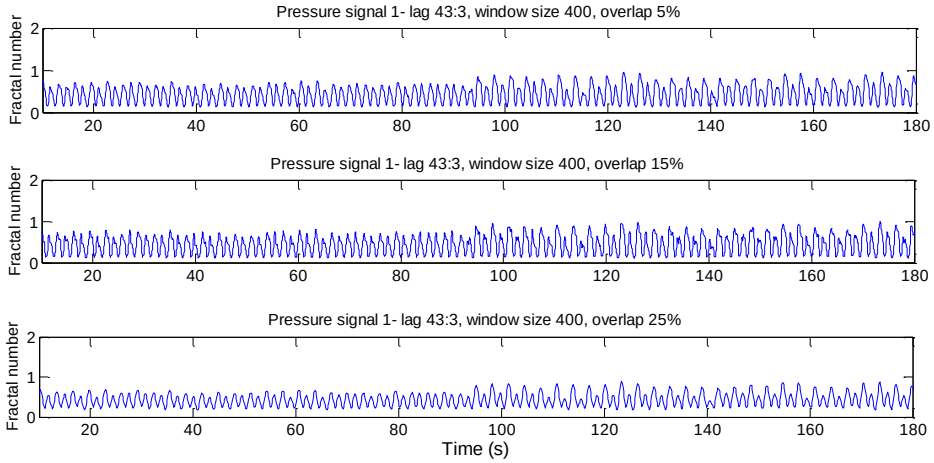

Figure 6-18: Effect of overlap on ratio of metric lengths (fractal number) of pressure signal 1 for a medium leak of 1.2 L/min, window size 400, overlap 5%, 15%, 25%, Lag 43:3

Table 6-15: Percentage change in mean RMS value as a function of the overlap

Overlap (%)	Mean RMS before leak	Mean RMS after leak	(%) Change of Mean RMS
5	0.32771	0.37359	13.9992
15	0.33037	0.37648	13.9566
25	0.32526	0.37052	13.9126

6.4.4 Ratio of Metric Lengths Results (small leak of 0.98 L/min)

The preferred lag, window size and overlap are used for detecting a small leak. Figure 6-19 shows the result of the ratio of metric lengths computation using both chamber pressure signals with the introduction of leak at about 90 seconds using lag 43:3, window size of 400 data points and 5% overlap. A small leak of 0.98 L/min was simulated in the test rig. By visual examination, there is no resemblance in the ratio of metric lengths (fractal number) of both pressure signals though both show changes at about 90 seconds. The result depicts the algorithm is able to detect a leak of about 0.98 L/min.

In Table 6-16, the percentage change in mean RMS values between the leaking and non-leaking ratio of metric lengths is shown. While a percentage change of 3.5892% is obtained for pressure signal 1, a percentage change of 6.7725% is obtained for pressure signal 2. This shows a close relationship between the chamber pressure signals as mentioned earlier.

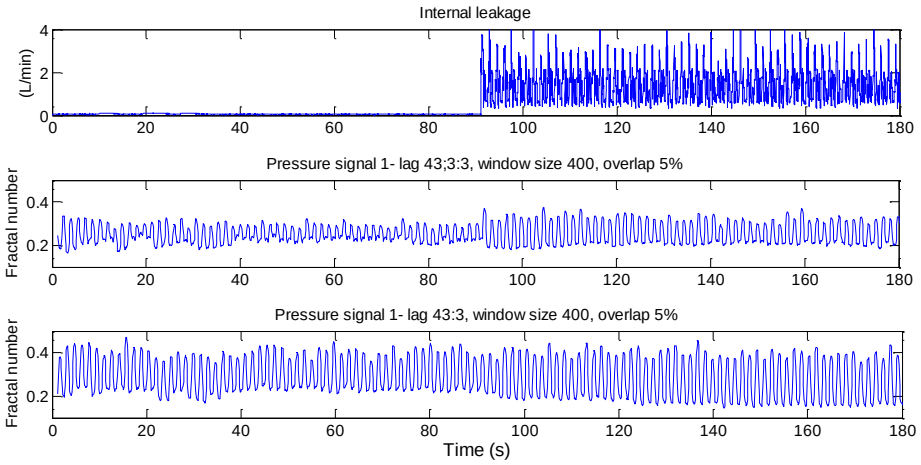

Figure 6-19: Ratio of the metric lengths (fractal number) of pressure signals 1 and 2 for a small leak of 0.98 L/min. Window size 400, overlap 5% and lag ratio 43:3.

Table 6-16: Percentage change in mean RMS values as function of small leak

Pressure signal	Mean RMS before leak	Mean RMS after leak	(%)Change of RMS
Pressure signal (P1)	0.25266	0.26172	3.5892
Pressure signal (P2)	0.31144	0.29035	6.7725

6.4.5 Sensitivity Analysis

The sensitivity analysis for varieties of leak (0.77 L/min-1.63 L/min) and load is performed Figure 6-20 shows the sensitivity of the ratio of metric lengths using pressure signal 1 to the severity of the internal leakage simulated. Generally, the percentage change in mean RMS values increases as the severity of the leak increases. The sensitivity is between 0% and 20%. This implies that a maximum change of 20% is obtainable for the range of leakage used.

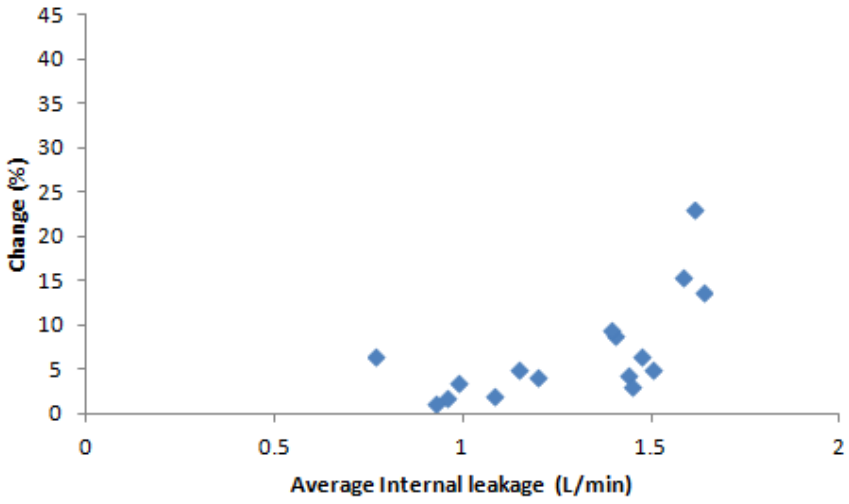

Figure 6-20: Sensitivity of the ratio of metric lengths of pressure signal 1 to the severity of internal leakage simulated.

6.5 Summary

All three methods can be successfully used to diagnose faults due to internal leakage for the EHA test rig. Autocorrelation of pressure signals gets better as the lag decreases and window size decreases. It performs well at a window size of 100 data points and lag 1. On the other hand, cross correlation of pressure signals performs well at lag 16 and window size of 200 data points. Cross correlation between control signal and piston displacement performs well at lag 8 and window size of 200 data points. Ratio of metric lengths of pressure signals gets better as the lag ratio increases and window size decreases. It performs well at a window size of 400 data points.

7 CONCLUSION

7.1 Contributions

This research considered internal leakage fault detection in valve controlled hydraulic actuation systems (VCA) and electrohydrostatic actuation systems (EHA). Motivated by developing a method that is independent of the system model or fault type, signal processing based techniques (autocorrelation, cross correlation and ratio of metric lengths concept) were employed for internal leakage fault detection. Various signals (pressure signals, piston displacement and control signals) were used for the identification purpose. For the excitation, pseudorandom inputs, in a closed position control loop, were used for the VCA and sinusoidal input signals to the pump were used for the EHA.

Experiments were performed using different magnitudes of internal leakage. The stationarity of the signals acquired from both systems were verified up to 4^{th} order using statistical moments. The results of these analysis showed that the signals were stationary for the application of autocorrelation, ratio of metric lengths and cross correlation. The following analysis were performed; autocorrelation of chamber pressure signals, cross correlation between chamber pressure signals, cross correlation between piston displacement and control signal and calculation of the ratio of metric lengths of pressure signals.

For the VCA, internal leakages in the ranges of 0.047 L/min-0.5 L/min were introduced to the test rig. Autocorrelation of pressure signal, cross correlation of pressure signals and cross correlation of piston displacement and control signal was found to perform well at window sizes in the range of 100-200 data points, overlap of 5% and lag 1.

Given the limitation of the system, the smallest leak simulated was 0.047 L/min and the highest leak was 0.5 L/min. Ratio of metric lengths for chamber pressure signals was found to be most sensitive to internal leakage as compared to cross correlation and autocorrelation methods.

For the EHA, internal leakages in the ranges of 0.77 L/min-1.63 L/min were introduced. Autocorrelation of pressure signal was found to perform well at a window size of 100 data

points, lag 1 and 10% overlap. Cross correlation of pressure signals was found to perform well at lag 16, window size of 100 data points and 10% overlap. On the other hand, cross correlation of piston displacement and control signal was found to perform well at a window size of 200 data points, lag 8 and 5% overlap. Ratio of metric lengths of pressure signal was found to perform well at a window size of 200, lag ratio of 43:3 and 5% overlap.

All three signal processing based methods can be employed for internal leakage fault diagnosis with a certain degree of success. However, the concept of the ratio of metric lengths using pressure signals, was found to be more sensitive to internal leakage as low as 0.047 L/min (VCA).

Finally, for the first time, leakage as low as 0.047 L/min can be detected for the valve controlled actuation system. The feasibility of employing input signal and piston displacement for internal leakage detection has also been investigated; a method which will require no pressure sensors and as such attractive for industrial implementation.

7.2 Future Work

The EHA analysis performed was for open loop conditions, as no fault tolerant controller has yet been designed for this system. The next phase of this work would require designing a closed loop fault tolerant controller for the EHA system. Also, this work will be improved such that the exact time the fault occurs can be determined automatically.

REFERENCES

An, L. and Sepehri, N. (2005) "Hydraulic actuator leakage fault detection using Extended Kalman filter." *International. Journal of Fluid Power, Vol. 6,* 41-51..

Bowerman, B. and O'Connell, R. (1979) "Time Series and Forecasting," *Duxbury Press, North Scituate, Massachusetts.*

Box, G., Jenkins, E. and Reinsel, G. (1994) "Time series analysis: forecasting and control*,"* (Third ed.).

Challis, R.E. and Kitney, R.I. (1991) "Biomedical signal processing, Time-domain methods*" Medical & Biological Engineering & Computing ,* 509-524.

Chinniah, Y. A. (2004.) "Fault Detection in the Electrohydraulic Actuator Using Extended Kalman Filter", *PhD Thesis, University of Saskatchewan.*

Chinniah,Y.A., Burton, R. and Habibi, S. (2003) "Viscous damping coefficient and effective bulk modulus estimation in hydrostatic actuatuation system using extended kalmer filtering" *International journal of fluid power Vol 4* , 27-34.

Gao, Y., Zhang, Q. and Kong, X. (2005) Comparison of hydraulic pump fault diagnosis methods, wavelet vs. spectral analysis, *Proceedings, ASME International Mechanical Engineering Congress and Exposition,* 73-78

Garimella, P. and Yao, B. (2005) Model-based fault detection of an electro-hydraulic cylinder. *American Control Conference*, 484-489.

Goharrizi, A. Y. (2011) Leakage Detection in Hydraulic Actuators based on Wavelet transform, *PhD thesis University of Manitoba.*

Goharrizi, A. and Sepehri, N. (2010.) "A wavelet- based approach to internal seal damage diagnosis in hydraulic actuators. *" IEEE Transactions on Industrial Electronics, Vol. 57, no. 5,* 1755-1763.

Goharrizi, A. and Sepehri, N. (2011.) "A Wavelet-based approach for external leakage detection and isolation from internal leakage in Valve Controlled hydraulic actuators", *IEEE Transactions on Industrial Electronics, Vol. 58, No. 9,* 4374-4384.

Goharrizi, A. and Sepehri, N. (2012.) "Internal Leakage Detection in Hydraulic Actuators using Empirical Mode Decomposition and Hilbert Spectrum. *" IEEE Transactions on Instrumentation and Measurements, Vol. 61,* 368-378.

Habibi, S. and Goldenburg, A. (2000) "Design of a New High Performance Electrohydraulic Actuator", *IEEE/ASME Transactions on Mechatronics, Vol. 5, No. 2.*

Huang, S. and Hsieh, C. (1998) "Feasibility of fractal-based methods for visualization of power system disturbances." *International Journal of Electrical Power & Energy Systems Vol 23, Issue 1,* 31–36.

Karpenko, M. (2008) "Quantitative fault tolerant control design for a hydraulic actuator with a leaking piston seal" *Ph.D. thesis, University of Manitoba, Winnipeg, Canada.*

Karpenko, M. and Sepehri, N. (2010) "Quantitative fault tolerant control design for a hydraulic actuator with a leaking piston seal." *ASME Journal of Dynamic Systems, Measurement, and Control, Vol. 132, No. 5.*

Karpenko, M. and Sepehri, N. (2005.) "Fault-tolerant control of a servohydraulic positioning system with crossport leakage." *IEEE Trans. on Cont. Sys. Tech. Vol.13, No. 1,* 155-161.

Khan, H., Abou, S. and Sepehri, N. (2002.) "Fault Detection in Electro-Hydraulic Servo Positioning Systems Using Sequential Test of Wald". *Proceedings, Canadian Conference on Electrical and Computer Engineering, Vol.3,* 1628-1633.

Leugner, L. (2010) "Hydraulic System Leakage - The Destructive Drip" http://www.machinerylubrication.com/Read/21/hydraulic-system-leakage

Linaric, D. and Koroman, V. (2003) "Fault diagnosis of a hydraulic actuator using neural network" *Industrial Technology, 2003 IEEE International Conference Vol. 1* 108 - 111

Liu, H., Ouyang, P. and Wang, S. (2006) "Fault Detection Based on RBF Neural Network in a Hydraulic Position" Servo System *Intelligent Control and Automation, 2006. WCICA 2006. The Sixth World Congress Vol.2* 5708 - 5712.

Loughmiler, J. (2009) "Emerging Technologies, Distributed Electro-Hydraulic Systems." *http://www.designnews.com/document.asp?doc_id=228724&dfpPParams=ind_182,aid_228724&dfpLayout=article.*

Mamishev, A., Russell, B., Carl, B. (1996). "Analysis of High Impedance Faults." *IEEE transaction on power systems, Texas,* 1-3.

May, M. (2012). "Internal leakage detection in hydraulic actuators using autocorrelation and cross correlation of pressure signals," *B.eng thesis, University of Manitoba.*

Merrit, H. E. (1967) " Hydraulic control systems," *Wisely New york.*

Murphy, B.J., Banks, J.C. and Richard, K. (2006) "Modeling of hydraulic systems tailored to diagnostic fault detection systems" Aerospace Conference, 2006 IEEE"

Nwachukwu, I. U. (2012) " Techniques for improving uniformity in direct mapped caches. *Proquest 2012, Masters Thesis, University of North Texas May 2011*

Paz, M. and Pilar, G. (2003) "Univarate Time Series Modelling-Computer-Aided Intorduction to econometrics" *Springer Link.* 163-224,

Preston, G.J., Shields, D.N. and Daley, S. (1996) "Application of a robust nonlinear fault detection observer to a hydraulic system" *Control '96, UKACC International Conference Vol.2* 1484 - 1489.

Skormin, V. A., Apone, J. and Dunphy, J. J. (1994.) "Online diagnostics of a selfcontained flight actuator." *IEEE Trans. Aerospace and Electronic Systems.*

Song, Y. and Habibi, S. (2013) "Electro-Hydrostatic Actuator Fault Detection and Diagnosis" *McMaster University, Masters in science Thesis* , 2.

Tan, H. and Sepehri, N. (2002) "Parametric fault diagnosis for electrohydraulic cylinder drive units." *IEEE Trans. Industrial Electronics, Vol. 49,* 96-106.

Ting-Tao, M., Yong-Xiang, Z. and Xi-Young. (2009) " Fault Detection for Electro-Hydraulic Valve-Controlled Single Rod Cylinder Servo System Using Linear Robust Observer" *Measuring Technology and Mechatronics Automation, 2009. ICMTMA '09. International Conference Vol. 1*, 639-642.

Thakur, A. (2011) "Understanding the Effect and Diagnosis of Internal Leakage in Hydrostatic Actuation Systems," *Masters Thesis.* University of Manitoba.

Theiler, J., Eubank, K., Longtin, A., Galdrikian, B. and Farmer, D. (1992) "Testing for Nonlinearity in Time Series: the Method of Surrogate Data. Copyright © 1992 Published by Elsevier B.V.

Umeh, K., Mohamed, A., Mohamed, R. and Hussain, A. (2004)" Characterizing nonlinear load harmonics using fractal analysis" *ISCAS '04. Proceedings of the 2004 International Symposium on Vol 5*.

U.S. Commerce Department. (Engineering statistic Handbook. Online) (2010) *http://www.itl.nist.gov/div898/handbook/eda/section3/eda35c.html.*

Wang, X. and Syrmos, V.L (2008) "Fault detection, identification and estimation in the electro-hydraulic actuator system using EKF-based multiple-model estimation" *Control and Automation, 2008 16th Mediterranean Conference* 1693 - 1698.

Watton, J. and Pham, D. T. (1997) Fault classification of fluid power systems using a dynamics feature extraction technique and neural networks. *Proc. Instn Mech Engrs, Vol. 212, Part I,* 87-96.

Zavarehi, M. K., Lawrence, P. D. and Sassani, F. (1999) Nonlinear modeling and validation of solenoid controlled pilot-operated servovalves. *IEEE/ASME transaction Mechatronics, Vol.4* , 324-334.

Zhang, Y.M. and Jiang, J. (2002) "Active fault-tolerant control system against partial actuator failures" *IEEE proceddings of control theory application Vol.149* , 25-149.

Zhiyong, L. and Weilin, W. (2006) "Detection and Identification of Power Disturbance Signals Based on Nonlinear Time Series" 2006 *6th World Congress on Intelligent Control and Automation, Vol.2*, pp.7646-7650.

"http://web.iitd.ac.in/~suniljha/MEL334/TermProjects2012/ElectroHydraulicServoValve.pdf?hsimp=yhse-001"

http://www.daerospace.com/HydraulicSystems/ServovalveDesc.php?

http://www.tree.ltrr.arizona.edu/~dmeko/geos585a.html?